NUMERICAL MODELING OF GEOPHYSICAL PROBLEMS

Dr. Attila Galsa

Eötvös Loránd University
Faculty of Science
Department of Geophysics and Space Science

Budapest, 2020

PREFACE

In these lecture notes I apply the COMSOL Multiphysics 5.3a finite element numerical software package to present the fundamentals of the numerical modeling from the selection of the appropriate module, via building the geometry, prescribing the initial and boundary conditions, discretization, solving the problem to visualizing the solution. After a brief theoretical summary of the operation of finite element method, I suggest to follow the Introduction to COMSOL Multiphysics which facilitates step by step to acquire the basal functions and capabilities of the program by a typical 'multiphysical' example. The main body of the course is getting an insight into the numerical phrasing of a given practical or theoretical geophysical problem, thus several topics in Geophysics, such as vertical electrical sounding, magnetic surveying, induction borehole sounding, borehole exchanger, solute transport in groundwater flow, thermal and thermochemical mantle convection etc., will be discussed. These notes were primarily written for geophysicists, however it could be useful for both students and modelers who are interested in scientific research.

CONTENTS

1 FUNDAMENTALS OF FINITE ELEMENT METHOD

Finite element method (FEM) was developed to solve partial differential equations (PDEs) and integral equations. The method is especially useful and suggested, if

- the geometry of the problem is complex (e.g. racing car in wind channel), or
- the areal density of incoming or outgoing data is strongly variable (e.g. meteorological observations).

1.1 Historical background

Originally, FEM was developed to investigate the elastic and/or structural behavior of tools having complex geometry in engineering. In 1941, Hrenikoff introduced rectangular mesh, one year later Courant applied the triangular discretization. Since 1950' structure of airframes has been investigated by FEM, and from 1960' FEM started to spread in civil engineering. In 1973, Strang framed the exact mathematical description of FEM, and proved that it is adaptable to compute and solve arbitrary physical problem, e.g. Electromagnetism, Fluid dynamics, Heat transport.

1.2 An example for the functioning of FEM

Generally, a FEM solution consists of three main steps:

- Transformation of the original PDE to variational/weak form. Usually, it is simple, it can be done analytically.
- Finite element discretization of the weak form.
- Solution of a large-sized linear algebraic system (LAS).

As an example, let us take a 1D boundary problem, where

$$u''(x) = f(x) \quad where \quad x \in [0,1] \quad and \quad u(x = 0,1) = 0. \tag{1.1}$$

Obviously, this problem can be solved by integration of the equation, but $u''(x)+u'(x)=0$ cannot be done.

1.2.1 Weak form

First, Eq. (1.1) should be transformed to weak form. Let us multiply both sides of the equation by any smooth function $v(x)$ that satisfies the boundary conditions, that is $v(x=0)=v(x=1)=0$. Then, it should be integrate for the whole domain, we get

$$\int_0^1 f(x)v(x)dx = \int_0^1 u''(x)v(x)dx. \tag{1.2}$$

Integrating partially the right term,

$$\int_0^1 f(x)v(x)dx = \left[v(x)u'(x)\right]_0^1 - \int_0^1 u'(x)v'(x)dx. \tag{1.3}$$

The term in the bracket is equal to zero due to the definition of the base function $v(x)$, so the weak form of the original differential equation Eq. (1.1) is

$$\int_0^1 f(x)v(x)dx = -\int_0^1 u'(x)v'(x)dx. \tag{1.4}$$

It can be proved, that the solution of the original equation Eq. (1.1) and the weak form Eq. (1.4) is equivalent, although the verification is not trivial (e.g. Hilbert transformation, Riesz representation), and not essential for this course.

1.2.2 Discretization

Let us define a smooth base function system $v_k(x)$ that satisfies the boundary condition at x=0 and 1! It can be

$$v_k(x) := \begin{cases} \dfrac{x - x_{k-1}}{x_k - x_{k-1}} & \text{if} \quad x \in [x_{k-1}, x_k] \\ \dfrac{x_{k+1} - x}{x_{k+1} - x_k} & \text{if} \quad x \in [x_k, x_{k+1}], \\ 0 & \text{otherwise} \end{cases} \tag{1.5}$$

where k=1..n. *Figure 1.1.a* illustrates the 1D base function system, which linearly varies between zero and one.

Using $v_k(x)$ the unknown solution $u(x)$ can be discretized,

$$u(x) = \sum_k u_k v_k(x). \tag{1.6}$$

With this transformation, the unknown vector u_k should be determined instead of the unknown function $u(x)$. *Figure 1.1.b* shows the relation between the solution $u(x)$ and the solution of the discretized problem (right term of (1.6)).

Turning back to the weak form of Eq. (1.4), the right side can be rewritten using the discretized solution of Eq. (1.6),

$$-\int_0^1 u'(x)v'(x)dx = -\int_0^1 \left(\sum_k u_k v_k(x)\right)' v_j'(x)dx = -\int_0^1 \sum_k u_k v_k'(x) v_j'(x)dx. \tag{1.7}$$

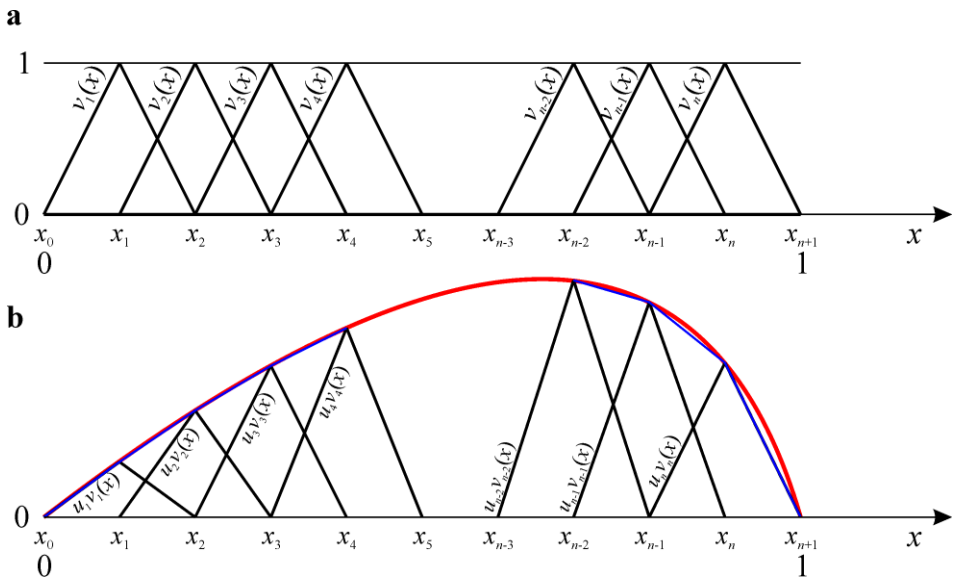

Figure 1.1 (a) The base function set and (b) the illustration of the solution of the original (u(x), red) and the discretized problem (blue).

Since the constants can be extracted from the integration, the right side of the discretized weak form is,

$$-\int_0^1 u'(x)v'(x)dx = -\sum_k u_k \int_0^1 v_k'(x)v_j'(x)dx =: -\sum_k u_k L_{kj}. \tag{1.8}$$

Here, L_{kj} is the so-called stiffness matrix, which can be calculated from the base functions,

$$L_{kj} = \int_0^1 v_k'(x)v_j'(x)dx. \tag{1.9}$$

The known function $f(x)$ can be discretized similarly to the unknown solution $u(x)$,

$$f(x) = \sum_k f_k v_k(x), \tag{1.10}$$

thus the left side of the weak form in Eq. (1.4) is

$$\int_0^1 f(x)v(x)dx = \int_0^1 \sum_k f_k v_k(x)v_j(x)dx = \sum_k f_k \int_0^1 v_k(x)v_j(x)dx = \sum_k f_k M_{kj}. \tag{1.11}$$

In Eq. (1.11) M_{kj} is the so-called mass matrix that can be computed by the integration of base functions,

$$M_{kj} = \int_0^1 v_k(x)v_j(x)dx. \tag{1.12}$$

So, we managed to discretize the weak form using the linear base function system $v_k(x)$,

$$\sum_k f_k M_{kj} = -\sum_k u_k L_{kj}. \tag{1.13}$$

1.2.3 Linear algebraic system

In order to highlight the LAS, it is worth rephrasing Eq. (1.13) into a vector equation from,

$$-\mathbf{L}\mathbf{u}^{\mathbf{T}} = \mathbf{M}\mathbf{f}^{\mathbf{T}}, \tag{1.14}$$

where T denotes the transposed vector. It is clear from Eq. (1.9) and (1.12), that matrix **L** and **M** can be calculated from the base function, while **f** is a known vector obtained from the value of $f(x_k)$. The unknown solution is the vector **u**, which should be determined by the solution of the large-sized LAS in Eq. (1.14).

Finally, the solution of a PDE was reduced to the solution of a LAS. The method is practical (i.e. time- and memory-consuming), when the structure of **L** and **M** are simple. In case of PDEs, these matrices are sparse matrices, that is the most of the elements are zero. It is instructive to calculate the elements of **M** in the given example.

Figure 1.2a reveals that **M** and **L** are zeros, when x_k and x_j are far from each other. More precisely,

$$M_{kj} = L_{kj} = 0 \quad if \quad |k-j| > 1. \tag{1.15}$$

It means that non-zero elements are grouped in the diagonal and next above and below it. In a word, **M** and **L** are tridiagonal matrices,

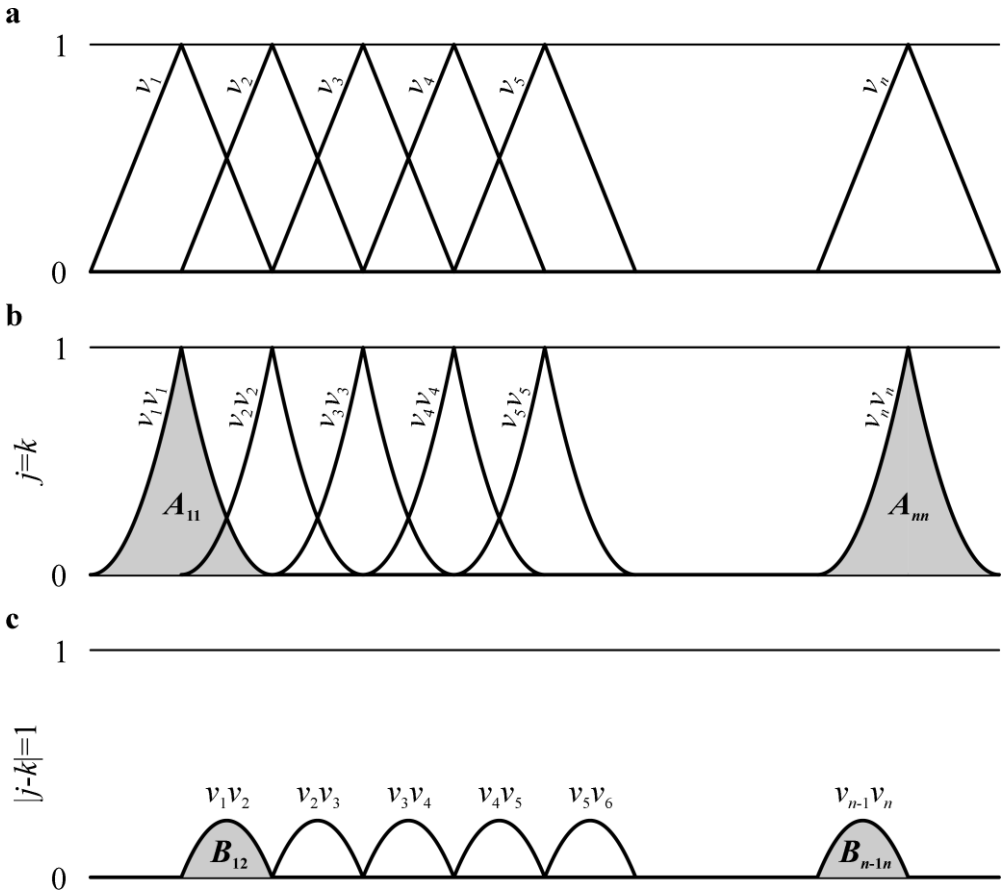

Figure 1.2 Illustration of (a) the base function and the structure of the mass matrix M including (b) the diagonal and (c) the non-diagonal elements.

$$M_{kj} = \begin{pmatrix} A_{11} & B_{12} & 0 & & 0 & 0 \\ B_{21} & A_{22} & B_{23} & & 0 & 0 \\ 0 & B_{32} & A_{33} & & 0 & 0 \\ & & & \ddots & & \\ 0 & 0 & 0 & & A_{n-1,n-1} & B_{n-1,n} \\ 0 & 0 & 0 & & B_{n,n-1} & A_{n,n} \end{pmatrix}, \tag{1.16}$$

where elements A_{kk} and B_{kj} are obtained from the integration of $v_k(x)v_k(x)$ and $v_k(x)v_j(x)$, respectively (*Figure 1.2.b* and *c*).

It is really funny to derive the elements of **M**. Using the definition of the mass matrix from Eq. (1.13),

$$A_{kk} = \int_0^1 v_k(x)v_k(x)dx = \int_{x_{k-1}}^{x_k} \left(\frac{x - x_{k-1}}{x_k - x_{k-1}}\right)^2 dx + \int_{x_k}^{x_{k+1}} \left(\frac{x_{k+1} - x}{x_{k+1} - x_k}\right)^2 dx . \tag{1.17}$$

Let us perform the integration,

$$A_{kk} = \frac{1}{(x_k - x_{k-1})^2}\left[\frac{(x - x_{k-1})^3}{3}\right]_{x_{k-1}}^{x_k} - \frac{1}{(x_{k+1} - x_k)^2}\left[\frac{(x_{k+1} - x)^3}{3}\right]_{x_k}^{x_{k+1}} ! \tag{1.18}$$

After some algebra we get

$$A_{kk} = \frac{(x_k - x_{k-1})^3}{3(x_k - x_{k-1})^2} + \frac{(x_{k+1} - x_k)^3}{3(x_{k+1} - x_k)^2} = \frac{x_{k+1} - x_{k-1}}{3}. \tag{1.19}$$

When the discretization is equidistant, namely x_{k+1}-x_k=Δx is constant, then

$$A_{kk} = \frac{2\Delta x}{3}. \tag{1.20}$$

The B_{kk+1} non-diagonal elements can be expressed from the multiplication of the decreasing part of $v_k(x)$ and the increasing part of $v_{k+1}(x)$,

$$B_{kk+1} = \int_0^1 v_k(x) v_{k+1}(x) dx = \int_{x_k}^{x_{k+1}} \frac{x_{k+1} - x}{x_{k+1} - x_k} \frac{x - x_k}{x_{k+1} - x_k} dx = \frac{1}{(x_{k+1} - x_k)^2} \int_{x_k}^{x_{k+1}} (x_{k+1} - x)(x - x_k) dx . \tag{1.21}$$

After partial integration,

$$\begin{aligned} B_{kk+1} &= \frac{1}{(x_{k+1} - x_k)^2} \left\{ \left[(x_{k+1} - x) \frac{(x - x_k)^2}{2} \right]_{x_k}^{x_{k+1}} + \int_{x_k}^{x_{k+1}} \frac{(x - x_k)^2}{2} dx \right\} = \\ &= \frac{1}{(x_{k+1} - x_k)^2} \left[\frac{(x - x_k)^3}{6} \right]_{x_k}^{x_{k+1}} = \frac{x_{k+1} - x_k}{6} \end{aligned} . \tag{1.22}$$

Using equidistant discretization,

$$B_{kk+1} = \frac{\Delta x}{6}. \tag{1.23}$$

The elements of the stiffness matrix L_{kj} can be calculated in similar way after the derivation of the base function,

$$v_k'(x) := \begin{cases} \dfrac{1}{x_k - x_{k-1}} & \text{if} \quad x \in [x_{k-1}, x_k] \\ \dfrac{-1}{x_{k+1} - x_k} & \text{if} \quad x \in [x_k, x_{k+1}]. \\ 0 & \text{otherwise} \end{cases} \tag{1.24}$$

Hereafter the diagonal and the non-diagonal elements can be derived simply. Since **M** and **L** are tridiagonal matrices, the LAS can be solved effectively by e.g. LU decompositon, conjugate gradient or any specialized method.

1.3 FDM vs FEM

Finite difference method (FDM) is a very popular method to solve differential equation. Owing to the simplicity of its programming, FDM is quite widespread, therefore it is worth making a qualitative comparison between FDM and FEM.

Probably, the most essential distinction between the two methods is that FDM approximates the PDE, while FEM approximates the solution of the PDE (*Table 1.1*). However, mathematically (incl. coding) FDM is much more simple than FEM which demands much deeper knowledge in numerical mathematics and programming. FDM can be effectively applied in regular/simple model geometry (rectangle, circle, block, sphere, cylinder etc.),

while FEM is very useful especially in complex model geometry. In FDM the solution is unknown between the grid points, while in FEM the solution among nodes can approximated by optional base functions. In general, it can be established that the accuracy of FEM solution exceeds the accuracy of FDM.

It is noted that the complexity of the applied base function can be enhanced, however it will increase the number of unknowns (degree of freedom) resulting in computations with longer CPU time, larger memory demand (larger size of **M** and **L**) and sometimes higher uncertainty. Additionally, adaptive mesh is able to estimate the accuracy of the solution through the propagation of error, and if it is necessary, the number of finite elements, the order of base functions can be modified during the solution process. It is called *r adaptivity*, when the mesh moves, which can be very useful e.g. in a fluid flowing in a pipe. It is called *h adaptivity*, when the resolution of FEM mesh is increased or decreased during the solution. Using *p adaptivity*, the order of the base function can be modified. Of course, the combination of the abovementioned adaptivities can be accomplished, e.g. *hp adaptivity*.

FDM	vs	FEM
Approximation of PDE	<	Approximation of the solution of PDE
Mathematically simple	>	Mathematically complex
Applicable in simple geometry	<	Applicable also in complex geometry
Solution is not known between grids	<	Solution among nodes can be approximated by arbitrary base function
Generally less accurate	<	Generally more accurate

Table 1.1 Qualitative comparison between FDM and FEM

2 INTRODUCTION TO COMSOL MULTIPHYSICS

The handbook entitled Introduction to COMSOL Multiphysics recommends several examples which facilitate the users to deepen the knowledge of using the software package. In order to catch the conception of solving multiphysical problems (coupled PDEs), the example busbar (page 54) directs the reader from the model building to the visualization of the numerical solution.

2.1 Physical description of electrical heating

The physical problem is well-known as the electrical heating or Joule heating which is called also the 1st Law of James Prescott (1940). Direct current flowing through a conductor produces heat. As the temperature increases, the resistivity of the conductor enhances, which decreases the current density. *Figure 2.1* illustrates qualitatively how the Laplace's equation describing the electric potential variation is coupled with the heat transport equation through Joule heating. The heat produced by electric current modifies the temperature distribution, which alters the resistivity of the conductor. This clearly affects the potential distribution again.

Before taking up the numerical solution of the example, it is worth considering the physical determination of the given problem. The 2nd Law of James Clerk Maxwell (Faraday's Law) for stationary problem is

$$\mathbf{rot}\,\mathbf{E} = -\frac{\partial \mathbf{B}}{\partial t} = 0\,, \tag{2.1}$$

where **E** and **B** denote the electric field and the magnetic flux density, while *t* is the time. Any non-rotational vector field can be generated as a gradient of a scalar field, that is

$$\mathbf{E} = -\mathbf{grad}V\,, \tag{2.2}$$

V is the electric potential.

Second, the general Ohm's Law serves for the current density **j** that

$$\mathbf{j} = \sigma\mathbf{E}\,, \tag{2.3}$$

if convective current and the Lorentz's motional electromagnetic field can be neglected, and here σ denotes electric conductivity of the medium.

Third, the charge conservation in stationary case results in

$$\mathbf{div}\,\mathbf{j} = 0 \tag{2.4}$$

without electric charge source. Assembling Eqs. (2.2)–(2.4) we get the Laplace's equation for electric potential,

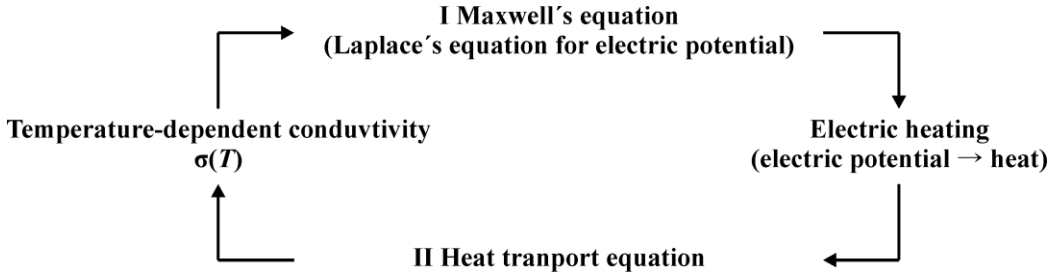

Figure 2.1 Sketch of the coupling of the electrical heating problem.

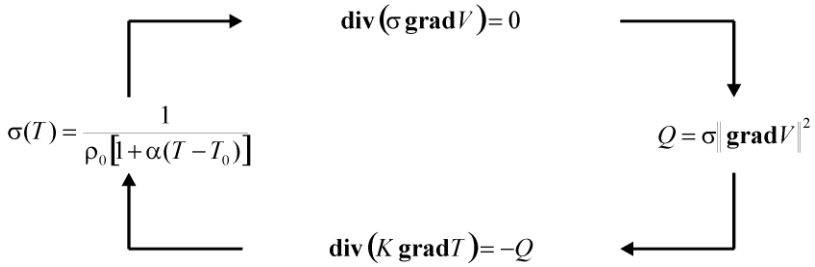

Figure 2.2 Coupling between Laplace's equation and heat transport equation describing the electrical heating problem

$$\mathbf{div}\left(\sigma\,\mathbf{grad}V\right)=0 \tag{2.5}$$

in homogeneous and isotropic medium.

The heat transport equation in stationary problem without advection is

$$\mathbf{div}\left(K\,\mathbf{grad}T\right)=-Q, \tag{2.6}$$

where K and Q are the heat conductivity and the volumetric heat source, while T denotes the unknown temperature. The heat source in the right-hand side of Eq. (2.6) comes from electrical heating. The linearized Ohm's Law says that the voltage is

$$U = R\,I, \tag{2.7}$$

where R and I are the resistance and the current. While the power of the direct current P is

$$P = U\,I = R\,I^2. \tag{2.8}$$

Based on Eq. (2.8) the differential form of the volumetric heat Q obtained from the volumetric electric power is

$$Q=\frac{dP}{dv}=\rho\,\mathbf{j}^2=\frac{1}{\sigma}\left(-\sigma\,\mathbf{grad}V\right)^2=\sigma\left(\mathbf{grad}V\right)^2, \tag{2.9}$$

where ρ and v denote the electric resistivity and the volume as well as Eqs. (2.2) and (2.3) were used in Eq. (2.9). This is the coupling between the Laplace's equation (Eq. (2.5)) and the heat transport equation (Eq. (2.6)).

Finally, we need to know the temperature-dependence of the electrical conductivity of the medium. For metals the conductivity decreases by increasing temperature,

$$\sigma(T)=\frac{1}{\rho_0\left[1+\alpha(T-T_0)\right]}, \tag{2.10}$$

where ρ_0 denotes the resistivity at temperature T_0, while α is an appropriate constant. Eq. (2.10) gives the feedback between the heat transport equation and Laplace's equation. *Figure 2.2* summarizes the quantitative relations of the system characterizing the physical problem of electric heating.

2.2 Example busbar as a multiphysical problem

Example busbar shows over how to compile a practical problem in COMSOL. The base task is the electrical heating in which parameter definition, building up model geometry, prescription of boundary and initial conditions, finite element mesh generation, solving PDE, visualization and interpretation of numerical results are presented. Additionally, the deformation of busbar due to heat expansion is calculated in order the multiphysical ability of the software to be highlighted. Finally, the busbar warmed by Joule's heating is located in a wind channel to ensure the cooling of the tool by air advection. Let us start with the busbar example in the Introduction to COMSOL Multiphysics!

3 ELECTRIC CURRENTS

It will be shown in this chapter that it is really easy and fast to compile a numerical model which functions wrong and serves false results. I will point out the two typical errors in numerical modeling which entail incorrect solution. Then, the vertical electrical sounding (VES) as a fundamental geophysical survey method will be realized in COMSOL both along the horizontal surface and in a cave.

3.1 Electric field of a point source

The very first step of a valid numerical model is the quantitative verification. Usually, it is a quite complex and time-consuming procedure, so here I am going only to flash the fundamentals of a typical testing process. It is clear, that our numerical results should be quantitatively compared with accepted analytical or numerical solutions. In the chapter of electric currents, the electric potential of a point current source in homogeneous and isotropic medium offers itself as a reference point.

The analytical solution of the above-mentioned problem is well-known from the course of Geoelectrical Methods. The potential of a point source in homogeneous and isotropic medium is

$$V(r) = \frac{I\rho}{4\pi}\frac{1}{r}, \tag{3.1}$$

where V is the electric potential at a distance of r from the point source, I and ρ denote the current flowing out from the current source and the resistivity of the medium, respectively (*Figure 3.1*). Let us assume that the current is 1 A and the resistivity is 10 Ωm! In this case the potential at a distance of 1 m is

$$V(r = 1\text{m}) = \frac{1\text{A}\cdot 10\,\Omega\text{m}}{4\pi}\frac{1}{1\text{m}} = 0.795775\ \text{V}. \tag{3.2}$$

Let us build up a model and check the validity of the numerical solution!

To open the software package COMSOL Multiphysics, double-click the icon  . After the program started, select **Model wizard**, then **3D** to use three-dimensional model, open the **AC/DC** module for the given problem, choose **Electric currents (ec)** and press the button **Add**. We do not need any modules to build up a multiphysical problem, thus you can press **Study**. Here, you can choose the type of the study, which is **Stationary** in this case, then press **Done** to get the base desktop.

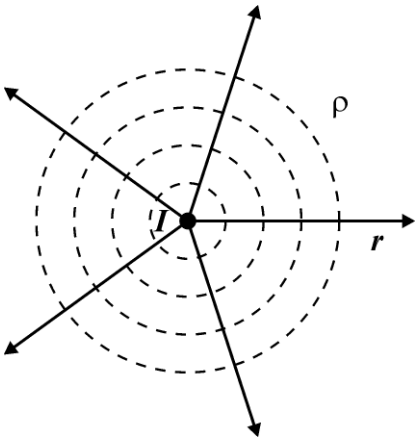

Figure 3.1 Sketch of the electric point source problem. Current is represented by radial solid lines. Dashed lines denote the concentric equipotential surfaces.

First, the simple model geometry must be created. Press the right click on **Geometry 1** (**Geometry 1_R**) in the Model Builder and choose **Sphere** to get the homogeneous and isotropic model domain. The radius of the sphere is **100 m**, which seems quite large to the effect of boundaries be negligible. In order to position the point source, right-click **Geometry 1_R**>**More Primitives**>**Point**. The coordinate of (0,0,0) is appropriate for the problem having spherical symmetry, so you can press **Build All Objects** in the Settings window to finalize the model geometry. If you would like also the interior of the solid domain, you can choose **Wireframe Rendering** in Graphics window (*Figure 3.2*).

You can check the applied equation to be solved by selecting the module **Electric currents** and opening **Equation** in Settings window. The equation of the stationary charge conservation with the source term (Eq. (2.4)), the reduced Ohm's Law (Eq. (2.3)) and the definition of electric potential (Eq. (2.2) appear. To fill up the domain with 'material', click **Current conservation 1**, switch the **Electrical conductivity** in Settings to **User defined**, and type **1/10** S/m to get the resistivity of 10 Ωm as in the analytical example (Eq. (3.2)). Since the boundary of the models are far (r=100 m) from the point where the electric potential will be checked (r=1 m), therefore the outer boundary of the sphere can be considered grounded. To set up the boundary conditions **Electric currents_R**>**Ground** and select **All boundaries** in Boundary Selection. All the 8 spherical surface segments will be marked. If you open the menu **Equation**, you can see the quantitative boundary of V=0. Last, we need to assign the point source, **Electric currents_R**>**Points**>**Point current source**, then you should select the central point (**#4**) in Graphics window, and write Qj,p=**1** A.

The most simple finite element mesh generation is if you right-click the **Mesh**, and select **Build All**. Messages below graphics window says, that the 'complete mesh consists of 8477 domain elements…'. To calculate the solution click simply **Sudy 1** and **Compute**.

Electric potential in **Results** shows the calculated 3D potential field using a Multislice visualization method. In order to represent the current lines **Results**>**Electric potential_R**>**Streamline**. Select streamline **Positioning**>**Start point controlled**>**Points: 100**, then press **Plot**. You can see that the current lines do not seem perfectly radial — especially in the surroundings of the point source —, as it would be required in homogeneous, isotropic medium (*Figure 3.3*).

As a next step, we will see the radial potential distribution near the point source. Click **Results**>**Data sets_R**>**Cut Line 3D**, then define the linear section by the two end points,

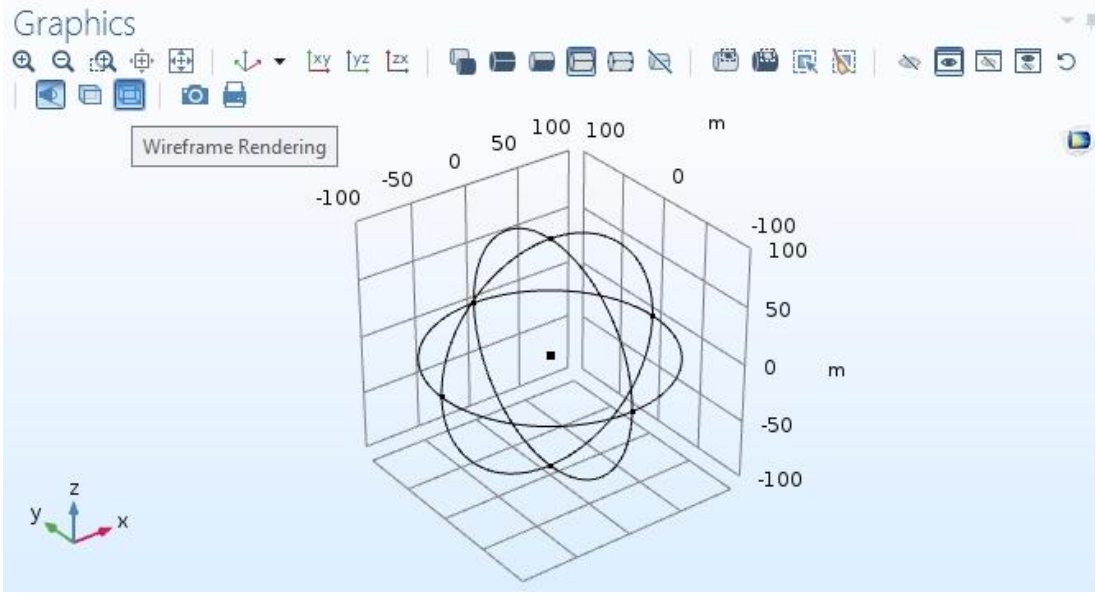

Figure 3.2 Geometry of the electric point source model

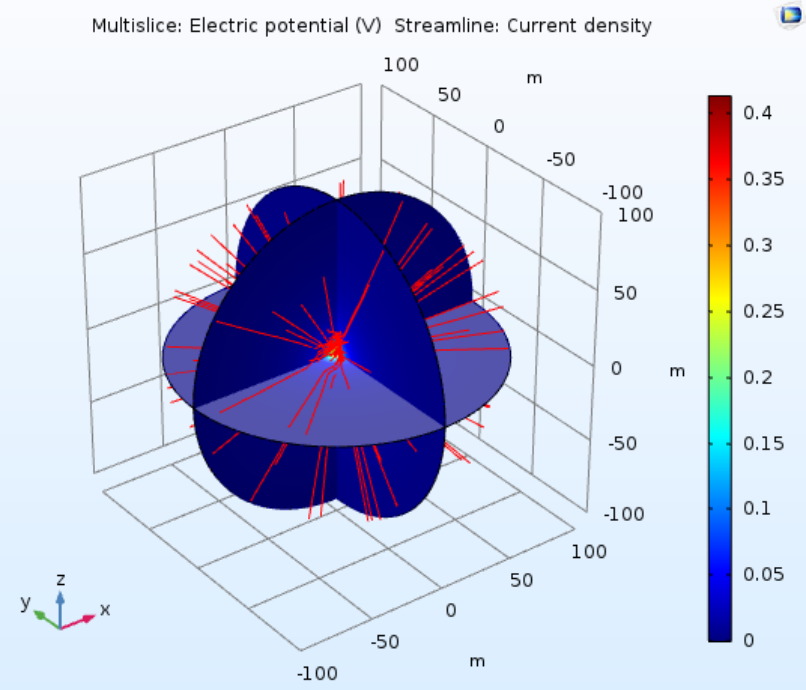

Figure 3.3 Inaccurate numerical solution of the electric potential and the current lines for the point source problem.

Point 1: 0.1, 0, 0 and **Point 2: 3, 0, 0**. It is suggested starting the section not from (0, 0, 0), where the potential tends to infinity. In addition, we need to insert a point, where the value of potential will be compared to the analytical solution, **Results**>**Data sets_R**>**Cut Point 3D: (1, 0, 0)**.

Now, we should visualize the potential along the above-defined section, **Results_R**>**1D Plot Group**, and then **1D Plot Group_R**>**Line Graph**. To select the defined line section, **Line Graph**>**Data set: Cut Line 3D**, and to select the defined point, **1D Plot Group_R**>**Point Graph**>**Data set: Cut Point 3D**, then press **Plot**. You can see that the potential decreases approx. linearly from the point source, although it should follow the ratio $1/r$ in Eq. (3.1). Let us check the quantitative values of the potential! **Results**>**Derived values_R**>**Point evaluation**>**Data set: Cut Point 3D**. Fill in the table, **Expression: V**, then press TAB to see the unit (V) and the description (Electric potential). Press the button **Evaluate**! In the Table 1 window (below the Graphics), the potential in the cut point appears: 0.349935 V. This numerical solution really differs from the analytical solution (Eq. (3.2)). What is the problem with our numerical solution?

One typical problem is the mesh with low resolution. To handle this trouble, we should go back to **Mesh** and select **Element size: Fine** instead of Normal, then press **Build All**. You get 17211 finite elements discretizing the model (see Messages). Now, you can solve the problem, **Study 1_R**>**Compute** and go to **Results**>**1D Plot Group** to check the potential variation. The solution is rather linear again than $1/r$ ☹ To check the potential value 1 m far from the point source, **Results**>**Derived Values**>**Point Evaluation** press **Evaluate**, the solution with finer mesh gives 0.456742 V, which is a bit better, but the deviation from the analytical value is really large. How can we increase the accuracy of the numerical solution?

It is a useful realization that mesh refinements should be done in the surroundings the point source, where the potential variation is high. In order to interfere with the mesh generation click **Mesh_R**>**Size**, then **Size 1**>**Geometric Entity Level**>**Point** and select the point number **4**, as the point source. If you cannot see the inner point, you can deselect **Mesh Rendering** and select **Wireframe Rendering**. Click the **Custom**, and set the **Maximum**

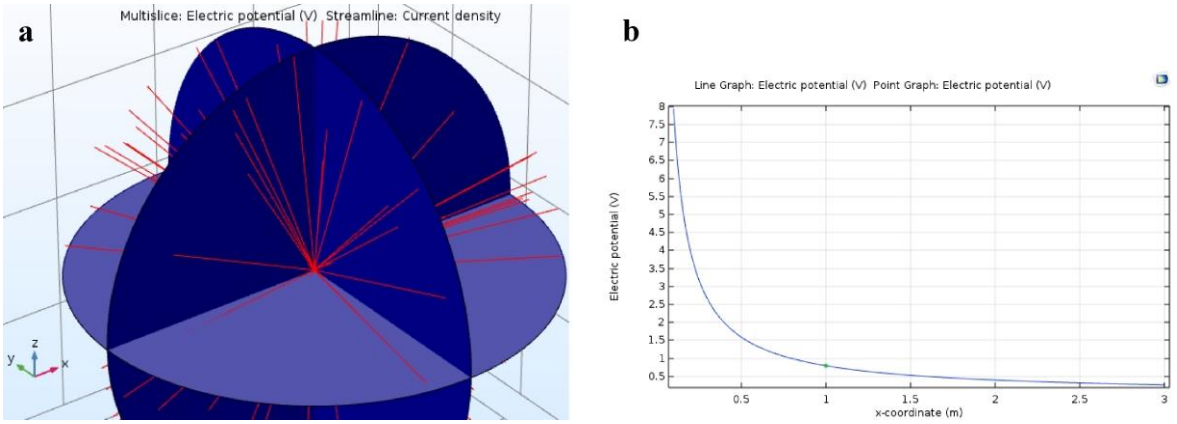

Figure 3.4 Verified numerical solution of the electric point source problem in homogeneous and isotropic medium. (a) Electric potential field and current lines, (b) Radial electric potential profile.

Element Size to **0.02** m. Now, you need to define the discretization method, **Mesh_R>Free Tetrahedral**. Press **Build All**, and you will see that 26396 finite elements were used for the new discretization, **Study>Compute**. Streamlines are much more linear in Graphics window, and the potential variation decreases following the ratio 1/*r* from the point source (**Results>1D Plot Group**). The evaluated electric potential 1 m far from the point source is 0.787384 V (**Results>Derived Values>Point Evaluation>Evaluate**). The numerical solution agrees quite well with the analytical one, but COMSOL Multiphysics should yield much more accurate solution.

It is worth refining the meshing also in the neighborhood of the point, where we look for the potential value. To do this, we need to go back to **Geometry_R>More Primitives>Point** with a coordinate **1, 0, 0** and **Build All Objects**. To actualize the mesh near the new point, **Mesh>Size 1** and select the point **#7** from the Graphics window. Set the **Size>Finer** instead of Fine, and select **Custom>Maximum element growth rate: 1.3**. So, you control that the size of the neighboring elements can increase less than 30% in the whole domain. Press **Buid All** to get 91916 elements in discretization. Then **Study>Compute**. You can see that the streamlines are radial, and the potential decreases following the analytical solution. The numerical solution 1 m far from the point source is 0.787723 V, which is only a bit better than the former solution. It seems that refining the mesh does not reduce the deviation between the numerical and the analytical solution. How can we lessen the difference?

Another typical problem, which appears in the verification process, is the inappropriate boundary condition. In the analytical solution the ‘outer boundary’ is in the infinity, where the potential is zero. Although the numerical model is quite large-sized (outer boundaries are farther from the point source by 2 orders of magnitude than the evaluated point), but the boundaries are not in the infinity which might result in approx. 1% deviation in the numerical solution. We can check the effect of the boundary conditions, if we change them. Fortunately, the analytical solution is known, and the equipotential surfaces are spherical. Thus, the exact boundary condition can be described along the outer boundaries, **Electric currents_R>Electric potential**, select **All boundaries** from **Selection** box (**#1–8**), and define the **Electric potential: 10/(4*pi*100)** as it is prescribed in the example. **Study>Compute**. *Figure 3.4a* illustrate the numerical solution of the 3D potential field with radial streamlines, and *Figure 3.4b* shows the potential variation between x=0.1–3 m. It is suggested graphing the potential as a function of x, **Results>Electric Potential>Line Graph>Parameter>Expression: x**, instead of Arc Length. The evaluated electric potential in the observed point is 0.795680 V, which is acceptable in this simple numerical verification

process. We should not forget saving the model, e.g. **Save>Point source**. In summary, we can conclude that it is very simple to build up a numerical model serving solution, but the validation of the model and the verification of the numerical solution are much more difficult and time-consuming task.

3.2 Point source in heterogeneous medium

In order to accentuate the advantage of the finite element numerical method, we present a model of which does not have analytical solution. Continuing the former model, an ellipsoid will be inserted into the homogeneous medium. To modify the geometry, **Geometry_R>More Primitives>Ellipsoid>Semiaxis: 3, 1, 1** and **Position: 5, 0, 0**, then **Build All Objects**. Since this object has different domain parameter, we need insert a new Electric currents sub-module from the first track of **Electric currents_R>Current Conservation**. Click the ellipsoid in Graphics window by scrolling the mouse, and **#2** will appear in the Selection box. This object will be a bad electric conductor, so **Electric conductivity>User defined: 1/1000** S/m. Because we do not already need the Ground boundary condition, we should delete it. From this moment all of boundary condition (#1–16) are reset to Electric potential defined above. Of course, the electric potential must be prescribed only on the outer boundary conditions (#1–8), thus surfaces of **#9–16** need to be **remove**d (- sign) from the Selection box.

After modifying the geometry, the mesh must be adjusted as well, **Mesh_R>Size**, then **Size 2>Geometric entity level (GEL)>Domain**, and select ellipsoid (**#2**), **Custom>Maximum element size (MES): 0.5** m, to maximize the size of the finite elements as 0.5 m. Buttons of Wireframe Rendering, Transparency, Zoom In/Out/Box, Zoom Extents and Go to Default View in Graphics window facilitate the navigation in a complex geometry. We need to move the **Size 2** menu above **Free Tetrahedral** to specialize the discretization method, and **Build All**. The mesh consists of 102,493 finite elements, **Study>Compute**.

After solving the problem, the selection of the appropriate visualization method is very important. To display the electric potential on the surface of the ellipsoid, we need to define the surface first, **Results>Data Sets_R>Surface: #9–16** in the Selection box. You can rotate the model in Graphics window, when you are moving the mouse while the left button is being pressed. You can move the model in Graphics window with the right button. To go back to

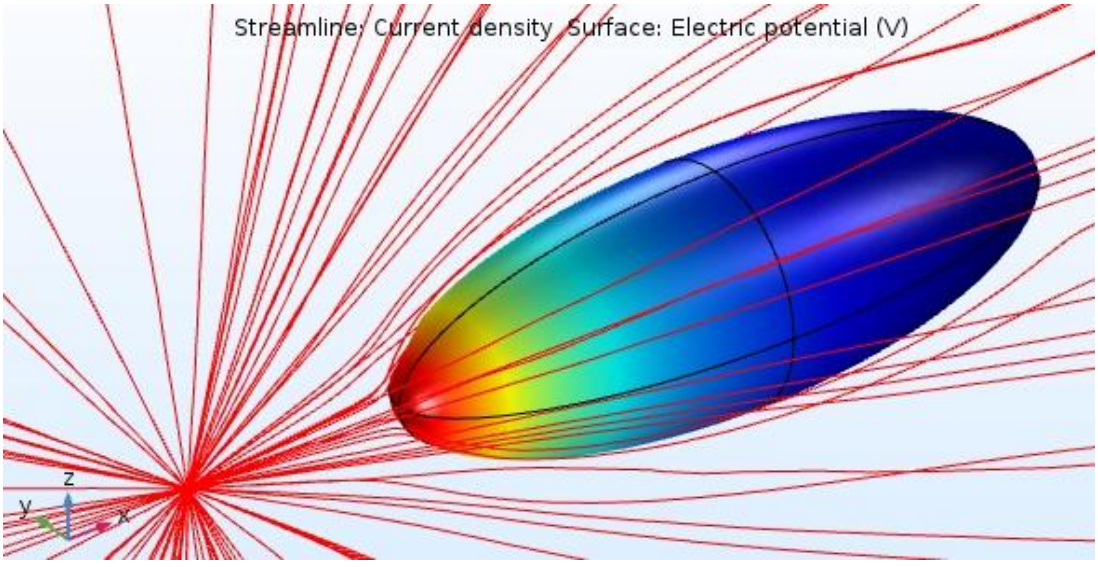

Figure 3.5 Electric potential on the surface of the high-resistivity ellipsoid, and current lines (red).

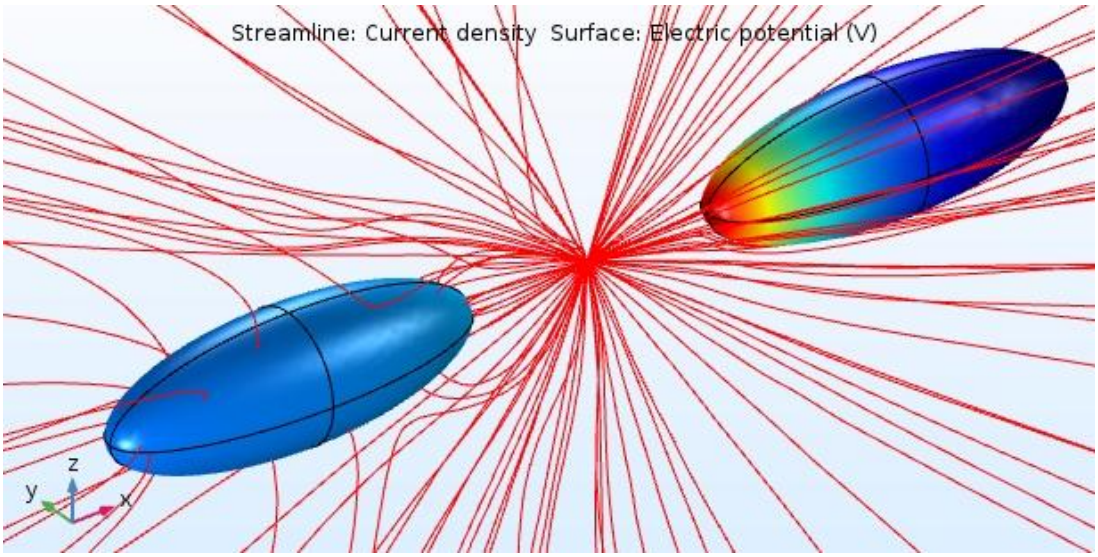

Figure 3.6. Electric potential on the surface of the low-resistivity (left) and the high-resistivity (right) ellipsoid, and current lines (red).

the normal view, just press Go to Default View. The electric potential on the surface of the ellipsoid can be visualized, **Results>Electric Potential_R>Surface>Data Set: Surface 1**, it is useful to remove the potential slices, **Results>Electric potential>Multisclice_R>Disable**. Zooming in the solution, the quasi-radial current lines try to avoid the high-resistivity ellipsoid (*Figure 3.5*). It is clear that the potential on the ellipsoid surface is higher near the point source.

As a check test, a low-resistivity object can be positioned in the model in symmetric manner. Turning back to the **Geometry_R>More Primitives>Ellipsoid>Semiaxis: 3, 1, 1** and **Position: -5, 0, 0**, then **Build All Objects**. To fill up the new domain, **Electric currents_R>Current Conservation**. Select the left ellipsoid in **Current Conservation 3**. Take care of that the numbering of the domains has already changed due the modification in the geometry! Click the new/left ellipsoid (**#2**) to appear in the Selection box, and specialize its conductivity, **Electric conductivity>User defined: 1/0.1** S/m, to get an object with low resistivity of 0.1 Ωm. Then select **#2** in **Mesh>Size 2** and **Build All** the mesh (#113,062), **Study>Compute**.

If you want to visualize the potential of both ellipsoid surfaces, you need to modify **Results>Data Sets>Surface 1** including **#5–12** and **#17–24**. Now you can see the numerical solution of the inhomogeneous problem, as the current lines are attracted by the low-resistivity ellipsoid (*Figure 3.6*). It seems that there is no relevant potential difference within this object.

Finally, we can quantify the solution along a section through these objects. Let us modify the former cut line, **Results>Cut Line 3D** from **(1,0,0)** to **(9,0,0)**, and create a new one, **Results>Data Sets>Cut Line 3D 1_R>Duplicate**, then define **Results>Data Sets>Cut Line 3D 2** from **(-9,0,0)** to **(1,0,0)**. If you press the button **Plot**, you can see the Cut Line 3D 1 to intersect the low-resistivity ellipsoid. You can duplicate the graph by **Results>1D Plot Group>Line Graph 1_R>Duplicate**, and switching in **Line Graph 2>Data set** to **Cut Line 3D 2**. Line graph illustrates the nonsymmetrical potential distribution around the point source in non-homogeneous medium. Do not forget to save the model as **Save as>Point source in heterogeneous medium**.

3.3 Vertical electrical sounding

In this chapter a simple numerical model of the vertical electrical sounding (VES) will be built up, which is one of the most popular geophysical survey method and it is used to reveal the resistivity distribution of the subsurface. **Model Wizard>3D>AC/DC>Electric Currents>Add**, then **Sudy>Stationary>Done**.

The subsurface is represented by a block, **Geometry_R>Block** with a **Width: 1000** m, **Depth: 1000** m and **Height: 500** m using a **Base position** of **(-500,-500,-500)** m. The four pointwise electrodes are positioned on the surface, **Geometry_R>More Primitives>Point** with a position of **(-4,0,0)** m, and **Geometry_R>More Primitives>Point** with a position of **(-1,0,0)** m. The VES arrangement is symmetrical, so you can duplicate them, select **Point 1** and **2_R>Duplicate** to **(1,0,0)** m and **(4,0,0)** m and **Build All Objects**. The four current and potential electrodes are aligned on the surface.

As a second step, we need to define the properties of the medium including the boundary conditions. Our model includes only one domain, **Electric currents>Current Conservation 1>Electrical conductivity>User defined: 1/10** S/m having a resistivity of 10 Ωm. Let us give the boundary conditions, the side walls and the bottom of the model are far from the current sources, **Electric currents_R>Ground>Selection: All boundaries** without the surface of **#4**, which is considered as an insulating boundary due to the high resistivity of the air. When the surface #4 is removed from the Selection box in Ground, you can see its appearance in the Selection box of Electric insulation, which is the default boundary condition in this module. All of other boundaries are overridden by Ground boundary condition. Current electrode A will be the left point, **Electric currents_R>Points>Point Current Source**, after selection the left pointwise electrode (**#5**), you need to define the P**oint current source>$Q_{j,p}$: 0.1** A. To set the current electrode B, **Point Current Source 1_R>Duplicate**, then remove **#5** from the Selection box of **Point Current Source 2** and insert the right electrode, **#8**. Do not forget modifying the Point current source of the return electrode to **$Q_{j,p}$:-0.1** A.

Finite element mesh needs to ensure better refinement near the point electrodes, **Mesh_R>Size**, then **Size>Custom>MEGR: 1.3** to decrease the variability of the element size in the whole domain. **Size 1>GEL>Point: #5–8** (electrodes), **Custom>MES: 0.2** m. We have to select the discretization method, **Mesh_R>Free Tetrahedral** and **Build All** resulting in 29656 finite elements, **Study>Compute**.

Multislices do not show any variation in electric potential, since it is zero in the mid-plane between A and B, and it tends to infinity crossing the pointwise current electrodes. Therefore, it is worth modifying the position of the planes, **Results>Electric Potential>Multislice>Multiplane Data>X-planes>Entry method>Coordinates: -100 100** m, while in **Y**- and **X-planes>Planes: 0**. It is instructive to display the current lines, **Results>Electric Potential_R>Streamline**, which shows the streamlines of the current density vector in Expression box: ec.Jx, ec.Jy and ec.Jz, where ec refers to the name of the module: Electric currents. Select **Streamline Positioning>Magnitude controlled** to the streamline be denser, where the current density is higher. *Figure 3.7* illustrate the current lines between the current electrodes, and the two vertical planes display the potential distribution on the side of electrode A (positive) and return electrode B (negative).

A possible verification method is, when the apparent resistivity computed from the electrode potential gives back the resistivity of 10 Ωm defined earlier. **Results>Derived Values_R>Point Evaluation**, select the inner electrodes (**#6** and **7**) as potential electrodes M and N, **Expression: V** and **Evaluate**. Table 1 serves the two potential values on electrode M and N, V_M=0.0212180 V and V_N=-0.212183 V, the symmetry is not perfect owing to the non-

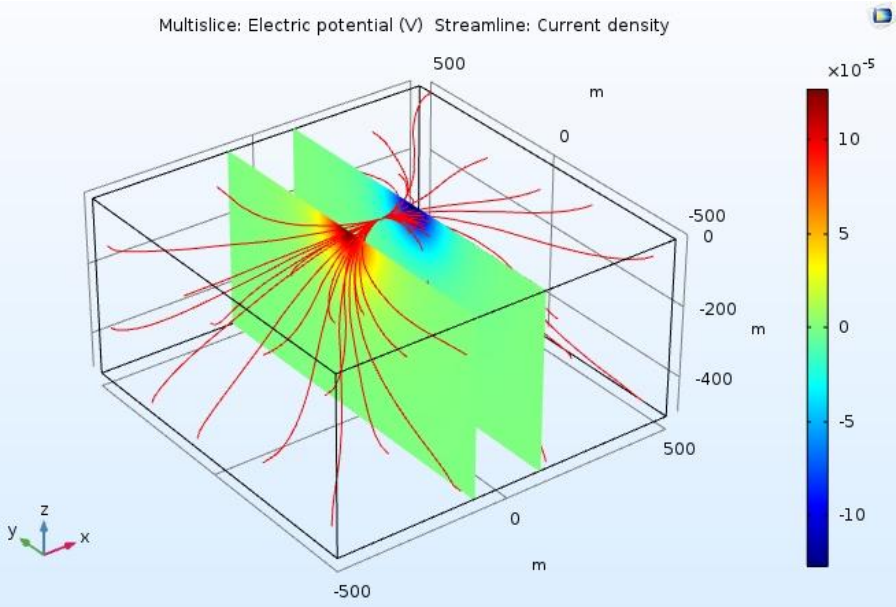

Figure 3.7 Numerical solution of the electric potential on two vertical slices and the current lines (red) in a given VES arrangement.

exact numerical solution. Based on the knowledge in the course of Geoelectrical Methods, the apparent resistivity ρ_a can be calculated,

$$\rho_a = K\frac{\Delta V}{I} = \frac{2\pi}{\frac{1}{r_{AM}} - \frac{1}{r_{AN}} - \frac{1}{r_{BM}} + \frac{1}{r_{BN}}}\frac{V_M - V_N}{I}, \tag{3.3}$$

where K, ΔV and I are the geometrical coefficient of the electrode arrangement, the potential difference between the potential electrodes and the current flowing out of the current electrode A, respectively, while r_{XY} denotes the distance between electrode X and Y. Using the symmetry of the arrangement, that is $r_{AM}=r_{BN}$ and $r_{AN}=r_{BM}$,

$$\rho_a = \frac{\pi}{\frac{1}{r_{AM}} - \frac{1}{r_{AN}}}\frac{V_M - V_N}{I}. \tag{3.4}$$

Substituting the computed and defined values,

$$\rho_a = \frac{\pi}{\frac{1}{3\,\mathrm{m}} - \frac{1}{5\,\mathrm{m}}}\frac{0.0212180\,\mathrm{V} + 0.0212183\,\mathrm{V}}{0.1\,\mathrm{A}} = 9.999\,\Omega\mathrm{m}, \tag{3.5}$$

which shows a quite good agreement with the given resistivity value of 10 Ωm. It is unfortunate, that there is no chance to get such an accurate result in the field.

There might be a second test, if we study, how varies the calculated apparent resistivity above the homogenous subsurface depending on the current electrode distance, r_{AB}. First, let us move the current electrode from the central point, **Geometry>Point 1>x: -16** m, and **Geometry>Point 4>x: 16** m, **Build All Objects**. Regenerate the mesh for the new geometry, **Mesh_R>Build All** resulting in 53529 elements, **Study>Compute**.

We can repeat the above calculation, **Results>Derived Values>Point Evaluation>Evaluate**, the electric potential on the potential electrodes is V_M=0.00124867 V and V_N=-0.00124773 V. It gives for the apparent resistivity,

$$\rho_a = \frac{\pi}{\frac{1}{r_{AM}} - \frac{1}{r_{AN}}} \frac{V_M - V_N}{I} = \frac{\pi}{\frac{1}{15\,\mathrm{m}} - \frac{1}{17\,\mathrm{m}}} \frac{0.00124867\,\mathrm{V} + 0.00124773\,\mathrm{V}}{0.1\,\mathrm{A}} = 9.999\,\Omega\mathrm{m}\,. \quad (3.6)$$

Accordingly, increasing the current electrode distance r_{AB}, that is the penetration depth of the VES arrangement does not modify the value of apparent resistivity above homogeneous subsurface. **Save** the COMSOL model as **VES in homogeneous medium**.

How does the implication of a deep, high-resistivity layer influence the apparent resistivity? We create the shallow layer, **Geometry_R>Block** with a **Width: 1000** m, **Depth: 1000** m and **Height: 10** m using a **Base position** of **(-500,-500,-10)** m and **Build All**. Let the resistivity of the lower layer be 100 Ωm, **Electric Currents>Current conservation 1_R>Duplicate**, **Electric Currents>Current conservation 2**, remove the upper layer (**#2**), and modify **Electrical conductivity>User defined: 1/100** S/m. **Mesh_R>Build All** results in 112,971 finite elements, **Study>Compute**.

We expect that the apparent resistivity obtained from electrode potentials gives a value between the resistivity of the upper (10 Ωm) and the lower (100 Ωm) layer. **Results>Derived Values>Point Evaluation>Evaluate**, V_M=0.00186768 V and V_N=-0.00186785 V. Thus the 'measured' apparent resistivity,

$$\rho_a = \frac{\pi}{\frac{1}{r_{AM}} - \frac{1}{r_{AN}}} \frac{V_M - V_N}{I} = \frac{\pi}{\frac{1}{15\,\mathrm{m}} - \frac{1}{17\,\mathrm{m}}} \frac{0.00186768\,\mathrm{V} + 0.00186785\,\mathrm{V}}{0.1\,\mathrm{A}} = 14.9627\,\Omega\mathrm{m}\,, \quad (3.7)$$

which serves an intermediate value.

Finally, we show, how the current density varies in the mid-plane, **Results>Electric potential>Multislice>Multiplane Data>X-plane>Coordinates: 0** m, as well as **Expression>Replace Expression>Component 1>Electric Currents>Currents and charge>Current density norm (ec.normJ)** in unit A/m^2 and **Plot**. If you change the streamline method, **Results>Electric Potential>Streamline>Streamline Positioning>Start point controlled>Number of points>Points: 100**, and refine the streamlines **Quality>Resolution>Finer**, you will realize the enhanced current density in the upper, low-resistivity layer after zooming in the model (*Figure 3.8*). **Save>VES in heterogeneous medium**.

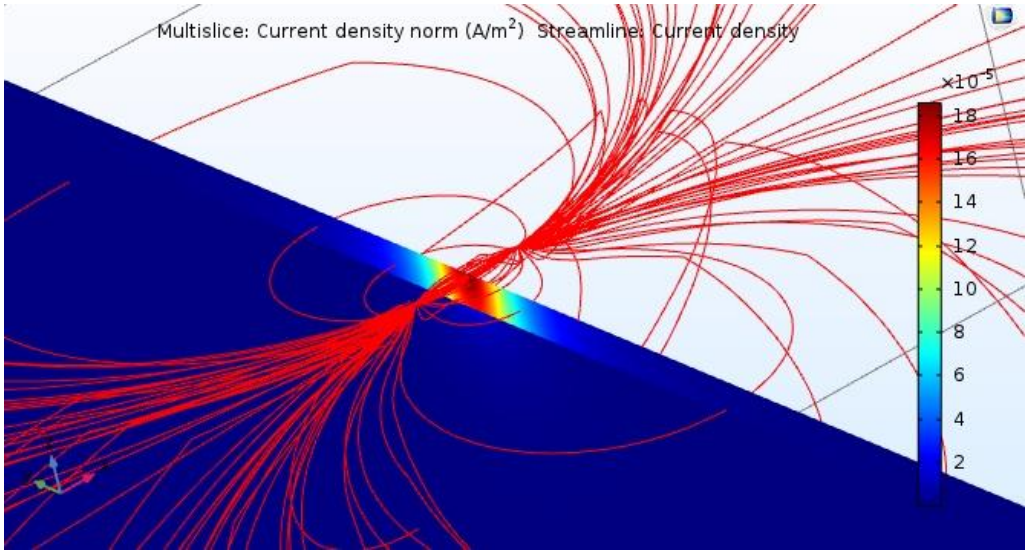

Figure 3.8 Normal (horizontal) current density distribution in the midplane and the current lines (red) in the two-layer VES model.

3.4 VES in a cave

In this last part, I would like to draw attention to the importance of the geometry of the medium. VES model is valid only for measuring above horizontally layered homogeneous and isotropic medium by point-wise electrodes, although filed-site circumstances are never in perfect accordance with the theoretical models. Nevertheless, the analytical solutions have to be re-interpreted in several geological situations, e.g. in case of VES measurements completed in cave.

Model Wizard>3D>AC/DC>Electric Currents>Add, then **Study>Stationary> Done**. VES measurement is accomplished in a cave bored in granite formation, so the rock and the cave are represented by a cylinder, **Geometry_R>Cylinder** with a **Radius: 200** m and **Height: 1000** m positioned at **x=-500** m and **y=z=0**. The axis of the cylinder should be parallel to *x*, **Axis>Axis type: x-axis**. To create the cave, **Geometry>Cylinder 1_R> Duplicate** and modify the **Cylinder 2>Radius: 3** m, **Build All Objects**. We need to crop the cave from the rock, **Geometry_R>Booleans and Partitions>Difference**, click the formation (**cyl1**) to add to **Objects to add** box, then click the cave (**cyl2**) to add to **Objects to subtract** box, and press **Build All Objects**. If you press the button **Go to YZ View**, you can see through the model along the cave. Let us locate the electrodes on the side walls of the cave, **Geometry_R>More Primitives>Point** at **x=-1** m, **y=-3** m and **z=0**. Duplicate the first electrode, **Geomtery_R>Point 1** to **Point 2>x=-0.5** m. Then **Duplicate Point 2** to **Point 3>x=0.5** m, and **duplicate Point 3** to **Point 4>x=1** m. **Build All Objects**, **Go to Default View** and press **Wireframe Rendering** to see into the model geometry.

Set the resistivity of the homogeneous rock of 1000 Ωm, **Electric Currents>Current Conservation 1>Electrical conductivity>User defined: 1/1000** Ωm. The boundary of the rock and the cave is electrically insulated as the default boundary condition, but other boundary should be grounded, **Electric Currents>Ground** adding the outer boundaries of **#1, 2, 3, 6, 9, 10** to Selection box. Now, we need to define the current flowing out of electrodes, **Electric Currents_R>Points>Point Current Source**, then click the left electrode to be A (**#9**), and set **$Q_{j,p}$: 0.1** A. To set also the return electrode B, **Electric Currents>Point Current Source 1_R>Duplicate**, and remove #9 from Selection box and add the right electrode (**#12**) in **Point Current Source 2**, then type the **Point current source> $Q_{j,p}$: -0.1** A.

We need to refine the mesh near the electrodes, **Mesh_R>Size**, decrease the element growth, **Size>Custom>MEGR: 1.3**, and **Size 1>GEL>Point: #9–12**, and set **Custom>MES: 0.1** m. For discretization we can use **Mesh_R>Free Tetrahedral** and **Build All**, which generates 48475 finite elements. If you would like to check the refined meshing in the surroundings of the electrodes, press the button **Click and Hide** in Graphics window, select the outer cylinder surface and use **Zoom Box**. Solve the problem by **Study>Compute**.

In order to visualize the current density in the mid-plane, **Results>Electric Potential>Multislice>Multiplane Data>X-planes>Coordinates: 0** m, and **Number of planes: 0** in **Y-** and **Z-planes**. You should select **Expression>Replace Expression>Component 1>Electric currents>Currents and charge>Current density norm (ec.normJ)**. Let us display the current lines, **Results>Electric Potential_R>Streamline>Streamline Positioning>Start point controlled>Points: 50**, and press the button **Plot**. If you zoom in the electrodes, you can see the higher current density behind the wall of the cave, as a half-space model (*Figure 3.9*).

To calculate the apparent resistivity, we can repeat the method presented in part 3.3, **Results>Derived Values_R>Point Evaluation**, add electrodes M and N (inner electrodes) to the Selection box by clicking **#10, 11**, then **Expression: V** and **Evaluate**. The potential on potential electrodes is V_M=19.9421 V and V_N=-19.9304 V, which gives the value of

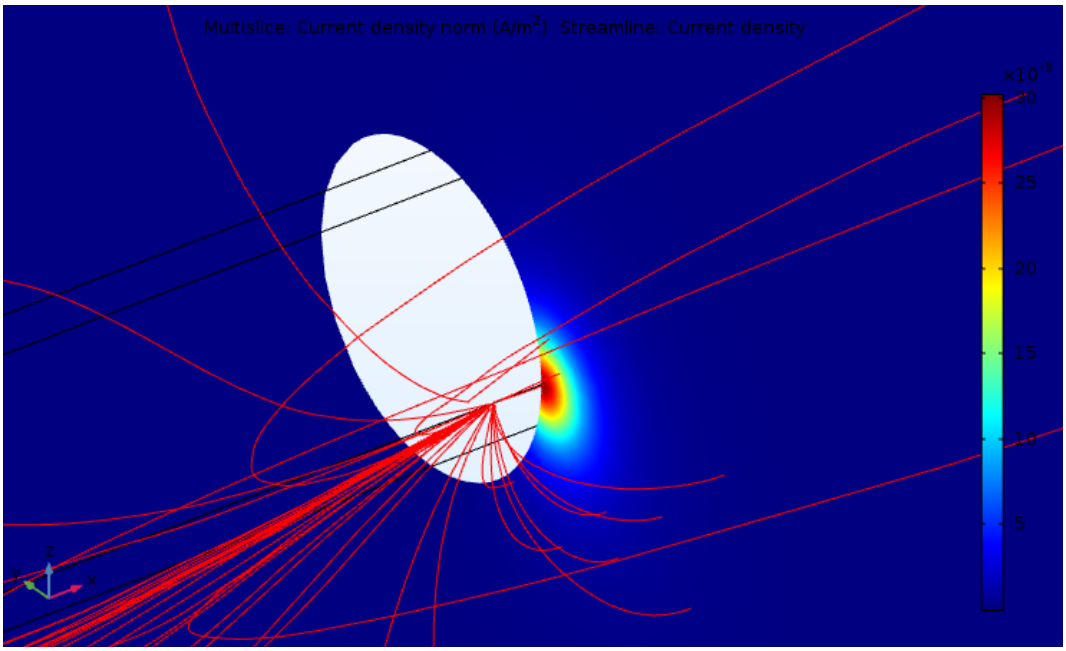

Figure 3.9 Current density field in the midplane of near current electrodes (r_{AB}=2 m). Current lines are denoted by red lines.

$$\rho_a = \frac{\pi}{\frac{1}{r_{AM}} - \frac{1}{r_{AN}}} \frac{V_M - V_N}{I} = \frac{\pi}{\frac{1}{0.5\,\mathrm{m}} - \frac{1}{1.5\,\mathrm{m}}} \frac{19.9421\,\mathrm{V} + 19.9304\,\mathrm{V}}{0.1\,\mathrm{A}} = 939.47\,\Omega\mathrm{m} \qquad (3.8)$$

for the apparent resistivity. It seems too low relative to the rock resistivity of 1000 Ωm defined earlier.

Increasing the current electrode distance r_{AB}, i.e. deepening the penetration of VES, we can investigate the variation of the apparent resistivity. Let us move A and B farther from the central point, **Geometry>Point 1>x: -30** m and **Geometry>Point 4>x: 30** m, **Build All Objects**. Regenerating the mesh, **Mesh>Build All** results in 83388 elements, then **Solve>Compute**.

Results>Electric Potential shows that current is able to encompass the cave (*Figure 3.10*). We can compute the apparent resistivity again, **Results>Derived Values>Point Evaluation>Evaluate**. The potential electrodes give V_M=0.00904019 V and V_N=--0.00917432 V, thus the apparent resistivity is

$$\rho_a = \frac{\pi}{\frac{1}{r_{AM}} - \frac{1}{r_{AN}}} \frac{V_M - V_N}{I} = \frac{\pi}{\frac{1}{29.5\,\mathrm{m}} - \frac{1}{30.5\,\mathrm{m}}} \frac{0.00904019\,\mathrm{V} + 0.00917432\,\mathrm{V}}{0.1\,\mathrm{A}} = 514.86\,\Omega\mathrm{m} \qquad (3.9)$$

For the first though, it is surprising, since the granite formation is homogeneous. However, if we remember the VES model, we can realize that it has already not been valid for this case, because the surface is not horizontal. To conclude, as the distance r_{AB} increases, the penetration deepens and the applied half-space model becomes rather a complete space model. It is reflected in the solution of the apparent resistivity, $\rho_a \approx 1000$ Ωm for near current

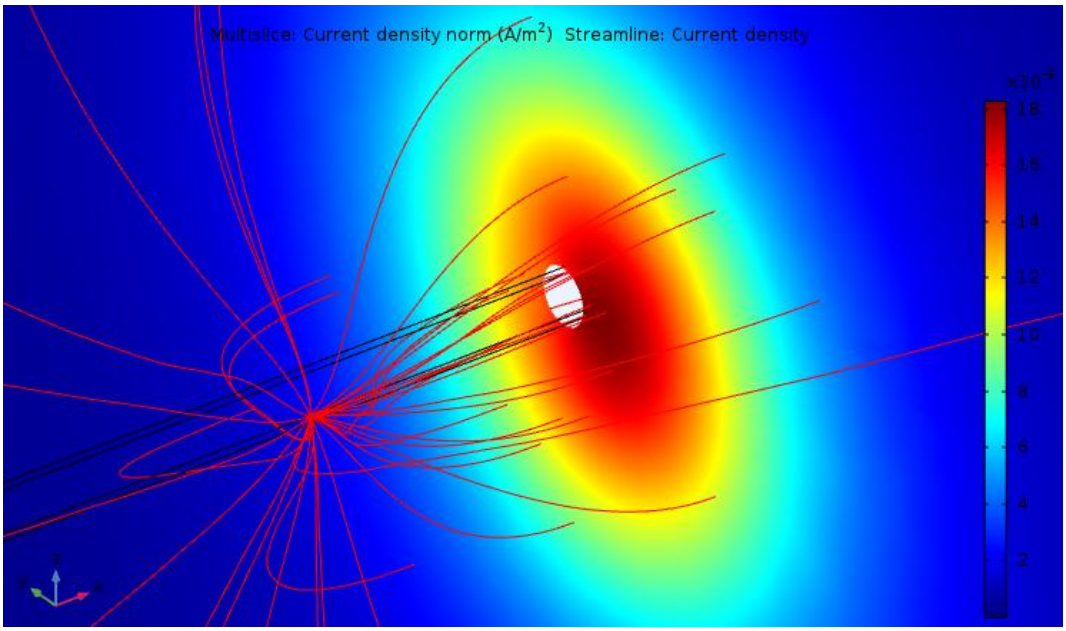

Figure 3.10 Current density field in the midplane of far current electrodes (r_{AB}=60 m). Current lines are denoted by red lines.

electrodes decreases continuously to $\rho_a \approx 500\ \Omega$m for far current electrodes. It could be corrected by a gradually increasing geometry coefficient from

$$K = \frac{\pi}{\frac{1}{r_{AM}} - \frac{1}{r_{AN}}} \quad \text{to} \quad K = \frac{2\pi}{\frac{1}{r_{AM}} - \frac{1}{r_{AN}}}, \tag{3.10}$$

however the rate of the growth is not trivial. One solution might be the numerical modeling to determine the correct growth rate. Please, don not forget saving the model, **Save>VES in cave**.

4 MAGNETIC FIELD

In this chapter, we shall compile a simple numerical model which reflects the stationary magnetic dipole field of the Earth using an axial and central elementary magnetic dipole approximation. Second, a typical magnetic field survey will be presented above buried iron objects, then, such a model will be built up, which is not a typical geophysical task.

4.1 Magnetic dipole field of the Earth

Model Wizard>3D>AC/DC>Magnetic Fields>Add, then press **Study>Stationary> Done** to start the necessary module. It is useful to learn how parameters can be defined in a COMSOL model. **Global Definitions>Parameters**, and no we need to fill in the table as in *Table 4.1*. The third column is filled up automatically in the software.

Name	Expression	Value	Description
Rf	6.37e6 [m]	6.37E6 m	Earth radius
md	7.768e22 [A*m^2]	7.768E22 $m^2 \cdot A$	Magnetic dipole momentum

Table 4.1 Parameters defined for the Earth's magnetic field

Next step is creating the geometry, **Geometry_R>More Primitives>Point**, which denotes the position of the elementary magnetic dipole. The Earth and the magnetosphere will be approximated by spheres, **Geometry_R>Sphere>Radius: Rf**, the radius of the magnetosphere is five times larger than that of the Earth, **Geometry>Sphere 1_R>Duplicate**, and **Sphere 2>Radius: 5*Rf**, and press **Build All Objects**, then **Zoom Extents** and **Wireframe Rendering** to look into your model.

Now, we need to fill up the model with physics in **Magnetic Fields** row. You can check the **Equation**, which is solved by COMSOL, this is the first law of Maxwell in stationary state (Ampère's Law), the definition of vector potential and the Ohm's Law with conductive and external current. Let us set the elementary magnetic dipole in the origin,

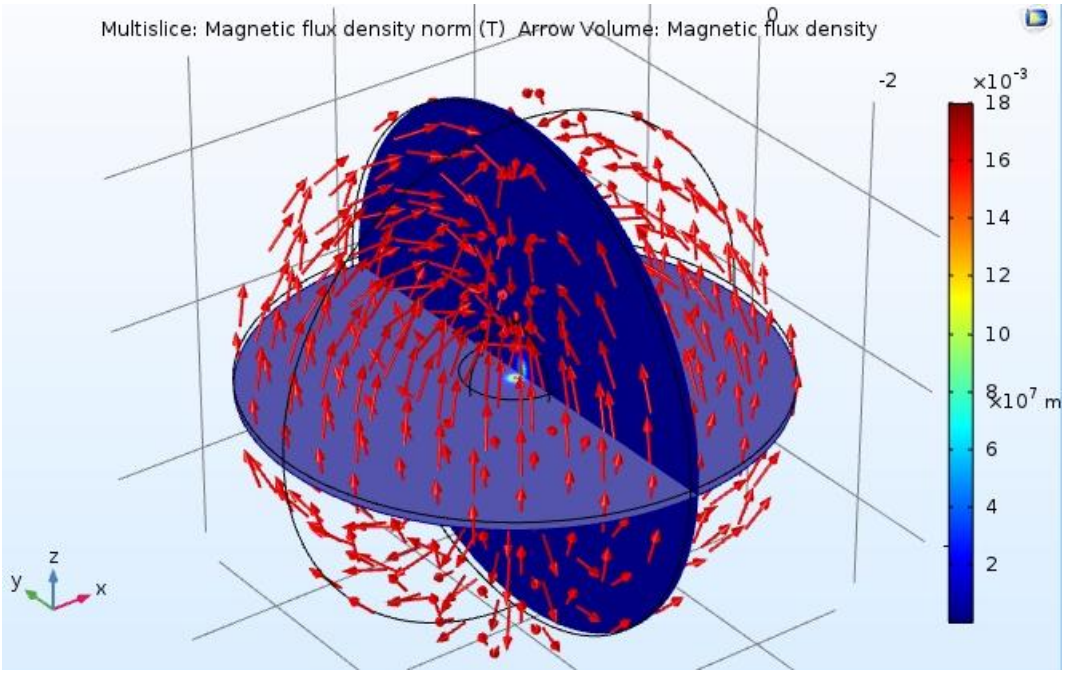

Figure 4.1 Central and axial magnetic dipole field of the Earth illustrated by the direction (normalized red arrows) and the magnitude of the magnetic flux density (two sections).

Magnetic Fields_R>Points>Magnetic Point Dipole and add **#7** (origin) to the Selection box. We should define the direction and the magnitude of the point dipole, **Magnetic dipole momentum direction>z: -1** and **Magnetic dipole moment, magnitude: m_d**. In the **Magnetic Fields>Ampère's Law** the **Relative permeability**, the **Electrical conductivity** and the **Relative permittivity** should be set to **User defined** (**μ_r=1**, **σ=0**, **ε_r=1**), which are unimportant in calculating the magnetic field.

Last step before the solution is the mesh generation, **Mesh_R>Size**, and **Size 1>GEL: Boundary: #5–8, 11, 12, 14, 15** (the Earth's surface), you can use the scroll of the mouse to enter the interior of the model, and left button to rotate it. To refine the discretization, **Custom>MES: Rf/10**. In order to increase the resolution in the surroundings of the magnetic source, **Mesh_R>Size**, and **Size 2>GEL>Point: #7**, **Custom>MES: Rf/100**. We should not forget the method of the discretization, **Mesh_R>Free Tetrahedral** and **Build All** to get 54201 finite elements, then press **Study>Compute**. In the **Progress** menu you can see that the software chooses an iteration method FGMRES to solve the problem, the iteration can be followed in the **Convergence Plot**.

Visualizing the solution **Results>Magnetic Flux Density Norm>Multislice>Y-Planes: 0**, while **X-Planes>Entry method>Coordinates: 1e6** m and **Z-Planes>Entry method>Coordinates: -1e6** m. To see the direction of the magnetic field, **Results>Magnetic Flux Density Norm_R>Arrow Volume>Entry method>Number of points: 10** in all directions. The length of the arrows should be **Arrow length>Normalized** to show only the direction of the field without the magnitude. *Figure 4.1* illustrates the simplified magnetic field of the Earth by two sections and the direction pointing from the geographic south to north.

Finally, it is worth quantitatively checking also the magnitude of the magnetic field, **Results_R>1D Plot Group**, and **1D Plot Group_R>Line Graph**, then sections **#6, 7** (a line of longitude on the Earth's surface) should be added to Selection box. We should use **Unit: nT**, and press **Plot**. *Figure 4.2* shows that the magnitude of the total magnetic flux has a maximum on the poles (60000 nT), and it has a minimum at the magnetic equator (30000 nT). We can visualize also the components of the magnetic flied separately, **Line Graph>y-Axis Data>Replace Expression>Component 1>Magnetic Fields>Magnetic>Magnetic Flux Density: mf.Bx - Magnetic Flux Density, x component** and **Plot**. As you can see, there is no

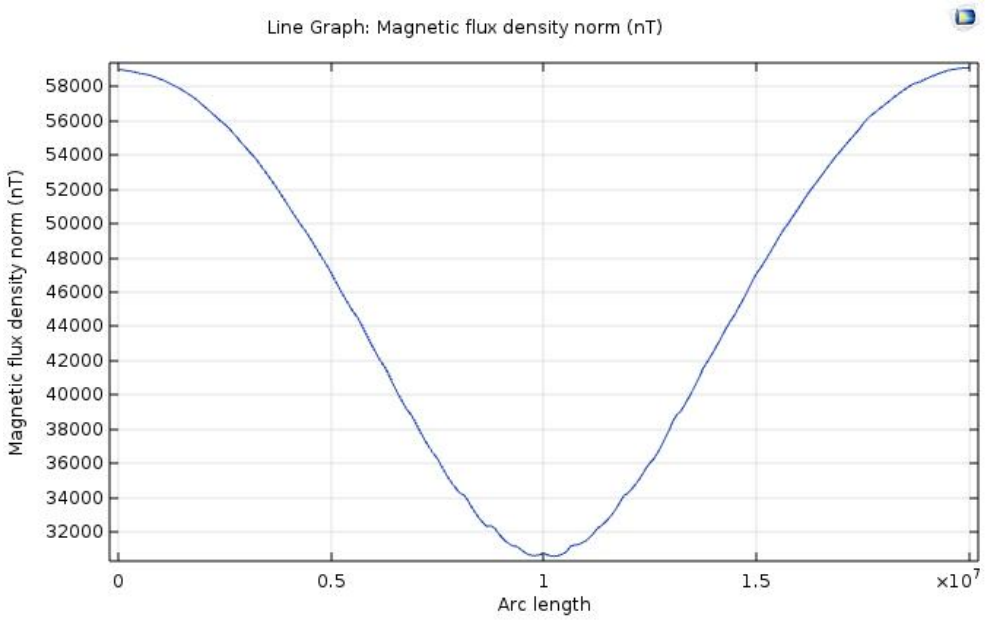

Figure 4.2 Magnitude of the magnetic flux density along a longitude from the south to the north pole of the Earth.

x component at the poles and the equator, and it has a minimum (-45000 nT) and a maximum (45000 nT) between those. To display the *y* component, rewrite **Expression: mf.By**, and press **Plot**, where mf is the abbreviation of the name of the module, Magnetic Fields. You can see a random variation between -20 and 200 nT, which is the numerical error of the solution, since along the given section the *y* component of the magnetic field should be zero. The vertical component of the magnetic field (in COMSOL coordinate!!), **Expression: mf.Bz**, and **Plot**, shows that the magnetic flux density points 'downwards' at the poles and 'upwards' at the equator. The latter explains, that here the magnetic field does not have *x*, *y* components. You should save the model, e.g. **Save>Earth's magnetic field**.

4.2 Buried objects

4.2.1 Iron barrels

Searching buried objects using non-invasive method is a typical task of the exploration geophysics. If the buried object has an induced or remanent magnetic field, magnetic exploration is an effective method to reveal the spatial position of the objects. In this example the magnetic anomalies induced by subsurface iron barrels and pipes will be computed.

As a first step, we need to choose the appropriate module, **Model Wizard>3D> AC/DC>Magnetic Fields, No Currents (mfnc)>Add**, then **Study>Stationary>Done**. The air above the surface is **Geometry_R>Block** with W**idth: 100** m, **Depth: 50** m and **Height: 10** m. To get the subsurface, **Geometry>Block_R>Duplicate** and set **Block 2>Position>z: -10** m, then **Build All Objects**. The surface is the internal boundary at *z*=0. Let us build into the model four buried barrels with different parameters, **Geometry_R>Cylinder>Radius: 0.5** m to the **Position>x: 10** m, **y: 10** m and **z: -2** m, which is 1 m beneath the surface. To get the 2nd barrel, **Geometry>Cylinder 1_R>Duplicate**, and modify **Height: 2** m, **x: 20** m and **z: -3** m. The 3rd barrel, **Geometry>Cylinder 2_R>Duplicate**, and modify **Height: 1** m, **x: 30** m. And the last one, **Geometry>Cylinder 3_R>Duplicate**, and modify **Radius: 1** m, **Height: 1** m, **x: 40** m. Press **Build All Objects** and **Wireframe Rendering** to see as the objects with different height, radius or depth are aligned parallel with the axis *x*. In order to be able to refine the mesh direct above the barrels, we need to insert four points, **Geometry_R>More Primitives>Point: (10, 10, 0)** m, the other three points should be created by duplication to the

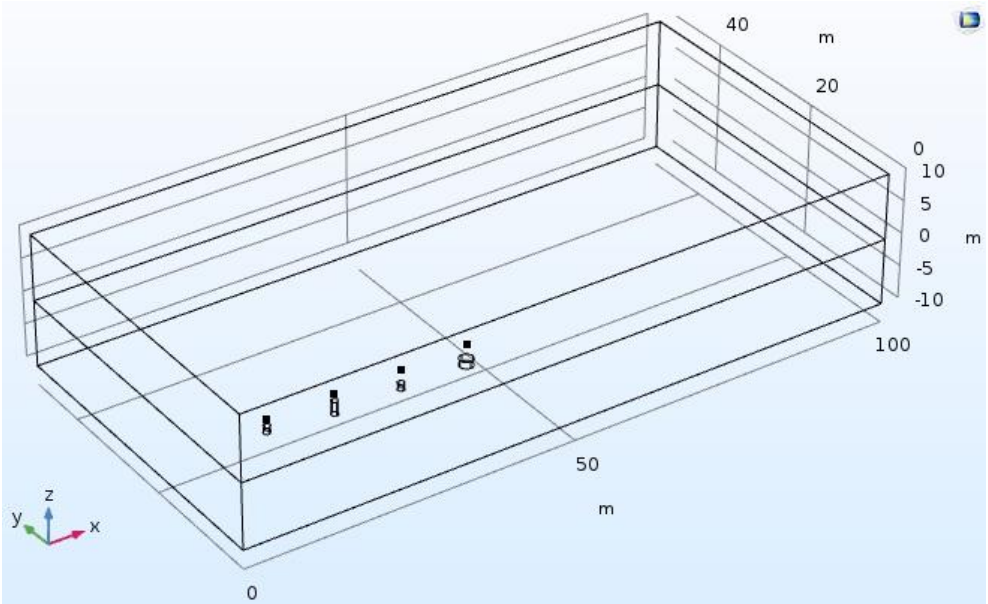

Figure 4.3 Geometry of the model including the air, the subsurface and the four buried iron barrels.

given position, **Point 2: (20, 10, 0)** m, **Point 3: (30, 10, 0)** m and **Point 4: (40, 10, 0)** m, and **Build All Objects**. *Figure 4.3* shows the model geometry.

The equations solved in module **Magnetic Fields, No Currents>Magnetic Flux Conservation>Equations** are shown as the 1st Maxwell's Law without currents, the relation between the magnetic flux density and the magnetic field as well as the definition of the magnetic potential. Set the **Relative permeability>μ_r>User defined: 1** for the air and the ground, while **Magnetic Fields, No Currents_R>Magnetic Flux Conservation>Relative permeability>μ_r>User defined: 1000** for the iron barrels (**#3–6**). For the configuration of the appropriate boundary condition, we need to take a little loop-way.

The magnitude of the total magnetic flux density in Hungary is approx. T=48700 nT, the inclination is about I=65º, while the declination is D=2º. *Figure 4.4* illustrate the above-mentioned parameters, the horizontal (H) and the vertical (Z) components of the magnetic field in a local coordinate system, where X and Y point to the geographical north and east, while Z shows downwards. The vertical,

$$Z = T \sin I = 44140\,\mathrm{nT}, \tag{4.1}$$

and the horizontal components,

$$H = T \cos I = 20580\,\mathrm{nT} \tag{4.2}$$

are calculated based on the Fig. 4.4, while the northern and the eastern components of the horizontal magnetic field are

$$X = H \cos D = 20570\,\mathrm{nT} \quad \text{and} \quad Y = H \sin D = 720\,\mathrm{nT}, \tag{4.3}$$

respectively. These values of the magnetic flux density will be given as outer boundary conditions, but we need to reconcile the coordinate system used in COMSOL and used in magnetic exploration presented in Fig. 4.4. In COMSOL x points to the east (Y), y points to the north (X) and z points upwards ($-Z$). Thus the boundary conditions specified in COMSOL are **Magnetic Fields, No Currents_R>Magnetic Flux Density>Type: Magnetic Flux Density>x: 720** nT, **y: 20570** nT and **z: -44110** nT, and to add **All boundaries** to Selection box. I note that this boundary condition is not applicable to the inner boundary, the surface (#6).

The mesh is suggested refining within the barrels, **Mesh_R>Size**, then **Size 1>GEL>Domain: #3–6** (barrels), **Custom>MES: 0.2** m, and on the surface above the barrels, **Mesh_R>Size**, then **Size 2>GEL>Point: #11, 20, 29, 38**, **Mesh_R>Size**, **Custom>MES: 0.2** m. The discretization is made by **Mesh_R>Free Tetrahedral**, resulting 49208 finite elements after **Build All**. If one would like to look into the interior parts of the

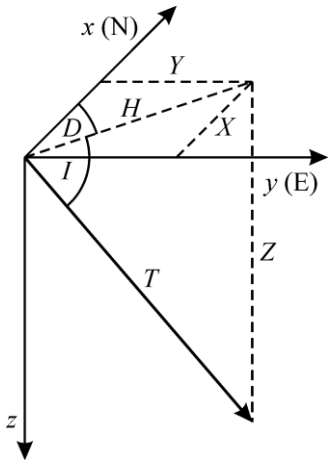

Figure 4.4 Local coordinate system of the magnetic field.

meshed model, in Graphics window press **Select Boundaries**, **Click and Hide**, then choose the upper and the lower boundary of the model. After rotating your model, you can see the finer mesh on the surface of the barrels. You can go back by clicking **Go To Default View**. Solve the problem by **Study>Compute**. The iterative Conjugate gradients method is chosen by COMSOL as you can see in **Convergence Plot** of **Graphics** window. After 22 steps the iteration reached the predefined threshold for the error, 10^{-3}.

Let us see the computed magnetic flux density on the surface, **Results>Magnetic Flux Density Norm>Multislice>Multiplane Data>X-planes: 0** and **Y-planes: 0**, while **Z-planes>Coordinates: 0** m, then press **Plot**. The value of **B** varies between 48000 and 60000 nT, **Unit: nT**. These extreme anomalies on the surface appear owing to that the barrels are thought to be compact iron. One can see that the maximum magnetic anomaly is observed above the 2nd barrel, because it is higher (2 m) than the other barrels, and it is situated shallower than barrel 3 and 4. We can easily investigate how the magnetic field varies upwards. At z=1 m, **Multiplane Data>Z-planes>Coordinates: 1** m, the value of the magnetic flux density ranges between 48500 and 51500 nT. At z=2 m, **Multiplane Data>Z-planes>Coordinates: 2** m, the value of the magnetic flux density ranges between 48600 and 49900 nT. At z=3 m, **Multiplane Data>Z-planes>Coordinates: 3** m, the value of the magnetic flux density ranges between 48600 and 49300 nT. It is clear that the horizontal extension of the magnetic anomalies increases, while the amplitude of those decreases. We can continue the investigation downwards, too, as a downward continuation, at **Z-planes>Coordinates: -0.2** m, or at **Z-planes>Coordinates: -0.5** m. The conclusion is obvious, the extension of the anomalies decreases, while the amplitude of the anomalies increases. Looking the surface magnetic field from above, **Z-planes>Coordinates: 0** m, and click **Go To XY View**, a minor negative anomaly appears north to the main positive anomalies. If we visualize the x component of the magnetic field, **Replace Expression>Component 1>Magnetic Fields, No Currents>Magnetic>Magnetic Flux Density>mfnc.Bx - Magnetic flux density, x component**, a positive and a negative anomaly appear on the left-side and on the right-side of the barrels, respectively. Changing **Expression: mfnc.By**, a positive and a negative anomaly appear south and north of the barrels, resp. In order to explain the phenomenon, click **Go To Default View** and visualize also the streamlines of the magnetic field, **Magnetic Flux Density Norm_R>Streamline>Streamline Positioning>Start Point controlled>Number of Points: 100**. After rotating and zooming in the solution, you can see that the magnetic flux lines are attracted by the barrels having high relative magnetic permeability (μ_r=1000) and resulting in negative/positive anomalies north and east/south and west of the barrels (*Figure 4.5a*). The total magnetic field can be presented along a section above the barrels, **Data Sets_R>Cut Line 3D>Point 1: (0, 10, 0)** to **Point 2: (80, 10, 0)**, then **Results_R>1D Plot Group**, **1D Plot Group_R>Line Graph>Data Sets>Cut Line 3D 1**, **Expression>Replace Expression>**

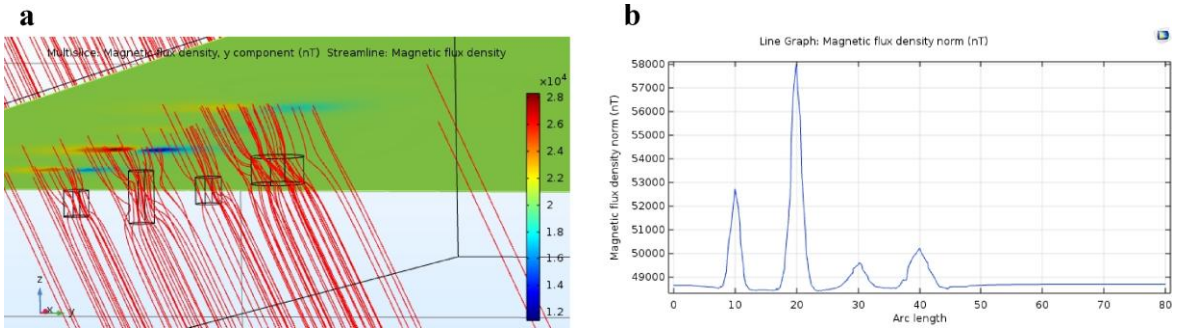

Figure 4.5 (a) y component of the magnetic flux density on the surface and the flux lines of the magnetic field (red). (b) Magnitude of the magnetic flux density on the surface above the buried barrels.

Component 1>Magnetic Fields, No Currents>Magnetic>mfnc.normB - Magnetic flux density norm using **Unit: nT**. Although the resolution of the solution is not satisfied for a quantitative solution, it is clear that the 2nd barrel produces the highest (~9000 nT), while the 3rd barrel generates the lowest (~1000 nT) magnetic flux density anomaly (*Figure 4.5b*). It is worth saving the model, **Save>Buried objects 1**.

4.2.2 Iron pipe in W-E direction

A buried iron pipe results in different magnetic anomaly on the surface, **Geometry_R>Cylinder>Radius: 0.5** m, **Height: 30** m, and **Position: (10, 30, -1.5)** m, **Axis>Axis type: x-axis**, then click **Build All Objects**. Here the axis of the pipe is situated at a depth of 1.5 m being parallel to axis *x*, and its diameter is 1 m. Add pipe to the Selection box of **Magnetic Flux Conservation 2: #3–7**, and also to the finer mesh, **Mesh>Size 1: #3–7**, then regenerate the mesh, **Build All** (#162 144), **Study>Compute**.

If you go to **Results>Magnetic Flux Density Norm>Multisclice>Go To XY View**, an asymmetry appears in the case of the pipe. It is more eye-catching, if you clear away the flux lines, **Results>Magnetic Flux Density Norm>Streamline_R>Disable**. The *y* component of **B** (mfnc.By) decreases from west to east due to the deviation between the magnetic and the geographic north directions (D=2º). (You can check it, if you set the *x* component of the magnetic flux density from 720 nT to 0 at the boundary condition.) You should save this model, e.g. **Save As>Buried Objects 2**.

4.2.3 Iron pipe in N-S direction

By a last modification of this example, we can study how alters the solution if the iron pipe is quasi-parallel to the horizontal component of the magnetic field. Locate a new pipe in the model, **Geometry>Cylinder 5_R>Duplicate>Position: (60, 10, -1.5)** m and **Axis type: y-axis**, then **Build All Objects**. We need to add this new pipe to the Selection box in both **Magnetic Fields, No Currents>Magnetic Flux Conservation 2: #3–8** and **Mesh>Size 1: #3–8**, then the mesh needs clicking **Build All** (#270 948). Press **Study>Compute** to solve this geophysical problem by the iterative conjugate gradients method, which includes approx. 80 steps to reach the error threshold (see **Convergence Plot**).

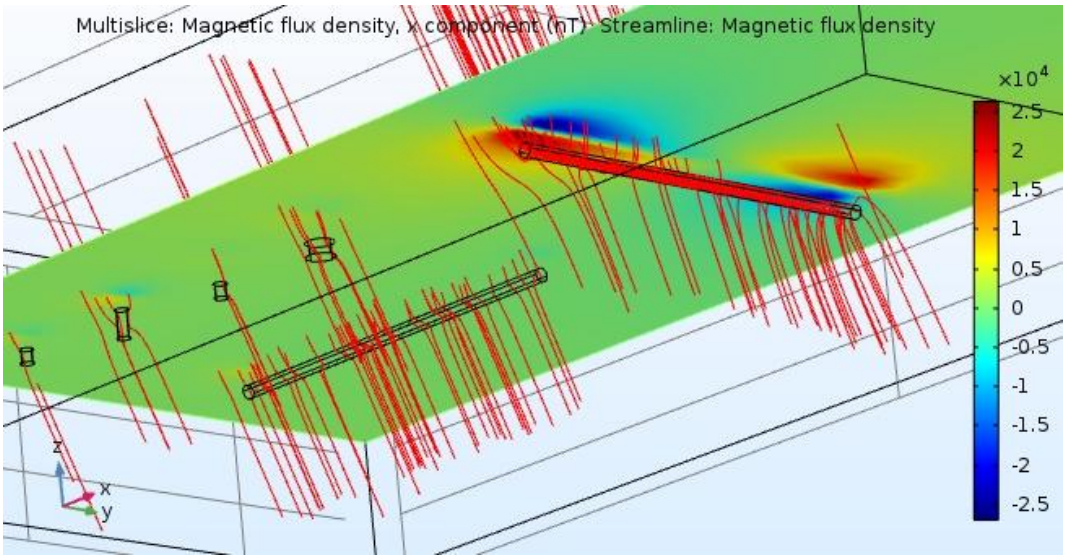

Figure 4.6 Final solution of the magnetic field of the buried objects: four barrels and two pipes. x component of the magnetic flux density on the surface and the flux lines of the magnetic field (red).

As you can see in the solution, **Results>Magnetic Flux Density Norm>Multislice> Expression: mfnc.normB** in **Unit nT** at a depth of **Multiplane Data>Z-planes>Coordinates: 0** m, the magnetic flux density varies within a much wider range, between 15000–107 000 nT. The anomaly caused by the new iron pipe suppresses the anomalies of the other buried objects. Investigating the effect of the different magnetic components, **Results>Magnetic Flux Density Norm>Multislice>Expression: mfnc.Bx** a quadrupole, while **Expression: mfnc.By** a three-pole anomaly structure appears. The observed phenomenon can be understood, when the magnetic flux lines are shown again, **Results>Magnetic Flux Density Norm>Streamline_R>Enable**. By rotating and zooming in the model, it is clear that the flux lines are attracted at the southern end of the pipe and they discharge at the northern end of the pipe resulting the quadrupole anomaly in B_x (*Figure 4.*6).On the other side, B_y component is enhanced at both ends of the pipe. You can check at **Results>1D Plot Group**, that the effect of the new pipe in the total magnetic flux density exceeds the anomalies generated by the barrels. Do not forget to save the modified model, **Save as>Buried objects 3**.

4.3 U-magnet

In this section the field of a permanent U-magnet will be modeled, **Model Wizard>3D>AC/DC>Magnetic Fields, No Currents>Add**, then **Study>Stationary>Done**. The model geometry of the U-magnet a bit complicated, **Geometry_R>Work Plane>Plane: yz-plane** at **x-coordinate: 0.08** m. Beneath the Work Plane, **Plane Geometry_R>Rectangle>Width: 0.02** m and **Height: 0.02** m at a **Position>xw: 0.03** m and **yw: 0** m, then click **Build All** and **Zoom Extents**. This square must be rotated to get a U-magnet, **Geometry_R>Revolve>Revolution Angles>Angles: -180**°and **Build All Objects**. We need to fit four pieces to finalize the geometry, **Geometry_R>Block>Width: 0.02** m, **Depth: 0.02** m and **Height: 0.04** m at the **Position>x: 0.04** m, **y: 0.03** m, **z: 0.02** m using **Axis type: x-axis**. Click **Build All Objects** to check whether the block fits to the U-piece. If yes, we can continue the geometry building, **Geometry>Block 1_R>Duplicate>Position>x: 0** m, **Geometry>Block 1_R>Duplicate>Position>y: -0.05** m, and **Geometry>Block 3_R> Duplicate>Position>x: 0** m. Now, we have to locate the U-magnet in a closed model domain, **Geometry_R>Block>Width: 0.4** m, **Depth: 0.3** m and **Height: 0.3** m at a **Position: (-0.20, -0.15, -0.15)** m. Click **Build All Objects** and **Wireframe Rendering**, and you can see that is shown in *Figure 4.7a*, if you worked well.

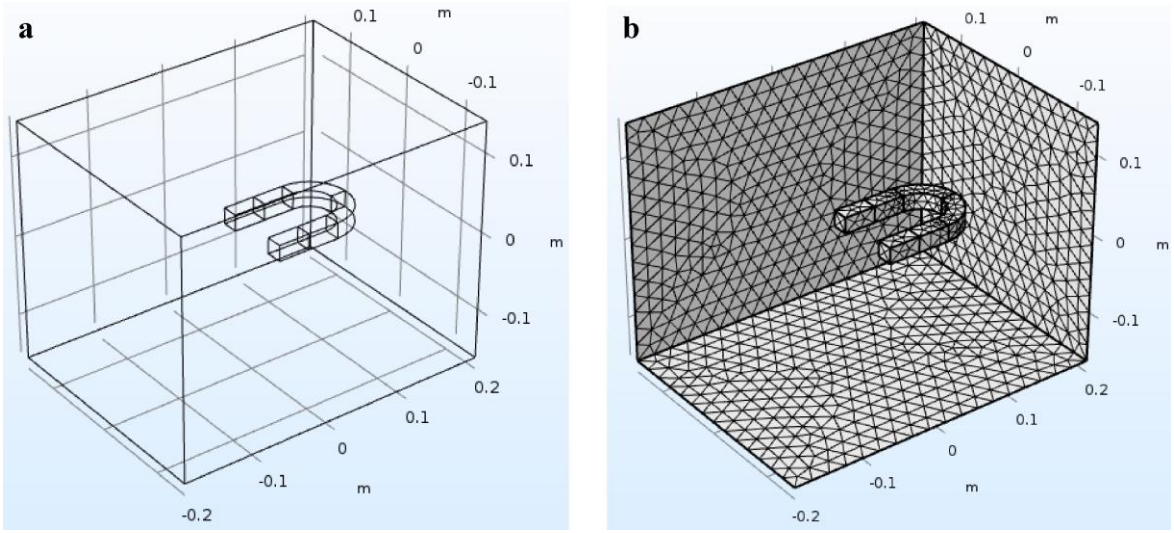

Figure 4.7 (a) Model geometry and (b) finite element mesh of the U-magnet problem.

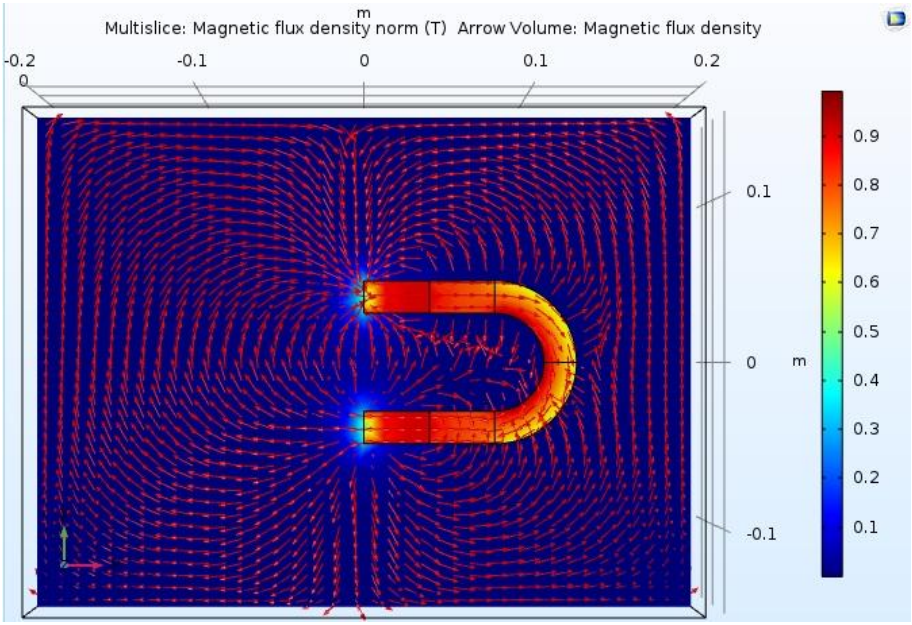

Figure 4.8 Magnetic flux density in the horizontal midplane of the U-magnet and the direction of the magnetic field illustrated by normalized red arrows.

In this example the material properties will be chosen from the **Materials_R>Add Material from Library>Built-In>Iron_R>Add to Component 1**. Since the U-magnet is located in air, we need to repeat it, **Materials_R>Add Material from Library>Built-In>Air_R>Add to Component 1**. The model box must be added to the Selection box in **Materials>Air: #1**. Now, you can close the **Add Material** window. If you click **Materials>Iron**, you can see that only the U-magnet consists of iron.

In Magnetic Fields, No Currents module, the magnetized parts of the magnet should be set, **Magnetic Fields, No Currents_R>Magnetic Flux Conservation>Domain Selection: #3** (farther end of the magnet), and **Magnetic Field>Constitutive relation>Magnetization>M: (750 [kA/m], 0, 0)**. You can copy this domain, **Magnetic Fields, No Currents_R>Magnetic Flux Conservation 2_R>Duplicate>Domain Selection: #2** (near end of the magnet), then **Magnetic Field>Constitutive relation>Magnetization>M: (-750 [kA/m], 0, 0)**. The part #3 must be removed from this Selection box.

Mesh generation is very simple, **Mesh>Element size: Finer** and **Build All** to get 57165 finite elements. To look into the model, click **Select Boundaries** in Graphics window, then **Click and Hide** and denote the three near sides of the model domain. *Figure 4.7b* shows the discretized model geometry. To solve the problem, click **Study>Compute**.

In order the magnitude and the direction of the magnetic flux density to be visualized, **Results>Magnetic Flux Density Norm>Multislice>Multiplane Data>X-planes: 0** and **Y-planes: 0**, while **Z-planes>Entry method>Coordinates: 0.01** m, which is the midplane of the magnet. Then **Results>Magnetic Flux Density Norm_R>Arrow Volume>Arrow Positioning>X grid points: 40** and **Y grid points: 40**, but **Z grid points>Entry method>Coordinates: 0.01** m. If you click **Plot**, you can see the direction of the magnetic field only within the U-magnet, because the magnitude of **B** is much higher there. A possible solution is, **Coloring and Style>Arrow length>Normalized**. If you think that the arrows are too long, you can scale them by e.g. **Scale factor: 0.015**. You see better the solution of the magnetic flux density, if you click **Go To XY View** in Graphics window (*Figure 4.8*). Save the model, **Save As>U-magnet**.

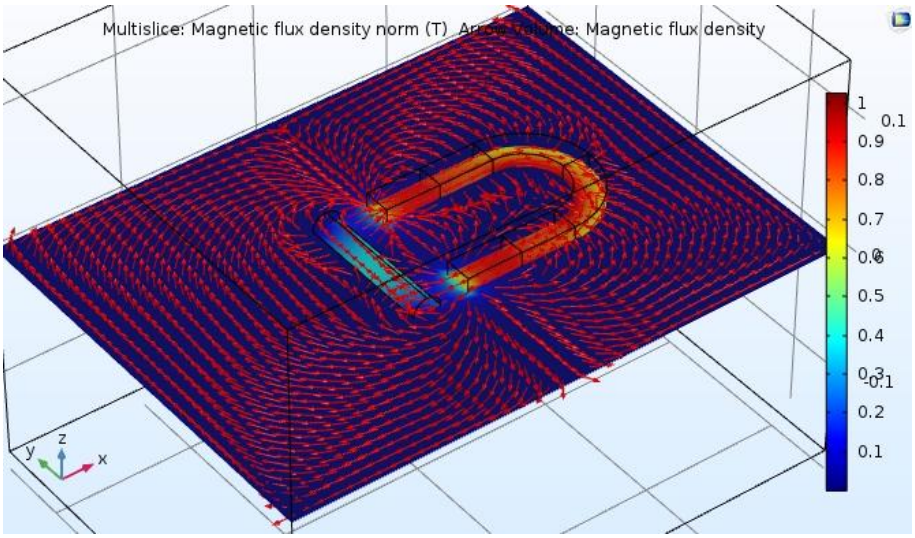

Figure 4.9 Magnitude and direction (red arrows) of the magnetic flux density of a U-magnet and an iron rod in the horizontal midplane of the model..

Electromagnetic force acting to an iron object can be computed in this model. **Geometry_R>Cylinder>Radius: 0.01** m and **Height: 0.1** m at a **Position: (-0.03, -0.05, 0.01)** pointing parallel to the **Axis>Axis type: y-axis**. Clicking **Build All Objects**, you will see the iron rod in the front of the U-magnet. You can check, whether the rod consists of iron in **Materials>Iron: #2**. For calculation, **Magnetic Fields, No Currents_R>Force calculation>Force name: rod** and add the rod (**#2**) to the Selection box. Remesh the modified model by **Mesh>Build All** (#74971) and **Study>Compute**.

In **Results>Magnetic Flux Density Norm** you can see how the iron rod conducts the magnetic flux lines (*Figure 4.9*). We can calculate the attraction force between the rod and the magnet, **Results>Derived Values_R>Global Evaluation>Expression>Replace Expression>Component 1>Magnetic Fields, No Currents>Mechanical>Electromagnetic Force: mfnc.Forcex_rod - Electromagnetic force, x component**. You can click =**Evaluate** to see the *x* component of the force, 5.9683 N. In the case of perfectly symmetrical model and exact numerical solution, *y* and *z* component would be zero. We can check it, **Expression: mfnc.Forcey_rod** and **Evalute**, $F_y \approx -7.200 \cdot 10^{-4}$ N, while the *z* component is $F_z \approx -0.032$ N. Just save the model, **Save As>U-magnet with rod**.

5 ELECTROMAGNETISM

In this chapter two popular geoelectrical tools will be numerically modeled using electromagnetic phenomena, the induction geophysical probe used in boreholes and the ground penetrating radar (GPR) as a surface exploration tool.

5.1 Induction borehole probe

As in the most problems in borehole geophysics, 2D axisymmetric model geometry will be used, **Model Wizard>2D Axisymmetric>AC/DC>Magnetic Fields>Add**, but here the solution is time-dependent, **Study>Time Dependent>Done**. Usually, the geometry will be as simple as possible, the model domain is a cylinder, **Geometry_R>Rectangle>Width: 1** m and **Height: 3** m at the **Position: (0, -1)** m. Three points will be inserted, the first is the transmitter loop generating electromagnetic (EM) field, **Geometry_R>Point: (0.05, 0)** m, the second denotes the transmitter loop, **Geometry_R>Point: (0.05, 1)** m, and the third one is a loop between the transmitter and the receiver to measure the current induced in the rock, **Geometry_R>Point: (0.5, 0.5)** m. We should not forget that the rectangle and the points are a cylinder and circles in 2D axisymmetric geometry, where red line denotes the symmetry axis.

The Ampère's Law has already been introduced in part 3.1, but here the problem time-dependent, therefore the electric field can be calculated from the time-variation of the magnetic flux density (Maxwell's 2nd Law) and the motional induction is also allowed in the general Ohm's Law, see **Magnetic Fields>Equation**. Let us give the electromagnetic parameters of the medium, **Magnetic Fields>Ampère's Law>Relative permeability>μ_r: 1**, **Electrical conductivity>σ: 1/100** S/m and **Relative permittivity>ε_r: 1**. Now, we need to define the time-dependent exciting current in the transmitter loop, **Magnetic Fields_R>Points>Line Current (Out-of-Plane)**, select point **#3** (transmitter loop), and give

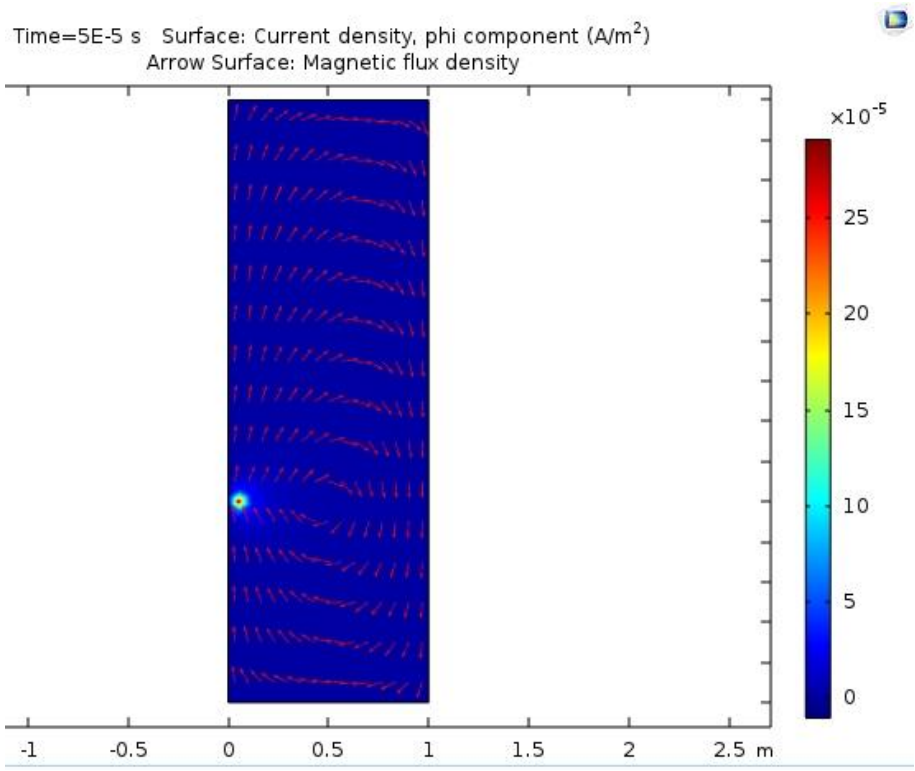

Figure 5.1 φ component of the current density excited by the transmitter loop and the direction of the magnetic flux density at a time of 5·10-5 s.

the current, **Out-of-plane current>I_0: 1[A]*sin(2*pi*t*10[kHz])**, where 1 A and 10 kHz are the amplitude and the frequency of the current, while *t* denotes the time. Let us use a simple automatic mesh, **Mesh>Build All**, which results in only 311 finite elements.

In time-dependent study we must define the parameters of the time stepping, **Study>Step 1: Time Dependent>Times: range(0, 2e-6, 1e-4)** s, which means that the calculation starts at t=0 and ends at 10^{-4} s, solutions will be kept in memory at each times of $2 \cdot 10^{-6}$ s (output times). Now, we can start the solution, **Study>Compute**.

In order to visualize the φ component of the induced current density, **Results>Magnetic Flux Density Norm>Surface 1>Expression: mf.Jphi** with the direction of the magnetic flux density, **Results>Magnetic Flux Density Norm>Surface 1_R>Arrow Surface>Coloring and Style>Arrow length: Normalized**, but we do not need the contour plot, **Contour_R>Disable**. *Figure 5.1* shows the φ component of the induced current density and the direction of the magnetic field at a time of t=$5 \cdot 10^{-5}$ s. To view the time-dependent exciting and induced current, **Results_R>1D Plot Group**, then **1D Plot Group_R>Point Graph>Expression>Replace expression>Component 1>Magnetic Field>Currents and charge>mf.Iop - Out-of-plane current** and add **#3** (transmitter loop) to Selection box, then click **Plot**. You can see the sinusoid exciting current with an amplitude of 1 A (*Figure 5.2a*). We should duplicate the graph, **Results>1D Plot Group>Point Graph 1_R>Duplicate>Expression: mf.Jiphi**, remove #3 and add **#5** (medium) to Selection box. Since the exciting current is much larger than the induced one, so **Results>1D Plot Group>Point Graph 1_R>Disable**, the time resolution seems very poor. The induced current at the place of the receiver loop, **Results>1D Plot Group>Point Graph 2_R>Duplicate**, change #5 to **#4** (receiver loop), and **Results>1D Plot Group>Point Graph 2_R>Disable**. Because the receiver is farther from the transmitter than the point in the medium, so the induced current is lower. It is obvious that the time step is not fine enough,

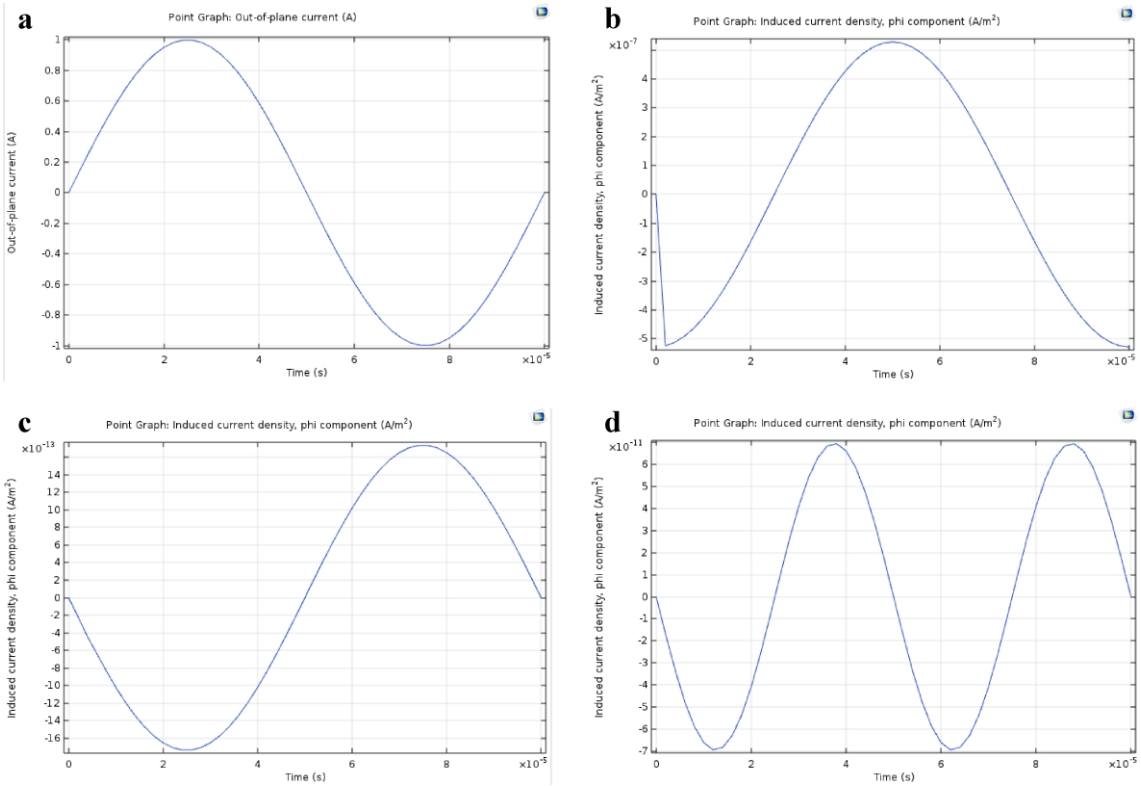

Figure 5.2 Time variation of (a) the exiting current in the transmitter loop, φ component of the current density induced (b) in the medium, (c) in the receiver loop after double induction, and (d) the induced current density in the receiver loop with higher exciting current frequency and rock conductivity (see text for details).

thus the time-dependent solution should be tuned.

As a default, the solution uses **Study>Solver Configurations> Solution>Time-Dependent Solver>Time Stepping>Steps taken by solver: Free**, which means that the time step can be as large as the solution is stable, and the output times will be interpolated afterwards. Usually, it results in low accuracy, so let us set it to **Strict**, so the solution will be computed at each output time, **Study>Compute**. The time resolution is much more satisfying, **Results>1D Plot Group**. One can see that the induced current follows a -cos function (*Figure 5.2b*), as a $\pi/2$ shift from the exciting current due to Maxwell's 2nd Law (see Eq. (2.1)). The amplitude of the induced current density in the receiver loop is $j_R \approx 1.4 \cdot 10^{-8}$ A/m^2, while in the medium, **Point Graph 2_R>Enable**, $j_m \approx 5 \cdot 10^{-7}$ A/m^2. It is worth creating an animation about the time variation of the induced current density and the direction of the magnetic flux density, **Results>Export_R>Animation>File>Format: AVI** and **Filename: Induction probe.avi**, then click **Export**. You can start the animation from your file browser, and see that (1) induced current is higher near the transmitter loop, and (2) it has $\pi/2$ shift from the magnetic field, which follows right-hand rule (Ampère's Law). The only problem is that we need the current induced by the current flowing in medium (and not by the transmitter loop), since it yields information about the resistivity of the rock. In one word, we should use double induction. But how?

In order to calculate the current in the receiver induced by the current flowing in the medium induced by the transmitter loop ☺, we need to add the module again, **Component 1_R>Add Physics** and select **Recently Used>Magnetic Fields**, which becomes the module **Magnetic Fields 2 (mf2)**. Let us set **Magnetic Fields 2>Ampère's Law>μ_r: 1**, **σ: 1/100** S/m and **ε_r: 1**. In this double induction model, the inducing current is prescribed as an external current, **Magnetic Fields 2_R>External current density>External current density>J_e: (0, mf.Jphi, 0)** A/m^2, and the domain **#1** must be added to the Selection box. We can solve it again, **Study>Compute**.

To look at the double induced current density curve, **Results>1D Plot Group>Point Graph 2_R>Disable** and **Point Graph 3>Expression: mf2.Jiphi**. Since the graph is quite ugly, we should refine the time-dependent solution again by decreasing the maximum time step, **Study>Solver Configurations> Solution>Time-Dependent Solver>Time Stepping> Maximum step: 1e-7** s. We can follow the solution in real-time manner, when we click **Study>Step 1: Time Dependent>Results While Solving>Plot: 1D Plot Group**. Let us start the solution again, **Study>Compute**. Now, the current density in the receiver loop after double induction, **Results>1D Plot Group**, shows $2 \cdot \pi/2$ phase shift, and its amplitude is only $j_R \approx 1.7 \cdot 10^{-12}$ A/m^2 (*Figure 5.2c*).

Remembering the point-like coil approximation in the course of Borehole Geophysics, the voltage in the receiver coil after double induction is

$$\varepsilon_R(t) = -\omega^2 \mu^2 n_T n_R s_T s_R I_T(t) \int_{-\infty}^{\infty} \int_{0}^{\infty} \sigma(r,z) \frac{r^3}{R_T(r,z)^3 R_R(r,z)^3} dr dz, \qquad (5.1)$$

where ω, μ are the angular frequency and the magnetic permeability of the medium, n_T and n_R denote the numbers of turns of the transmitter and the receiver coil, s_T and s_R are the cross-sectional areas of turns of the transmitter and the receiver coil, I_T is the exciting current in the transmitter coil, r and z denote the radial and vertical coordinates in axisymmetrical model geometry as well as R_T and R_R are the distance between the arbitrary circular current induced in the rock and the transmitter/receiver coils. Eq. (5.1) says that the voltage/current induced in the receiver coil is proportional to the electrical conductivity of the rock, σ and the second power of the angular frequency, ω^2. It is worth checking this property of the model as a validation.

5.1.1 Parameter test

First, we increase the conductivity of the medium by one order of magnitude, **Magnetic Fields> Ampère's Law>Electrical conductivity>σ: 1/10** S/m, and **Study>Compute**. The current density induced in the 'receiver coil' increased by one order of magnitude, $j_R \approx 1.7 \cdot 10^{-11}$ A/m^2. Second, we can increase the exciting frequency by a factor of 2, **Magnetic Fields>Line current (Out-of-Plane)>Out-of-plane current: I_0=1[A]*sin(2*pi*t*20[kHz])**, then **Study>Compute**. During the solution we can see that the numerical duration includes two periods, and the amplitude of the current density induced in the receiver loop is four times larger, $j_R \approx 6.8 \cdot 10^{-11}$ A/m^2 owing to the double induction (*Figure 5.2d*), **Results>1D Plot Group**. If we are interested in the current density induced in the medium, **Results>1D Plot Group>Point Graph 2_R>Enable**, the current density is $j_m \approx 10^{-5}$ A/m^2, which involves an increase by a factor of 20 due to (1) one order of magnitude increase in σ and (2) an increase by a factor of 2 in ω (there is a single induction in the rock). This simple parameter analysis can be saved separately, **Save As>Induction probe - parameter test**.

5.2 Ground penetrating radar

5.2.1 Homogeneous medium

We need to choose the appropriate dimension and module, **Model Wizard>2D>Radio Frequency>Electromagnetic Waves, Frequency Domain (emw)>Add>Study>Frequency Domain>Done**. The air, **Geometry_R>Rectangle>Width: 20** m, **Height: 10** m at the **Position: (-10, 0)** m and the subsurface **Geometry>Rectangle 1>Duplicate>Position: (-10, -10)** m are represented by two rectangles. The transmitter is a point source just above the surface, **Geometry_R>Point** at the position of **(0, 0.1)** m, **Build All Objects**.

We add the material properties of the air from **Materials_R>Add Material from Library>Built-In>Air**. The module solves the Helmholtz equation for the electric field vector, **E**, **Electromagnetic Waves, Frequency Domain>Equation**. We need another domain for the subsurface, **Electromagnetic Waves, Frequency Domain_R>Wave Equation, Electric>Domain selection: #1** (subsurface - lower domain). To parameterize the subsurface, **Wave Equation, Electric 2>Relative permittivity>User defined>ε_r: 9**, **Relative permeability>User defined>μ_r: 1**, and **Electrical conductivity>σ: 1/100** S/m. To define the point source, **Electromagnetic Waves, Frequency Domain_R>points>Electric Point Dipole>Point Selection: #4** (point source), **Electric current dipole moment direction>n_p: (1, 0)** and **Electric current dipole moment, magnitude>p: 1** Am.

Meshing the simple model, **Mesh_R>Size** and for the whole model, **Mesh>Size>Calibrate for Predefined: Finer** and for the surroundings of the point source, **Mesh>Size 1>GEL>Point: #4**, **Custom>MES: 0.01** m, **Mesh_R>Free Triangular** and **Build All** to cover the model by 3896 finite elements.

In the solution we choose a typical frequency used by the ground penetrating radar (GPR), **Study>Step 1: Frequency Domain: 100 MHz**, **Study>Compute**.

To visualize the solution, **Results>Electric Field>Surface>Expression: Ex**, as the *x* component of the electric field. We can accentuate the variation of the field by the modification of the range, **Range>Minimum: -100** V/m and **Maximum: 100** V/m. The solution seems very noisy due to the imperfect boundary condition, which reflects the EM waves. We need to modify it, **Electromagnetic Waves, Frequency Domain_R>Scattering Boundary Condition>Boundary Selection>All boundaries**. Rerun the computation, **Study>Compute**, the solution is much nicer (*Figure 5.3*).

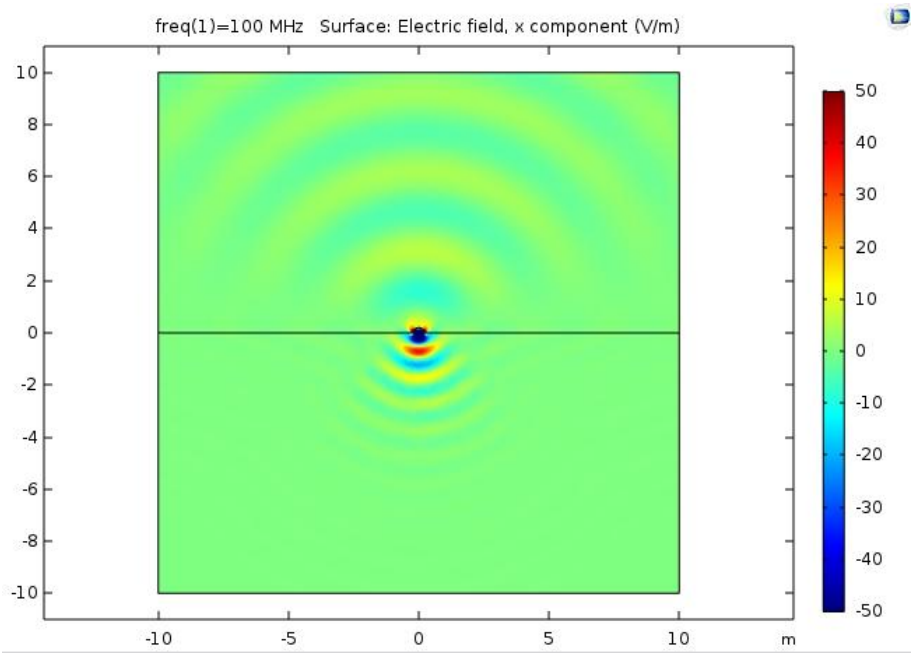

Figure 5.3 Horizontal component of the electric field in the air (upper domain) and in the subsurface (lower domain) excited by an electric point dipole with a frequency of 100 MHz..

It is a good idea to try to focus the EM wave downward, into the ground to increase the penetration of GPR. For this we modify the geometry by enveloping the point source, **Geometry_R>Circle>Radius: 0.2** m, **Sector angle: 180** deg, and **Build All Objects (BAO)**. A good conductor reflects EM waves, **Electromagnetic Waves, Frequency Domain_R>Perfect Electric Conductor>Boundary Selection: #11, 12** (encasement), then **Study>Compute**.

Now, the larger ratio of the energy of EM wave penetrates into the ground. Let us investigate also the magnetic field, **Results_R>2D Plot Group**, and rename it, **2D Plot Group 2_R>Rename: Magnetic Field**, then **Results>Magnetic Field_R>Surface> Expression: emw.Hz**, which direction is perpendicular to the plane of the display in emw module. To highlight the variation of **H**, **Range>Manual color range>Minimum: -0.5** A/m and **Maximum: 0.5** A/m. In isotropic medium the electric and the magnetic fields are perpendicular, and they are also perpendicular to the propagation of EM wave. Calling back the relation derived from Helmholtz equation in the course of Geoelectrical Methods,

$$\mathbf{E} = -\sqrt{\frac{\mu}{\varepsilon}}\,\mathbf{k}\times\mathbf{H} \quad \text{or} \quad \mathbf{H} = \sqrt{\frac{\varepsilon}{\mu}}\,\mathbf{k}\times\mathbf{E}, \tag{5.2}$$

where **k** denotes the unit vector pointing toward the propagation. Eq. (5.2) says that if **E** propagates in the plane (*x*, *y*), so **H** has only *z* component, which is perpendicular to the display. You can check it, **Results>Magnetic Field>Expression: emw.Hx**, then **emw.Hy**, then back to **emw.Hz**. Electric field does not have *z* component, **Results>Electric Field>Expression: Ez**, and **E** does not have *y* component beneath the point source, where EM wave propagates downward (-*y* direction), **Expression: emw.ey**, then we should set it back, **Expression>emw.Ex**. Let us save the model, **Save>GPR - homogeneous**.

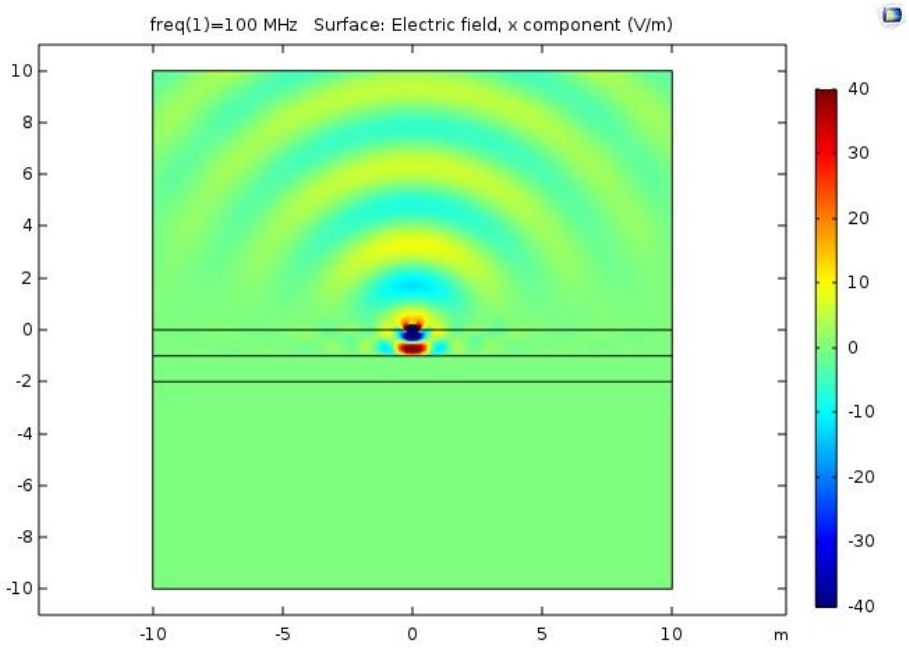

Figure 5.4 Horizontal component of the electric field in the air (upper half of the domain) and in the subsurface including sandy and clayey (middle) layers excited by an electric point dipole with a frequency of 100 MHz..

5.2.2 Clayey layer

It is very instructive to examine, how the EM wave behaves in inhomogeneous medium. The simplest geological inhomogeneity is a clayey layer inserting in the model, **Geometry_R>Rectangle>Width: 20** m at **Position: (-10, -2)** m, **BAO**. Define the parameters of the clayey layer, **Electromagnetic Waves, Frequency Domain>Wave Equation, Electric 2_R>Duplicate>** and **Wave Equation, Electric 3>Domain Selection: #2** (clayey layer at a depth of 1–2 m) removing other domains. The conductivity of the clay is much higher, **Electrical conductivity>σ: 1** S/m. Remeshing the model, **Mesh** and **Build All (BA)**, results in 2866 finite elements, then **Study>Compute**.

If you magnify the variation of the electric field, **Results>Electric Field>Surface>Range>Minimum: -40** V/m and **Maximum: 40** V/m, you can see better that the electric field is strong in the upper high-resistivity layer (ρ=100 Ωm), and tends to zero in the second, clayey layer (ρ=1 Ωm). *Figure 5.4* illustrates that there is a distinctly visible reflection from the top of the clay. Magnetic field shows similar behavior, **Results>Magnetic Field**. You can simply visualize the skin depth, **Results>Magnetic Field_R>Duplicate**, and **Magnetic Field 1>Surface>Expression: emw.deltaS**. Remove the tick from **Range>Manual color range** and click **Plot**. The skin depth, that is the depth, where the amplitude of the EM wave attenuates to the values of 1/*e*, is about 1.6 m in the high-resistivity, sandy layer. However, in the clay the skin depth reduces to 5 cm! It means that that a clayey layer with a thickness of couples of centimeters impedes the penetration of the EM wave. **Save As>GPR - clayey layer**. I note that the skin depth in air tends to infinity owing to its conductivity, σ≈0.

5.2.3 Buried iron pipe

Another typical utilization of GPR is searching buried iron objects, e.g. pipe lines. **Geometry>Rectangle 3_R>Delete** and **Geometry_R>Circle>Radius: 0.5** m at **Position: (0, -1.5)** m, **BAO**. Choose the parameters of iron from **Materials_R>Add Material from**

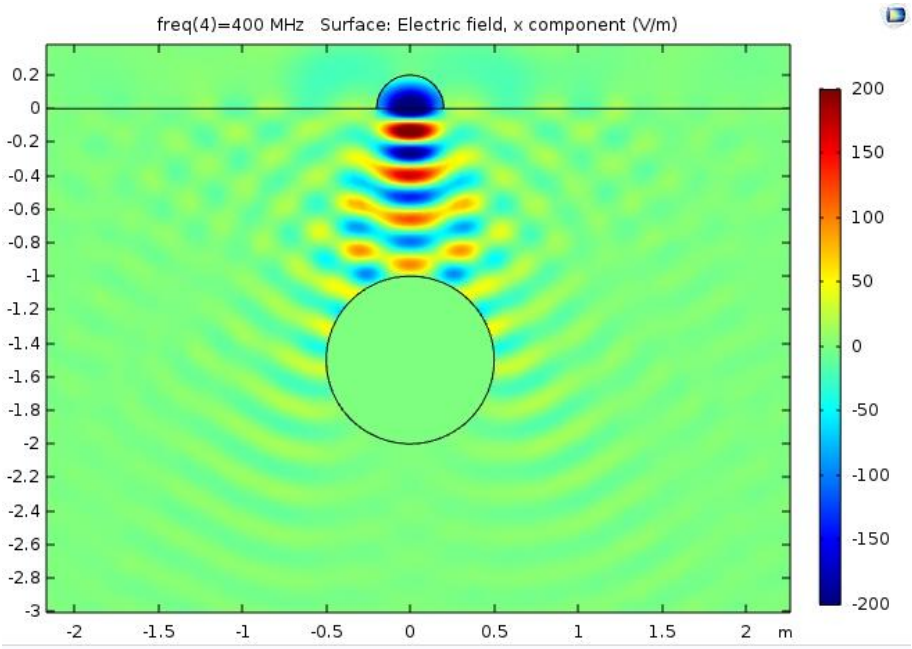

Figure 5.5 Horizontal component of the electric field in the surroundings of a buried iron pipe line (circle) excited by an electric point dipole with a frequency of 400 MHz.

Library>Built-In>Iron: #4 (iron pipe) and add to the Selection box. Delete **Electromagnetic Waves, Frequency Domain>Wave Equation, Electric 3_R>Delete**, which was used for the clayey layer. To refine the mesh, **Mesh_R>Size**, and you should move **Size 2** above **Free Triangular**, then **GEL>Boundary: #12, 15** (upper arc of the pipe), and **Custom>MES: 0.02** m, and reduce **Mesh>Size>Custom>MEGR: 1.1**, then click **BA** to get 14376 finite elements.

In order to solve the problem for more frequencies, **Study>Step 1: Frequency Domain>Frequencies>Range>Start: 100**, **Step: 100** and **Stop: 1000** MHz, and click **Replace**. Click **Results While Solving>Plot** to see the **Electric Field** during the solution procedure. We need to remove the manual range, **Results>Electric Field>Surface>Manual Range**, and we can start the solution by **Study>Compute**.

We can choose the case of **Results>Electric Field>Parameter Value (freq (MHz)): 400** from the solutions to interpret the physical phenomenon. *Figure 5.5* shows that there is (1) a strong reflection from the top of the iron pipe, (2) the electric field is zero within the pipe. The effect is very similar in the magnetic field, **Results>Magnetic Field>Surface>Range>Manual color range>Minimum: -4** and **Maximum: 4** A/m. The skin depth within the pipe is practically zero, **Results>Magnetic Field 1**, which means that the EM wave does not penetrate into the iron pipe. Copying this surface plot, **Results>Magnetic Field 1_R>Duplicate**, then typing **Magnetic Field 1.1>Surface> Expression: 3e8[m/s]/sqrt(emw.murAv*emw.epsrAv)**, we can display the propagation velocity of the EM wave, v based on the relation of

$$v = \frac{c}{\sqrt{\mu_r \varepsilon_r}}, \tag{5.3}$$

where c denotes the light speed. Accordingly, the propagation velocity in the air is $3 \cdot 10^8$ m/s, that is in the sand is approx. 10^8 m/s, while in the iron pipe is $5 \cdot 10^6$ m/s, notwithstanding the energy of the EM wave reflects from the top of the pipe.

Finally, we can visualize the electric field beneath the point source, **Results>Data Sets_R>Cut Line 2D>Line Data** from **(0, 0)** to **(0,-1.5)** m. By clicking **Plot**, you can check

the position of the cut line, which goes from the surface to the interior of the pipe line. To display it, **Results_R>1D Plot Group**, then **1D Plot Group_R>Line Graph>Data Sets: Cut Line 2D**, **Expression: Ex** as a function of the depth, **x-Axis Data>Parameter>Expression: y**. All solutions are shown in the figure, and each frequency dies away in the iron pipe. If you want to present only one electric wave frequency, you can choose it from **Parameter selection (freq)>From list: 400** and click **Plot**. Do not forget saving the model, **Save As>GPR - iron pipe**.

6 GEOTHERMICS

Via three simplex numerical models we present the phenomenon of heat conduction and heat source in homogeneous and inhomogeneous medium, we investigate how the output temperature and heat power depend on the amount of the circulating fluid in a borehole heat exchanger, and finally, we illustrate how the surface heat flux above a 3D cooling magma body varies in time.

6.1 Role of heat conduction and heat source

6.1.1 Homogeneous medium

Here we compile an artificial 2D model to get to know the operation of Heat Transport module, **Model Wizard>2D>Heat Transfer>Heat Transfer in Solids>Add** and **Study>Stationary>Done**. *Table 6.1* shows the necessary model parameters defined in **Global Definitions>Parameters**.

Name	Expression	Value	Description
T0	10 [degC]	283.15 K	Surface temperature
T1	60 [degC]	333.15 K	Bottom temperature

Table 6.1 Parameter definition

To create the model geometry, **Geometry_R>Square>Side length: 1000** m at **Position: (-500, -1000)** m, then **BAO**.

Defining the model properties and boundary conditions, **Heat Transfer in Solids>Solid>Thermal conductivity>User defined>k: 3** W/(m K), **Density>User defined>ρ: 2500** kg/m^3, and **Heat capacity at constant pressure>User defined>Cp: 1000** J/(kg K). **Equation** shows the heat transport equation including terms from the left-side: heat advection, heat conduction, heat source and other additional terms. Default boundary condition suggested by the module: Thermal Insulation, which is appropriate for the side walls. However, the horizontal boundaries will be isothermal, the surface is **Heat Transfer in Solid_R>Temperature>Boundary Selection: #3** (surface), where the temperature is **T_0: T0** from the defined parameters, and the bottom boundary is **Heat Transfer in Solid_R>Temperature>Boundary Selection: #2** (bottom), where the temperature is **T_0: T1**.

The mesh is just simply, **Mesh>BA** using for discretization 578 finite elements, then **Study>Compute**.

It is worth changing the color table from Thermal Light to **Results>Temperature>Surface>Coloring and Style>Color table: Rainbow**, thus cold zones are denoted by cold colors, and we should use **Unit: degC** and click **Plot**. Coloring suggests that the temperature increases continuously downwards, but we should display it quantitatively along a vertical section, **Results>Data Sets_R>Cut Line 2D>Point 1: (0, 0)** to **Point 2: (0, -1000)** m, you can click **Plot** to see the section. To plot the temperature profile, **Results_R>1D Plot Group**, then **1D Plot Group_R>Line Graph>Data set: Cut Line 2D** in **Unit: degC** as a function of **x-Axis Data>Parameter>Expression: y**, then **Plot**. It is clear that the temperature increases linearly downwards owing to this simple geometry, boundary conditions, homogeneous and isotropic medium etc. This base model should be saved, **Save>Geothermics - homogeneous medium**.

6.1.2 Layered model

In geology, the most common heterogeneity is the layering. As a first step, we insert a clayey layer with reduced thermal conductivity, **Geometry_R>Rectangle>Width: 1000** m and **Height: 200** m at **Position: (-500, -600)** m, then **BAO**. **Heat Transfer in Solids>Solid_R>Duplicate**, then **Solid 2>Domain Selection: #2** (middle, clayey layer) and **Thermal conductivity>k: 2** W/(m K). If you click **Study>Compute**, the mesh generation will be done automatically, because the geometry was modified after the last meshing.

Color scale does not show unequivocal variation in temperature distribution, but the graph covers, **Results>1D Plot Group**, that in the clayey layer with lessened thermal conductivity the temperature gradient is higher. It is clear, since the vertical heat flux has to be constant in stationary solution (if it would not be, some zones would be warming up, while others would be cooling down, but it would not be stationary). Knowing Fourier's 1st Law concerning heat conduction,

$$\mathbf{q} = -\mathbf{k}\,\mathbf{grad}T\,, \tag{6.1}$$

where **q**, **k** and *T* denotes the heat flux vector, the thermal conductivity matrix of the medium and the temperature, respectively. So, if **q** is constant and **k** is reduced, the temperature gradient must be enhanced, like in the clayey layer. The direction of the conductive heat flux can be illustrated by arrows, **Results>Temperature_R>Arrow Surface>Expression>X component: ht.dfluxx** and **Y component: ht.dfluxy**, then **Coloring and Style>Color>White**. You can save it separately, **Save As>Geothermics - layering**.

6.1.3 Good thermal conductor

To magnify the effect of thermal conductivity, an extremely good conductor will be inserted into the model, **Geometry_R>Circle>Radius: 100** m, **Position: (0, -800)** m, then **BAO**. We need to set the thermal conductivity of the new object, **Heat Transfer in Solids>Solid 2_R>Duplicate**, and **Solid 3>Domain Selection: #4** (circle), and other domains must be removed, then **Thermal conductivity>k: 100** W/(m K). Click **Study>Compute** to

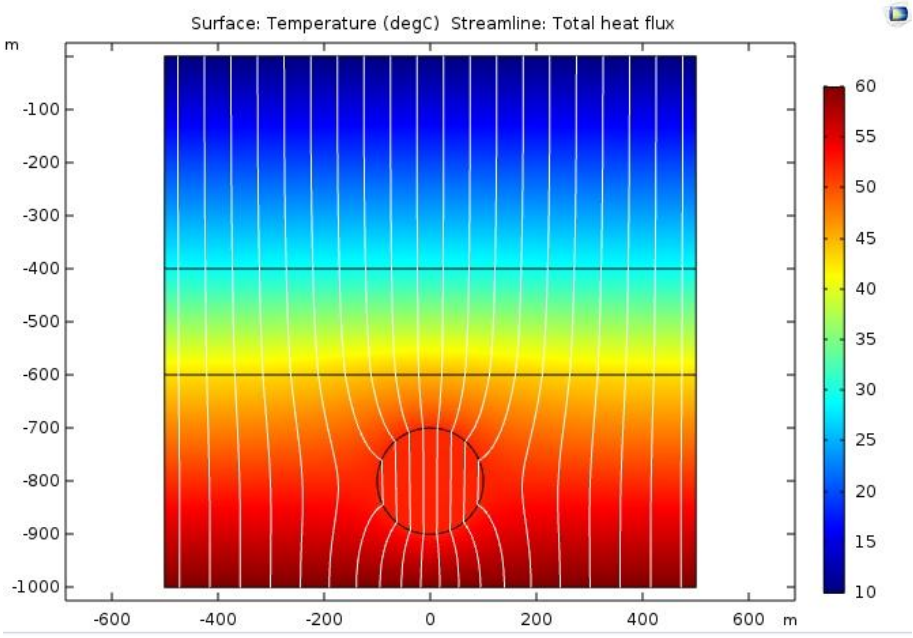

Figure 6.1 Temperature field and heat flux lines (white) in the model including a middle clay layer with reduced and the circle-shaped object with enhanced thermal conductivity.

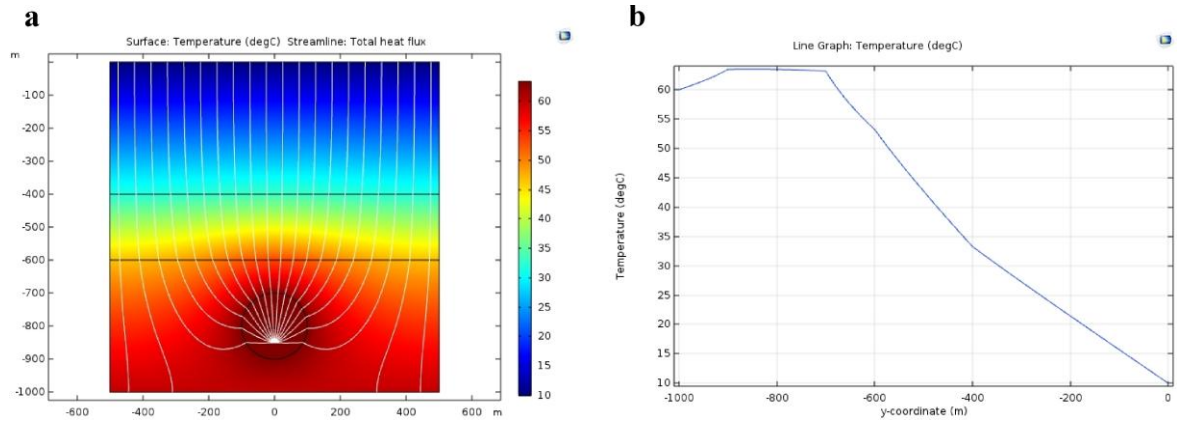

Figure 6.2 Stationary solution of the heat transfer for a model with a middle clay layer having low thermal conductivity and a circle-shaped thermally good conductor. In the latter object the heat production is 0.005 W/m^3. (a) Temperature field with heat flux lines (white), (b) Vertical temperature profile through the middle of the model domain.

be solved.

In order to highlight the path of the heat, **Results>Temperature _R>Streamline: #7** (surface) can be marked in the Selection box, as a boundary through which 20 streamlines overpass. You can choose **Coloring and Style>Color>White** and click **Plot**, to the total heat flux path be displayed. *Figure 6.1* shows the temperature field and the total heat flux streamline after the arrows were cleared away, **Result>Temperature>Arrow Surface_R>Disable**. Last, we should save it, **Save As>Geothermics - good conductor**.

6.1.4 Heat source

Finally, we study the effect of the heat source in the medium, **Heat Transfer in Solids_R>Heat Source>Domain Selection: #4** (circle), and **General source>Q_0: 0.005** W/m^3, then **Study>Compute**. *Figure 6.2a* emphasizes that the circular heat source has the maximum temperature, since more streamlines originate from its interior, and it heats also downwards. This suggestion is proved by **Results>1D Plot Group**, because within the heat source the temperature exceeds 60 ºC, that is the temperature of the bottom boundary (*Figure 6.2b*). Terminally, **Save As>Geothermics - heat source**.

6.2 Borehole heat exchanger

In this chapter we investigate how the output temperature and heat power depends on the fluid velocity circulating in a geothermal borehole heat exchanger. **Model Wizard>2D Axisymmetric>Heat Transfer>Heat Transfer in Solids>Add**, then **Study>Stationary> Done**. First, we define the necessary model parameters in **Global Definitions>Parameters**, which can be found in *Table 6.2*. Based on geometrical considerations, the fluid velocity flowing upwards in the inner pipe is,

$$w_u = w_d \frac{R_{out}^{\ 2} - R_{in}^{\ 2}}{R_{in}^{\ 2}} = 3w_d\,, \tag{6.2}$$

three times larger than the downward velocity in the outer pipe, since the cross sectional area of the inner pipe is lower by a factor of three.

The model includes three coaxial cylinders, the rock, where the only heat transfer mechanism is the conduction, **Geometry_R>Rectangle>Width: 100** m, **Height: 100** m at

Position: (0, -100) m, the outer pipe, where the cold fluid flows down, **Geometry_R>Rectangle>Width: Rout**, **Height: 80** m at **Position: (0, -80)** m, and the inner pipe, where the warm fluid flows upwards, **Geometry>Rectangle 2_R>Duplicate** and **Rectangle 3>Width: Rin**, then **BAO**. The size of the borehole heat exchanger (BHE) is much less than that of the model domain, but you can see it after zooming in the left upper corner of the model geometry.

Name	Expression	Value	Description
T0	285 [K[	285 K	Surface temperature
T1	289 [K]	289 K	Bottom temperature
Rout	0.1[m[	0.1 m	Outer pipe radius
Rin	Rout/2	0.05 m	Inner pipe radius
wd	1e-4 [m/s]	1E-4 m/s	Down velocity
wu	wd*((Rout^2-Rin^2)/Rin^2)	3E-4 m/s	Up velocity

Table 6.2 Parameter definition

For the first time, we will use probe plots to analyze easily the effect of fluid circulation. The first probe plot is a checking probe by which the velocity of the outflowing water will be measured, **Definitions_R>Probes>Boundary Probe>Source Selection: #5** (top of the inner pipe, where the fluid flows out), **Variable name: w_out**, **Expression: ht.uz** (vertical velocity in Heat Transfer module), **Table and Window Settings>Plot window>+** to get **Probe Plot 1**. The second probe plot is the average temperature at the bottom of the BHE, **Definitions_R>Probes>Boundary Probe>Source Selection: #7** (bottom of the outer pipe), **Variable name: T_b**, **Expression: T** (temperature), **Table and Window Settings>Plot window>+** to get **Probe Plot 2**. The third probe plot is the average temperature of the outflowing water, **Definitions>Boundary Probe 1_R>Duplicate>Source Selection: #5** (top of the inner pipe), **Variable name: T_out**, **Expression: T**, **Table and Window Settings>Plot window>Probe Plot 2**. And the last probe plot measures the outflowing heat power, **Definitions>Boundary Probe 3_R>Duplicate>Source Selection: #5** (top of the inner pipe), **Variable name: Q_out**, **Expression: ht.Cp*ht.rho*ht.uz*(T-T0)*Rin^2*pi**, **Table and Window Settings>Plot window>+** to get **Probe Plot 3**. The heat power defined above is

$$Q_{out} = c_p \rho w_u (T - T_0) A, \tag{6.3}$$

where c_p, ρ, w, T_0 and $A=R_{in}^2\pi$ denote the specific heat, the density and the vertical velocity of the water, the inflow water temperature and the cross-sectional area of the outflow water.

Now, we need to fill in the domains with materials, **Materials_R>Add Material from Library>Built-In>Water** for the BHE, and **Materials_R>Add Material from Library>Built-In>Material Library>Minerals, Rocks and Soils>Sandstone (quartzitic) >Sandstone (quartzitic)>Sandstone (quartzitic) [solid, parallel to bed]** for the medium, **Geometric Entity Selection: #1**. At this moment you get a warning, because the heat capacity of the sandstone is not defined, but needed for the calculation, so fill in the table with an appropriate value, **Material Contents>Cp: 1000** J/(kgK). The warning will disappear.

At this stage the domain properties and the boundary conditions must be prescribed. You need to add two fluid modules for the BHE, **Heat Transfer in Solids_R>Fluid>Domain Selection: #3** (outer pipe), **Velocity Field>u: (0, -wd)**, because the water flows downwards. And for the inner pipe, **Heat Transfer in Solids>Fluid 1_R>Duplicate>Domain Selection: #2** (inner pipe), **Velocity Field>u: (0, wu)**, because the water flows upwards. Going on the boundary conditions, the temperature of the surface and the inflow water is T_0, **Heat Transfer in Solids_R>Temperature>Boundary Selection: #8, 10**, **Temperature>T_0: T0**, and at the

bottom of the model, **Heat Transfer in Solids_R>Temperature>Boundary Selection: #2**, **Temperature>T_0: T1**. The temperature at the bottom of the inner pipe is equal to that of the outer pipe, here the water turns back, **Heat Transfer in Solids_R>Temperature>Boundary Selection: #4**, **Temperature>T_0: T_b**. You get a warning of 'Unknown variable T_b', because T_b will be calculated later, during the simulation as a boundary probe. So, you can skip the warning. At the top of the inner pipe, **Heat Transfer in Solids_R>Outflow>Boundary Selection: #5**, which ensures that the water does not cool through the boundary (zero heat flux, see **Equation**). Finally, the descending cool and the ascending warm pipes should be isolated by a low-conductivity material, **Heat Transfer in Solids_R>Thin Layer>Boundary Selection: #6**, **Layer thickness: 5e-3** m, **Layer thermal conductivity: 0.1** W/(m K), **Layer density: 2500** kg/m^3, **Layer heat capacity: 1000** J/(kgK). The outer side wall of the model is thermally insulated, and the axis is symmetrical, as it is prescribed by the default boundary conditions.

Meshing the model is much more simple, **Mesh_R>Free Quad>BA**, which gives 11468 finite elements. The problem will be solved for more circulation velocity values, thus we use a parametric sweep for w_d, **Study_R>Parametric Sweep>Study Settings>+** and we should choose **wd (Down velocity)** and type the values for the solutions: **1e-4 2e-4 5e-4 1e-3 2e-3 3e-3 5e-3 1e-2 2e-2** with **Parameter unit: m/s**. And now you can click **Study>Compute**. During the solution probe plots are calculated and shown in **Graphics** window.

Results>Temperature 3D shows the nine numerical solutions of the problem, it is worth changing color table, **Surface>Coloring and Style>Color table>Rainbow**. At highest water velocity (w_d=0.02 m/s) the BHE cools down its surroundings observably (*Figure 6.3a*), while at the lowest velocity (w_d=10^{-4} m/s), **Parameter value (wd (m/s)): 1e-4**, the solution for the temperature seems to reflect the conductive solution, T increases linearly downwards (*Figure 6.3b*). Let us look at the probe plots in **Graphic** window, **Probe Plot 1** shows that w_u increases linearly with w_d, and its values three times larger, as it was expected. **Probe Plot 2** displays that T_b decreases as the water velocity increases, since it has less time to be warmed up. The temperature of the outflow water has a maximum at w_d=0.002 m/s, because at this velocity the water is slow enough to be warmed up in the outer pipe, and it is fast enough not to be cooled down in the inner pipe. **Probe Plot 3** states that the outcome heat power monotonically increases with wd, however the slope of Q_{out} decreases. It can be explained by the fact that, although the outflow temperature (T_{out}) decreases with the circulation velocity (w_d), but the amount of the water ($w_u R_{in}^2 \pi$) increases. It is worth studying the temperature profile along the pipes, **Results_R>1D Plot Group**, then **1D Plot Group>Line**

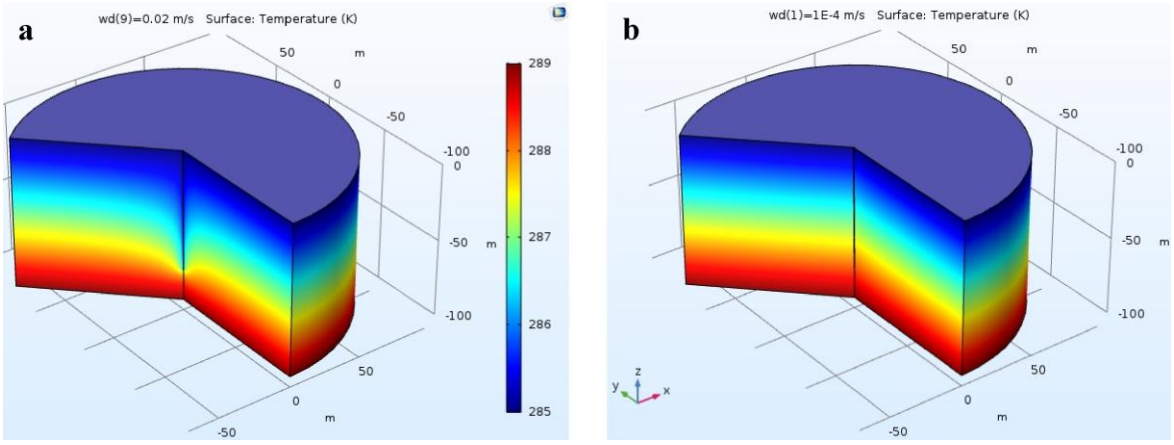

Figure 6.3 Temperature field in the ambient rock of the BHE with (a) high circulation velocity and (b) low circulation velocity.

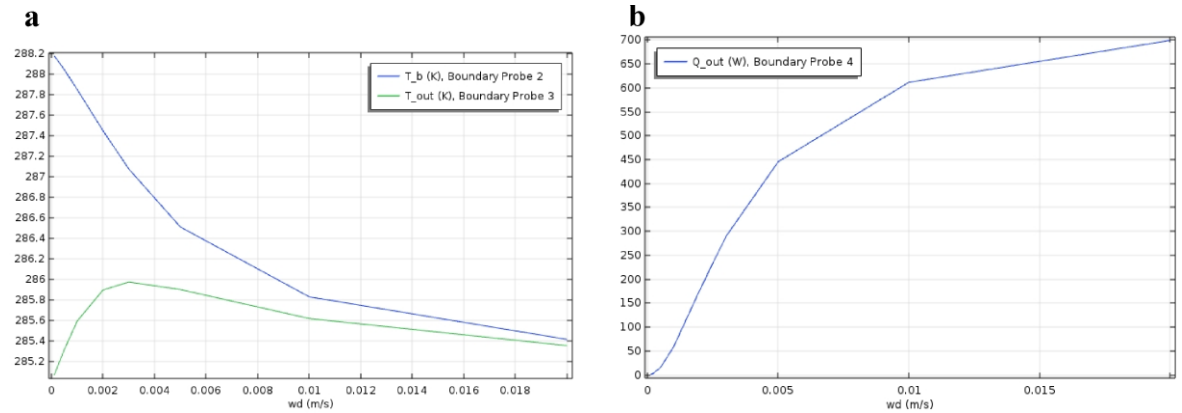

Figure 6.4 (a) The outflow and the bottom temperature of the BHE and (b) the outcome heat power from the BHE as a function of the circulation water velocity in the outer pipe.

Graph>Selection: #3, 9, **x-Axis Data>Parameter>Expression: z** and click **Legends>Show legends**, press the button **Plot**. At the lowest circulation velocity the water warms up linearly downwards, then it cools down almost linearly upwards. As w_d increases the deviation at the bottom of the BHE becomes larger. It must be an inconsistency in the numerical model, which should be eliminated. To understand the problem, **Results_R>1D Plot Group**, and **1D Plot Group_R>Line Graph>Selection: #4, 7** (bottom of BHE), **x-Axis Data>Expression: r**, then **Plot**. For the first look, it is strange, because the temperature varies radially within the outer pipe. The reason for this unrealistic behavior is that the module uses laminar approximation, so if one particle starts along the verge of the outer pipe, it will move here till the bottom of the BHE. Therefore, the radial heat transport occurs only by conduction. In natural circumstances, the flow in the BHE is rather turbulent, thus the flow has also radial component, which mixes the water and abolish the radial temperature differences. In order to eliminate this discrepancy from our model, we will artificially increase the radial thermal conduction within the pipes.

To increase the radial thermal conductivity within the pipes as a kind of imitation of turbulent flow, **Heat Transfer in Solids>Fluid 1>Thermal conductivity>User defined>Diagonal: (60, 0.6)** W/(m K), and also in the inner pipe, **Heat Transfer in Solids>Fluid 2>Thermal conductivity>User defined>Diagonal: (60, 0.6)** W/(m K). We can rerun the model, **Study>Compute**.

We managed to eliminate the problem, **Results>1D Plot Group 7** shows that there is no radial temperature variation within the pipe. **Probe Plot 2** illustrates that now the maximum outflow temperature occurs at w_d=0.003 m/s (*Figure 6.4a*), and **Probe Plot 3** says that the maximum circulating velocity results in approx. $Q_{out}\approx$700 W heat power (*Figure 6.4b*) in stationary calculation. Vertical temperature profiles within the pipes are shown in *Figure 6.5*, but some solutions were expelled, **Results>1D Plot Group 6>Data>Parameter Selection (wd)>From list: 1e-4, 0.001, 0.003, 0.01** and **Plot**. Now it is clear, that the downward velocity of $w_d=10^{-4}$ m/s is too slow, thus the water cools down in the ascending branch. On the other hand, $w_d=10^{-2}$ m/s is too fast, thus the water cannot warm up in the descending branch. From the point of view of the outflow water temperature, $w_d=3\cdot10^{-3}$ m/s is the optimum point.

Finally, we study also the radial temperature variation in the rock generated by the BHE, **Results>Data Sets_R>Cut Line 2D>Point 1: (0, -40)** m to **Point 2: (1, -40)** m, Plot shows that the section is situated at the middepth of the BHE. **Results_R>1D Plot Group>**, and **1D Plot Group 8>Line Graph>Data>Data set: Cut Line 2D**, **x-Axis Data>Expression: r**, then click **Show legends**. The plot illustrates that $w_d\geq$0.001 m/s is able

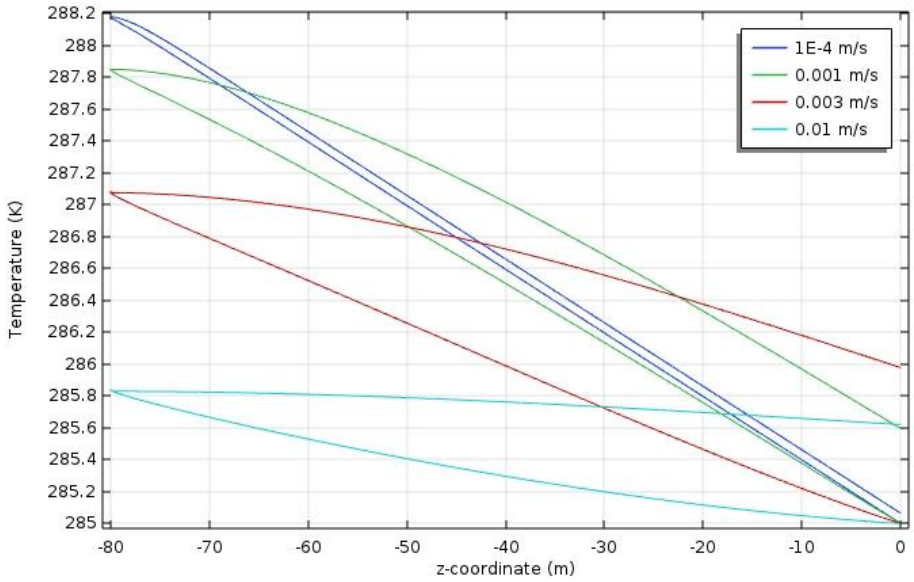

Figure 6.5 Vertical temperature profiles along the descending and the ascending branch of BHE at different water circulation velocities w_d.

to cool down the medium in the surroundings of the BHE, since the conductive temperature at the depth of 40 m is 286.6 ºC. We need to save the model, **Save>BHE**.

6.3 Cooling volcano

In the last model in Geothermics the temperature and the surface heat flux variation created by a 3D cooling magma body will be investigated, thus the only heat transport mechanism is the conduction. It permits for us the calculation of a time-dependent 3D numerical model, **Model Wizard>3D>Heat Transfer>Heat Transfer in Solids>Add**, and **Study>Time Dependent>Done**. *Table 6.3* summarizes the defined parameters in **Global Definitions>Parameters**. Since this problem is time-dependent, we need also an initial condition for the temperature, as a conductive temperature distribution increasing linearly downwards. It can be defined in **Global Definitions_R>Variables** (*Table 6.4*).

Name	Expression	Value	Description
T0	285 [K[	285 K	Surface temperature
T1	1100 [K]	1100 K	Bottom temperature
d	30 [km]	30000 m	Crust thickness

Table 6.3 Parameter definition

Name	Expression	Unit	Description
T_in	T0-(T1-T0)/d*z	K	Initial temperature profile

Table 6.4 Variable definition

The bedding medium is, **Geometry_R>Block>Width: 1e5** m, **Depth: 1e5** m, **Height: d**, at **Position: (-5e4, -5e4, -d)** m. The magma body is situated 3000 m deep, **Geometry_R>Cylinder>Radius: 3000** m, **Height: 5000** m at **Position: (0, 0, -8000)** m. For accurate calculation above the magma body, click **Geometry_R>More Primitives>Point**, then **BAO** and **Wireframe Rendering**.

We set the model parameters characterizing the material properties, boundary and initial conditions for the bedding sediments, **Heat Transfer in Solids>Solid>Thermal**

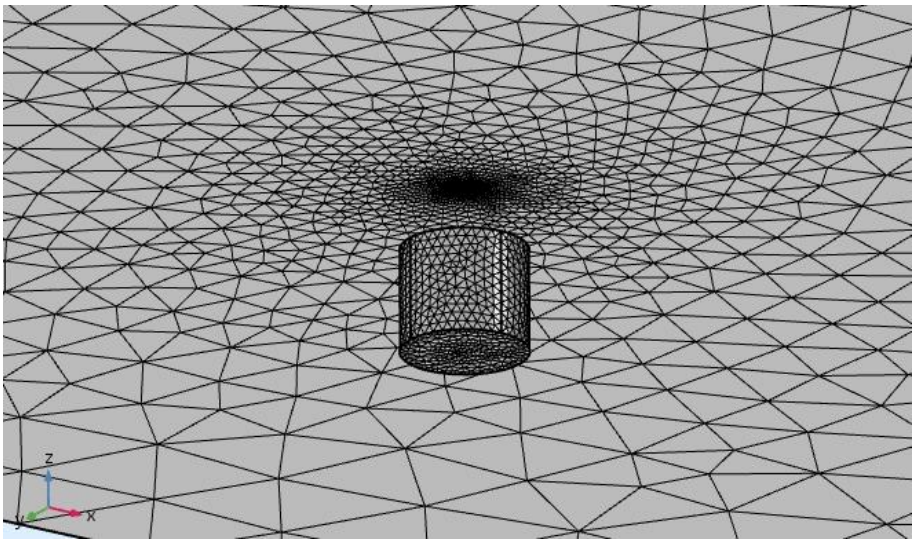

Figure 6.6 Illustration of the mesh of the magma chamber and the surface above.

conductivity>k: 2 W/(m K), **Density>ρ: 2500** kg/m^3 and **Heat capacity at constant pressure>C_p: 1000** J/(kgK) and for the magma body, **Heat Transfer in Solids>Solid_R>Duplicate**, and **Solid 2>Domain Selection: #2** (magma body), **Density>ρ: 3300** kg/m^3. The surface and the bottom of the model is isothermal, **Heat Transfer in Solids_R>Temperature>Boundary Selection: #4** (surface), **Temperature>T_0: T0**, and **Heat Transfer in Solids_R>Temperature>Boundary Selection: #3** (bottom), **Temperature>T_0: T1**. We can allow the isothermal boundary conditions for the side walls as a default. The initial condition for the temperature of the sediments is the conductive temperature profile defined in Table 6.4, **Heat Transfer in Solids>Initial Values>Temperature>T: T_in**. However, it is assumed that the magma body migrated suddenly from the mantle, so its temperature was kept, **Heat Transfer in Solids_R>Initial Values**, and **Initial Values 2>Domain Selection: #2** (magma body), **Temperature>T: T1**.

We compile an appropriate discretization for the problem, **Mesh_R>Size**, and **Size>Custom>MEGR: 1.3**, **Size 1>Geometric Entity Selection>GEL>Boundary: #6–11** (surface of magma body), then **Custom>MES: 500** m. For the surface, **Mesh_R>Size**, and **Size 2>Geometric Entity Selection>GEL>Boundary: #4** (surface), then **Custom>MEGR: 1.15**. For the point above magma chamber, **Mesh_R>Size**, and **Size 3>Geometric Entity Selection>GEL>Point: #9** (point above the magma chamber), then **Custom>MES: 50** m. As usual, we apply tetrahedral discretization, **Mesh_R>Free Tetrahedral>BA**, which results in 64064 finite elements. *Figure 6.6* shows the meshed magma body from below, after the side walls and the bottom boundary were hidden, click **Select Boundaries** in **Graphics** window and **Click and Hide**.

In order to check the initial condition, **Study_R>Get Initial Value**, then **Results>Temperature>Surface_R>Disable** and **Results>Temperature_R>Slice>Plane Data>YZ-planes>Planes: 1** creating a vertical section for the temperature profile. The temperature increases linearly in the ambient rock, while it is 1100 K in the magma body. It is worth removing the **Coloring and Style>Color legend**. Presenting the magnitude of total heat flux on the surface, **Results>Temperature_R>Slice>Plane Data>XY-planes>Planes**, **Entry method>Coordinates>Z-coordinates: 0** m, **Expression>ht.tfluxMag** in **Unit: mW/m^2**. At the initial state the surface heat flux is constant, 54.33 mW/m^2 (*Figure 6.7a*). Click **Go to Default View**.

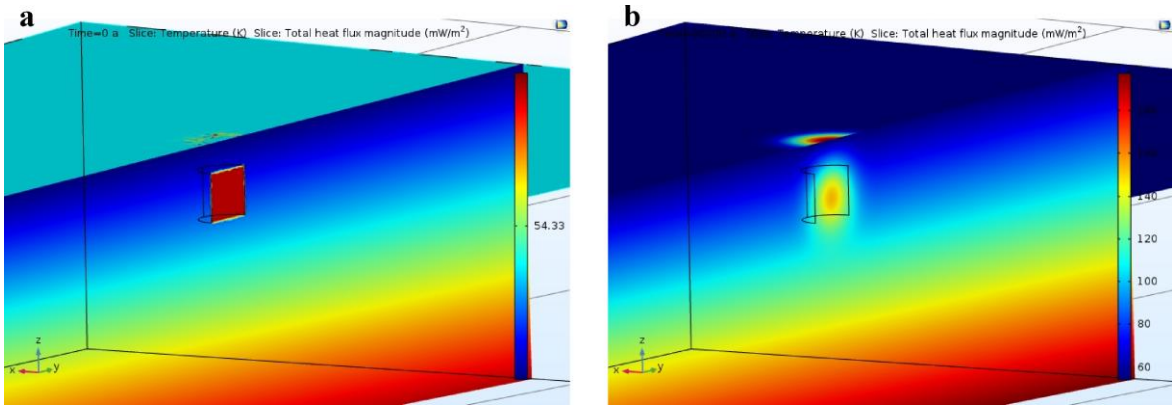

Figure 6.7 Vertical temperature profile crossing the magma body and surface heat flux (a) in the initial state and (b) 90 kyr later.

Let us set the parameters of the solution, **Study>Step 1: Time Dependent>Study Settings>Time unit: a** and **Times: range(0, 10000, 400000)** to simulate the solution to 0.4 Myr with an output time of 10 kyr. Click **Results While Solving>Plot Group: Temperature (ht)**, **Update at: Time steps taken by solver**, and set the time stepping method, **Study>Solver Configurations>Solution>Time-Dependent Solver>Time Stepping>Steps taken by solver: Strict**. Now, you can start the simulation, **Study>Compute**. During the computation you can rotate the model to look at the temperature of the magma chamber and the ambient rock, as well as the surface heat flux. The temperature of the magma body is likely to decrease with time resulting a time-dependent surface heat flux anomaly above that. *Figure 6.7b* displays the surface heat flux and the vertical temperature profile at a time of 90 kyr.

To study the temperature variation both in time and space, **Results>Temperature>Slice 1_R>Disable**, **Results>Data Sets_R>Cut Line 3D>Point 1: (-10000, 0, 5500)** m to **Point 2: (10000, 0, -5500)** m crossing the magma chamber at middepth, **Plot**. Then we create a graph, **Results_R>1D Plot Group**, **1D Plot Group_R>Line Graph>Data>Data set: Cut Line 3D**, **x-Axis Data>Parameter> Expression: x**, click **Plot**. *Figure 6.8* illustrates the temperature distribution crossing the magma body at each output time of 10 kyr. If you visualize only the initial state and the temperature after 160 kyr, **Data>Time selection>From list>Times (a): 0, 1.6E5**, and **Plot**, you can see that the initial temperature anomaly of the magma chamber reduced to approx. 1/*e*, which is the characteristic time scale of this conductive regime. Additionally, we can look at the time variation of the surface heat flux above the magma body, **Results_R>1D Plot Group**, and **1D Plot Group 4_R>Point Graph>Selection: #9** (point above the magma

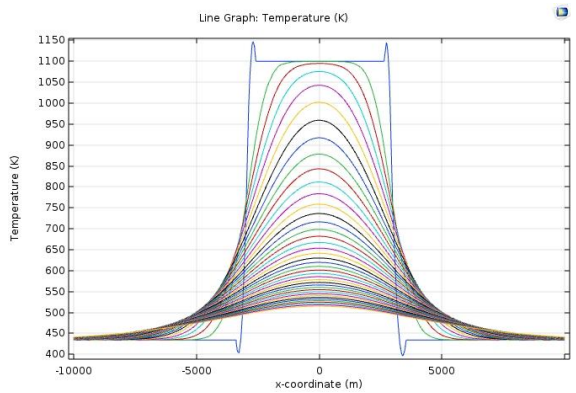

Figure 6.8 Horizontal temperature profiles crossing the magma body at each 10 kyr.

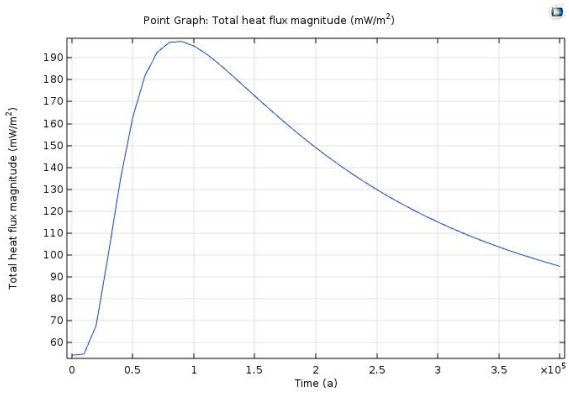

Figure 6.9 Time-variation of the surface heat flux above the magma body.

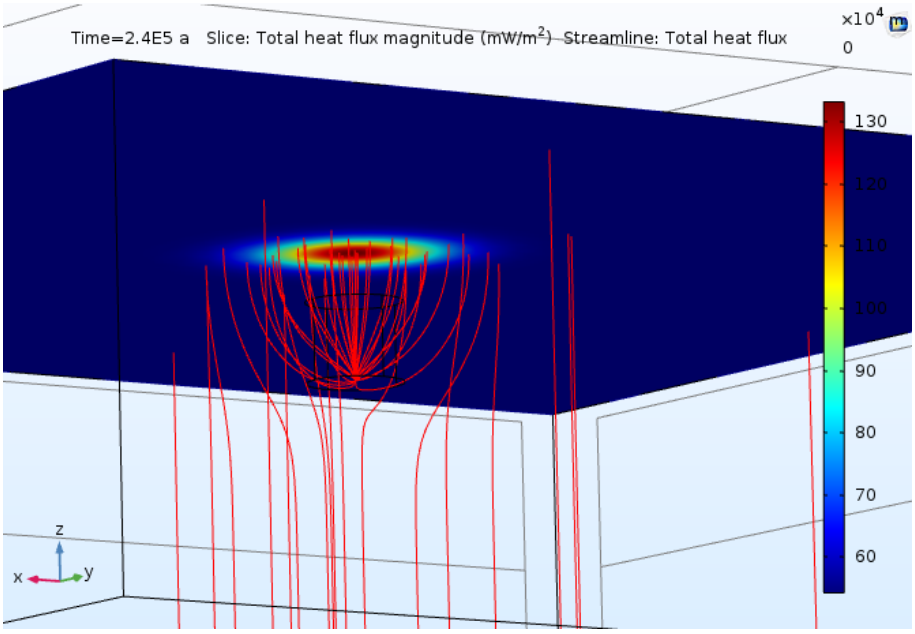

Figure 6.10 Surface heat flux and the heat flux lines (red) at a time of 240 kyr.

chamber), **y-Axis Data>Expression>ht.tfluxMag** in **Unit: mW/m^2**, then click **Plot**. *Figure 6.9* demonstrates that the surface heat flux has a maximum of almost 200 mW/m^2 at 90 kyr after the magma started cooling.

We can export the surface heat flux variation as an animation, **Results>Export_R>Animation>File>Format: AVI**, **Filename: Cooling volcano**, **Frames>Frame selection: All**, and click **Export**. Finally, we can study the heat flux streamlines, **Results>Temperature_R>Streamlines>Streamline Positioning>Start point controlled**, **Entry method>Number of points: 50**, then click **Plot**. Using the arrows in the upper part of **Settings** window, you can find that the magma chamber heats the ambient rock only if $t \leq 240$ kyr (*Figure 6.10*). Do not forget saving your model, **Save>Cooling volcano**.

7 GROUNDWATER FLOW

In this chapter groundwater flow modeling will be presented using Dracy's Law. In the first part a 2D stationary problem will be compared with the analytical solution, as well as the effect of anisotropy and inhomogeneity will be studied. Then, a hypothetical contamination transport problem will be investigated coupled with groundwater flow, and a possible treatment will be suggested.

7.1 Unit basin

7.1.1 Homogeneous and isotropic medium

We examine here how groundwater flow is controlled by a cosinusoid water table variation, **Model Wizard>2D>Fluid Flow>Porous Media and Subsurface Flow>Darcy's Law (dl)>Add>Study>Stationary>Done**. Model domain is a simple rectangle, **Geometry_R>Rectangle>Width: 1000** m and **Height: 300** m at **Position: (0, -300)** m, and **BAO**. Porous fluid, as water is added from **Materials_R>Add Material from Library>Built-In>Water, liquid**. Porosity and permeability are necessary parameters for the problem, but not respecting the water, so we can ignore the warning.

In **Darcy's Law>Fluid and Matrix Properties>Equation** we can check the relations consisting of the conservation of mass in stationary problem and the Darcy's Law, which uses the pressure *p* as unknown. Parameters for water are taken From material, but for **Matrix Properties>Porosity>User defined: 0.1** and **Permeability model>Hydraulic conductivity: 1e-4** m/s. Default boundary condition, No Flow are applicable for the boundaries excepting for the surface, where the cosinusoid water table must be prescribed as a driving force, **Darcy's Law_R>Hydraulic Head>Boundary Selection: #3** (surface) and **Hydraulic head>H_0: h_0**. Posteriorly, we need to define the water table, **Global Definitions_R>Variables>Name: h0**, **Expression: 10[m]*cos(pi*x/1000[m])**, **Description: Water table**. Now, the warning will disappear in the boundary condition.

Meshing is simple, **Mesh_R>Size**, and **Size>Custom>MES: 10** m, **MEGR: 1.2**. Then, **Size 1>GEL>Boundary>Selection: All boundaries**, **Custom>MES: 5** m. We need to select the type of meshing, **Mesh_R>Free Triangular**, and **BA** to get 12572 finite elements. Then, **Study>Compute**.

For visualization of the result, we can display the hydraulic head instead of pressure, **Results>Pressure>Surface>Expression: dl.H** and **Plot**. The hydraulic head varies within the range of (-10, 10) m in the whole domain, maximum is at the top left corner, and minimum is at the top right corner (*Figure 7.1*). Streamlines show the path of the flow, **Results>Pressure_R>Streamline>Streamline Positioning>Positioning: Magnitude controlled** and **Density: 10**. It is worth presenting also the hydraulic head contours by

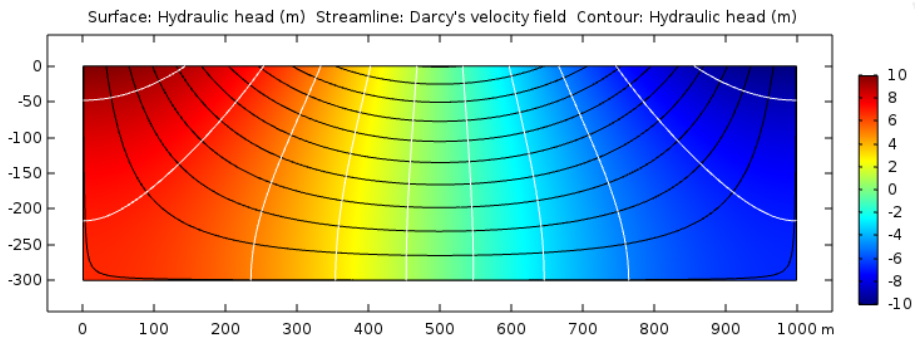

Figure 7.1 Hydraulic head field, Darcy flux lines (black) and head isocontours (white) of the groundwater flow under cosinusoid water table.

Results>Pressure_R>Contours>Expression: dl.H, **Levels>Number of levels>Total levels: 10**. We can choose a different color, **Coloring and Style>Color: White**. It is clear, that the water flows from left to right following the decrease of the head. In addition, streamlines are perpendicular to the head contours pointing out, that in isotropic medium the flow occurs toward the maximal head decrease. To look at the depth profile of different parameters, we define a vertical midsection, **Results>Data Sets_R>Cut Line 2D: (500, 0)** m to **(500, -300)** m, you can **Plot** the section.

- To create a graph, **Results_R>1D Plot Group**, and **1D Plot Group_R>Line Graph>Selection: #1** (left boundary), **Expression: dl.H**, **x-Axis Data>Parameter>Expression: y**. If you **Plot** the graph, you will see how the head decreases with the depth, which is typical in the recharge zones.
- On the other side, **Clear Selection**, and add **#4** (right boundary) to Selection box, then press **Plot**. Here the head increases with depth, as it is usual in the discharge zone. The rate of the head variation is known from analytical solution, which was solved in the course of Earth's Flow Systems I, the hydraulic head is

$$h(x,z)=\frac{H}{\cosh\frac{\pi d\sqrt{\varepsilon}}{l}}\cos\frac{\pi x}{l}\cosh\left[\frac{\pi\sqrt{\varepsilon}}{l}(y+d)\right], \tag{7.1}$$

  where H, d, l and ε denote the amplitude of the water table at the surface, the depth and the length of the model as well as the anisotropy coefficient, respectively. In this numerical model, H=10 m, d=300 m, l=1000 m, while $\varepsilon=K_{xx}/K_{yy}=1$ in isotropic medium. Eq. (7.1) reveals that the head varies with the depth as a cosh function.
- To get the horizontal Darcy flux along the surface, remove **#4** and add **#3** (surface) from/to Selection box, **Expression: dl.u** and **Parameter>Expression: x**, then **Plot**. You see that the horizontal velocity is maximal at the middle of the surface, where the slope of the water table is the largest.
- The vertical profile of the horizontal velocity along the midline, **Data>Data Sets>Cut Line 2D** and **x-Axis Data>Parameter>Expression: y**, **Plot** shows that the horizontal Darcy flux decreases with depth (~sinh), but it is nonzero at the bottom of the model. It means that there is horizontal flow along the bottom, which is also a flow path.
- The surface vertical velocity, **Data>Data Set: Study 1/Solution 1**, add **#3** (surface) to the Selection box, **Expression: dl.v**, then **x-Axis Data>Parameter>Expression: x**, then **Plot** it. The graph illustrates that the vertical flux is negative (downwards) on the left part of the model domain, while it is positive (upwards) on the right part. Former one indicates the recharge area, while the latter one indicates the discharge area.

Finally, let us visualize the magnitude of the Darcy flux, **Results>Pressure>Surface>**

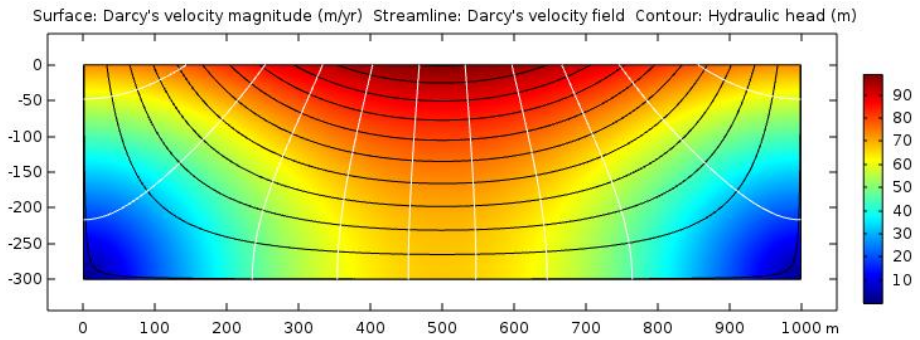

Figure 7.2 Darcy flux magnitude, Darcy flux lines (black) and head isocontours (white) of the groundwater flow under cosinusoid water table.

Expression: dl.U in **Unit: m/yr**. *Figure 7.2* displays that the flow is slow in the vicinity of the lower corners of the model domain, while it is more intense in the near-surface, and the Darcy flux is maximal in the shallow zone of the midline of the model. You should not forget to **Save>Groundwater flow - homogeneity**.

7.1.2 Anisotropy

In order to investigate the influence of hydraulic conductivity anisotropy on the flow and head distribution, we introduce a parametric sweep of ε to decrease gradually the vertical conductivity of the medium, **Global Definitions>Parameters>Name: e**, **Expression: 1** and **Description: Anisotropy coefficient**. **Darcy's Law>Fluid and Matrix Properties>Matrix Properties>Hydraulic conductivity>Diagonal: (1e-4, 1e-4/e)** m/s. Going to **Study 1_R>Parametric Sweep>Add (+)**, **Parameter name: e**, **Parameter value list: 1 10 100 1000**, **Parameter unit: 1**. Click **Plot** in **Output While Solving**. Now, you can start the computation by **Study 1>Compute**.

As the anisotropy increases, a slow/sluggish zone grows in the deeper domain, and the streamy zone contracts toward the surface (*Figure 7.3*), **Results>Pressure** (use arrows in Settings window). It can be easily explained, since the enhanced anisotropy reduces the vertical conductivity and so the vertical flow. If you set the **Data>Parameter value (e(1)): 10** and **Plot**, you can see that streamlines have not already been perpendicular to the head isocontours. Accordingly, the direction of the flow is controlled by both the head gradient and the hydraulic conductivity matrix.

We can see some Darcy flux and head sections of the solution, **Results>1D Plot Group>Line Graph>**

- **Selection: #1** (left side), **Expression: dl.v**, **x-Axis Data>Parameter>Expression: y**, and **Plot**. Obviously, as the anisotropy coefficient increases, the vertical velocity decreases due to the reduced vertical conductivity. You can click **Legends>Show legends** to be able to discriminate between the curves.
- You can check the horizontal velocity along the vertical midline, **Results>1D Plot Group>Line Graph>Data>Data set: Cut Line 2D**, **Expression: dl.u**, and **Plot**. The

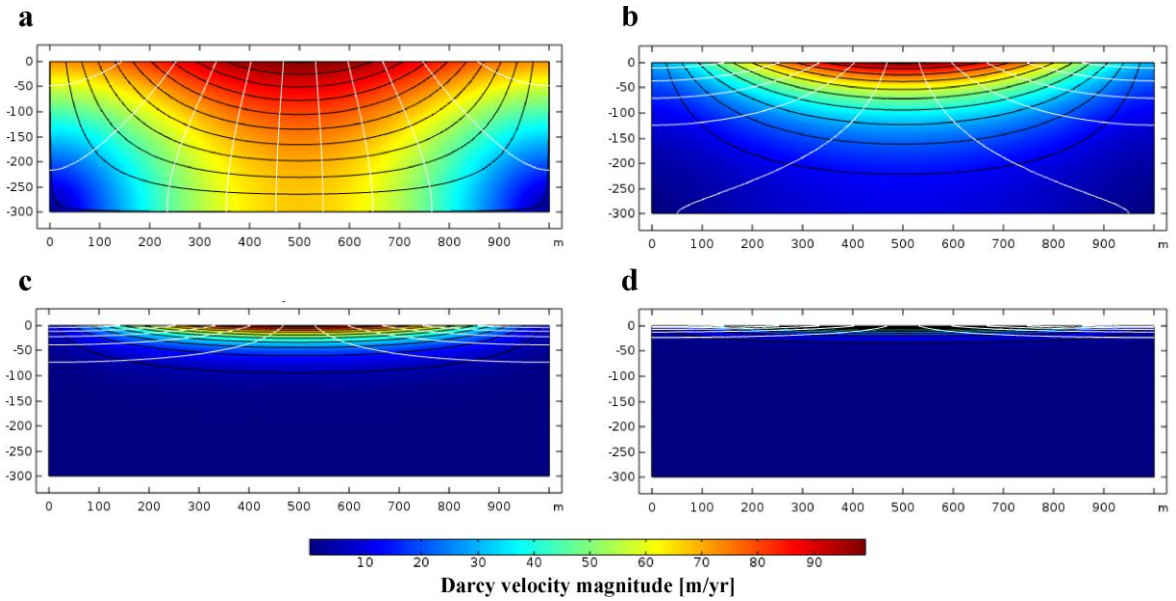

Figure 7.3 Effect of hydraulic conductivity anisotropy on the groundwater flow. Darcy flux magnitude, Darcy flux lines (black) and head isocontours (white) at different anisotropy ratios: (a) ε=1, (b) ε=10, (c) ε=100 and (d) ε=1000.

graph shows that the anisotropy ε=100 is high enough not to be present flow along the bottom of the model. If ε=1000 there is no relevant water motion below the depth of 50 m.

- The surface horizontal velocity, **Data>Data set: Study 1/Solution 1**, **Selection: #3**, **x-Axis Data>Parameter>Expression: x**, is not influenced by the anisotropy of the medium.
- However, the surface vertical velocity is affected by the anisotropy, **Expression: dl.v** and **Plot**. The higher the anisotropy is, the lower the vertical Darcy flux is.

Finally, we need to **Save As>Groundwater flow - anisotropy**.

7.1.3. Three-layer model

The most frequently occurrent heterogeneity in the nature is the geological layering, in this part the effect of a low-conductivity, clayey bedded layer will be analyzed by parametric sweep. The hydraulic conductivity of the middle, clayey layer is, **Global Definitions>Parameters>Name: K**, **Expression: 1e-4 [m/s]** and **Description: Hydraulic conductivity**. The model geometry must be modified, **Geometry>Rectangle 1_R> Duplicate**, and **Rectangle 2>Height: 100** m and **Position: (0, -200)** m. Press **BAO** to create the 3-layer model geometry.

A new module is needed for the bedded layer, **Darcy's Law_R>Fluid and Matrix Properties**, then **Fluid and Matrix Properties 2>Domain Selection: #2** (middle layer), **Matrix Properties>Porosity: 0.1** and **Permeability model>Hydraulic conductivity>K: K**. We should not forget that this model is isotropic, so **Darcy's Law>Fluid and Matrix Properties 1>Matrix Properties>Permeability model>Hydraulic conductivity>Isotropic**.

Mesh>BA results in 17230 elements. Let us choose in **Study 1>Parametric sweep>Parameter name: K (Hydraulic conductivity)**, **Parameter value list: 1e-4 5e-5 2e-5 1e-5 5e-6 2e-6 1e-6** in **Parameter unit: m/s**. Using this setting, the hydraulic conductivity of the bedded layer decreases by two orders of magnitude after **Study>Compute**.

Figure 7.4 illustrate that as *K* decreases in the middle layer, the flow slows down in the bedded and also in the lower layer, **Results>Pressure>Parameter value (K(m/s))**. It is unambiguous that streamlines (black) break at the layer boundaries. It is instructive recalling the law of refraction of current lines from Geoelectrical Methods,

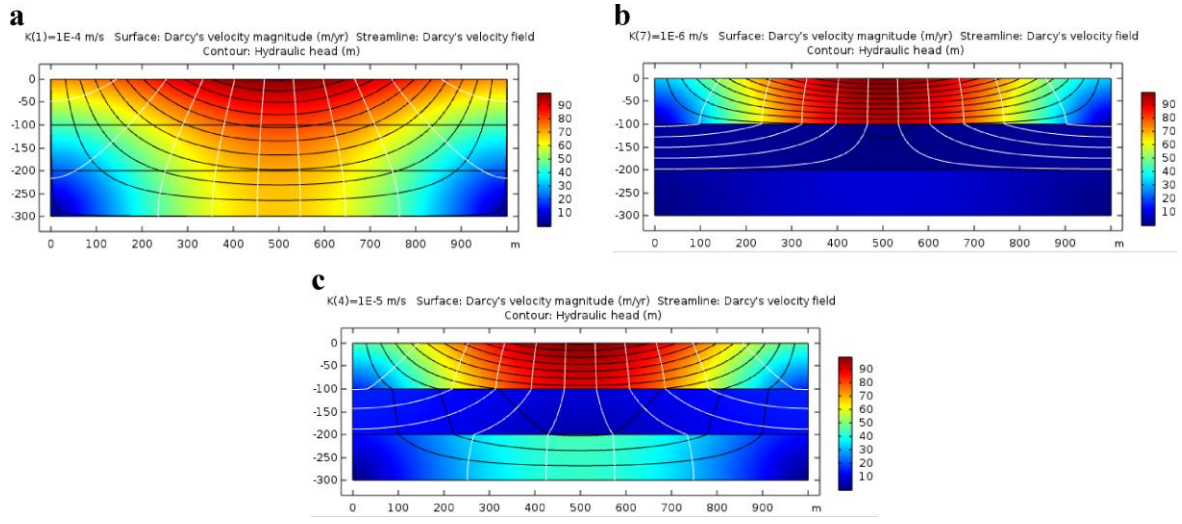

Figure 7.4 Effect of hydraulic conductivity of the bedded layer on the groundwater flow. Darcy flux magnitude, Darcy flux lines (black) and head isocontours (white) at different hydraulic conductivities of the middle layer: (a) K=10^{-4} m/s (homogeneous), (b) K=10^{-5} m/s and (c) K=10^{-6} m/s.

$$\rho_1 \tan\alpha_1 = \rho_2 \tan\alpha_2, \qquad (7.2)$$

where ρ and α denote the resistivity and the angle from the axis of incidence in medium 1 and 2. Eq. (7.2) proves that if the current enter the medium 2 with higher resistivity ($\rho_2>\rho_1$), the angle tends to the axis on incidence ($\alpha_2<\alpha_1$), since tangent is a monotonic increasing function within the range of α=0–90º. The analogy between the water flow and current flow is strong, Figure 7.4 validates that the flow enters from the upper layer to the middle, clayey layer with lower conductivity (higher resistivity), the flow paths break toward the axis of incidence, so α decreases.

We can investigate how the head and velocity profiles vary e.g. along the left-hand side of the inhomogeneous model, **Results>1D Plot Group>Line Graph>Selection: #1, 3, 5** (left side), **Expression: dl.H**, and **x-Axis Data>Parameter>Expression: y**, then **Plot**. As the hydraulic conductivity of the bedded layer decreases, the head is enhanced in the upper layer, but it is reduced in the deeper layers. The vertical velocity along this profile, **Expression: dl.v**, is lower, when *K* is decreased. The low-conductivity clayey layer retains the flow, so its role is similar to the increase in anisotropy. **Save As>Groundwater flow - 3-layer**.

7.1.4 Inhomogeneity

Another kind of heterogeneity occurring in geological situations is an embedded clayey lens, **Geometry_R>Ellipse>Size and Shape>a-semiaxis: 30** m and **b-semiaxis: 10** m at a **Position: (100, -50)** m related to the **Base: Corner**. Press **BAO**.

Suppose that the hydraulic conductivity of the clayey layer and the lens is less by one order of magnitude, **Darcy's Law>Fluid and Matrix Properties 2>Selection: #2, 4** (bedded layer and lens), **Matrix Properties>Hydraulic conductivity: 1e-5** m/s. To refine the discretization around the lens, **Mesh_R>Size**, move **Size 2** above **Free Triangular**, and **GEL>Domain>Selection: #4** (lens), then **Custom>MES: 3** m and **BA**. The new model geometry is recovered by 18508 finite elements. Now, you must delete parametric sweep, **Study 1>Parametric Sweep_R>Delete**, and you can solve the problem, **Study 1>Compute**.

Darcy flux maximums appear at the 'corner' of the clayey lens, where the flow accelerates to avoid the aquitard. Negative values of the horizontal velocity, **Results>Pressure>Surface>Expression: dl.u**, become visible near the surface of the lens, which were not present earlier in the model. This solution will be the initial condition of the next model including contaminant transport, so **Save As>Groundwater flow - inhomogeneity**.

7.2 Pollutant transport in groundwater flow

In this model the effect of a point-like pollutant emitter will be investigated. Although the near-surface source operates only one day long, still the pollution is dissolved and transported in the groundwater flow. In order to handle numerically the solution transport in porous medium, we need to add a new module, **Component 1_R>Add Physics>Chemical Species Transport>Transport of Diluted Species in Porous Media (tds)**. Change **Equation>Equation form>Time dependent** to see the relation describing the time-dependence of the solute concentration (1st term), which depends on the time-dependent rock structure (porosity), the molecular diffusion, the advection, the reaction and source terms (from left to right) as it was studied in the course of Earth's Flow Systems I. Let us click **Dispersion** to include this specific property (mechanical dispersion) of flow in porous medium.

We need to slightly modify the **Geometry_R>Point: (100, -1)** m to locate the pollutant point source just below the surface, **BAO**. Back to **Transport of Diluted Species in Porous Media>Porous Media Transport Properties>Velocity field: Darcy's velocity field** we can couple the two equations (Darcy's Law and mass transport equation), which is the strength of COMSOL. In this model the Darcy flux driven by water table topography influences the concentration distribution through advection and dispersion terms, but the concentration does not control the flow, supposing that the solute concentration is low to considerably increase the water density. Thus, it is a partly coupled PDE system. We need to define **Porosity: 0.1**, **Effective diffusivity model>No correction**, and **Dispersion tensor: Dispersivity**, **Dispersivity model>Isotropic>Longitudinal dispersivity: 1** m and **Transverse dispersivity: 1** m for the whole model domain. To define the point source, **Transport of Diluted Species in Porous Media_R>Points>Line Mass Source>Point Selection: #6** (pollutant point source defined above). The point source contaminates the soil one day long, **Species Source: t<1 [d]**.

To actualize the mesh in the surroundings of the point source, **Mesh_R>Size**, move **Size 3** above **Free Triangular**, and choose **GEL>Point: #6** (point source), **Custom>MES: 0.5** m, then **BA**, and the model geometry will be covered by 18910 finite elements.

Now, we are going to study the time-dependent transport of the contamination, thus we need a new study, **Groundwater flow - inhomogeneity.mph_R>Add Study>Time Dependent**. We can prepare the settings during the time-dependent solution, **Study 2_R>Get Initial Value**, then **Results>Concentration_R>Arrow Surface>Coloring and Style>Arrow length: Normalized**. To set the parameters characterizing the time-dependence of the study, **Study 2>Step 1: Time Dependent>Time unit: d** and **Times: range(0, 1, 120)** d, which is about four months. We would like to follow the variation of the solute concentration during the solution, **Results While Solving>Plot>Plot Group: Concentration** for each time step, **Update at: Time steps taken by solver**. We should not forget to regulate the time stepping, **Study 2>Solver Configurations>Solution 2>Time-Dependent Solver>Time Stepping>Steps taken by solver: Strict**. Now, we can start, **Study 2>Compute**.

During the solution you can follow the time-dependent contamination transport in the model in **Graphics** window (*Figure 7.5*). In **Progress** and **Log** menu below Graphics the chosen calculation method, time, time steps, output times etc. are presented. It is clear that the flow field does not vary in time, since the concentration does not influence the water density, and the water table is fixed. After 1 day the extension of the concentration anomaly increases, while the concentration maximum decreases due to the molecular diffusion and mechanical dispersion. The contaminated water is transferred from the recharge zone toward the discharge zone by advection, which results in that the pollutant penetrates deeper. One part of the contamination is trapped in the clayey lens and retained by the low-conductivity medium, thus the anomaly parts. Generally, it can be established that the main transport process in this model is the advection, while the role of diffusion and dispersion are less, but not negligible, since it causes the spreading of the contaminating substance. Finally, we can see e.g. the time-variation of the concentration in the position of the original point source, **Results_R>1D Plot Group>Data>Data set: Study 2/Solution 2**, **1D Plot Group_R>Point Graph>Selection: #6** (point source), **Expression: c** and **Plot**. We see that the concentration is high at the beginning, while the pollutant source is functioning, then *c* decreases owing to the processes of advection, diffusion and dispersion. Also this solution should be saved, **Save As>Solute transport**.

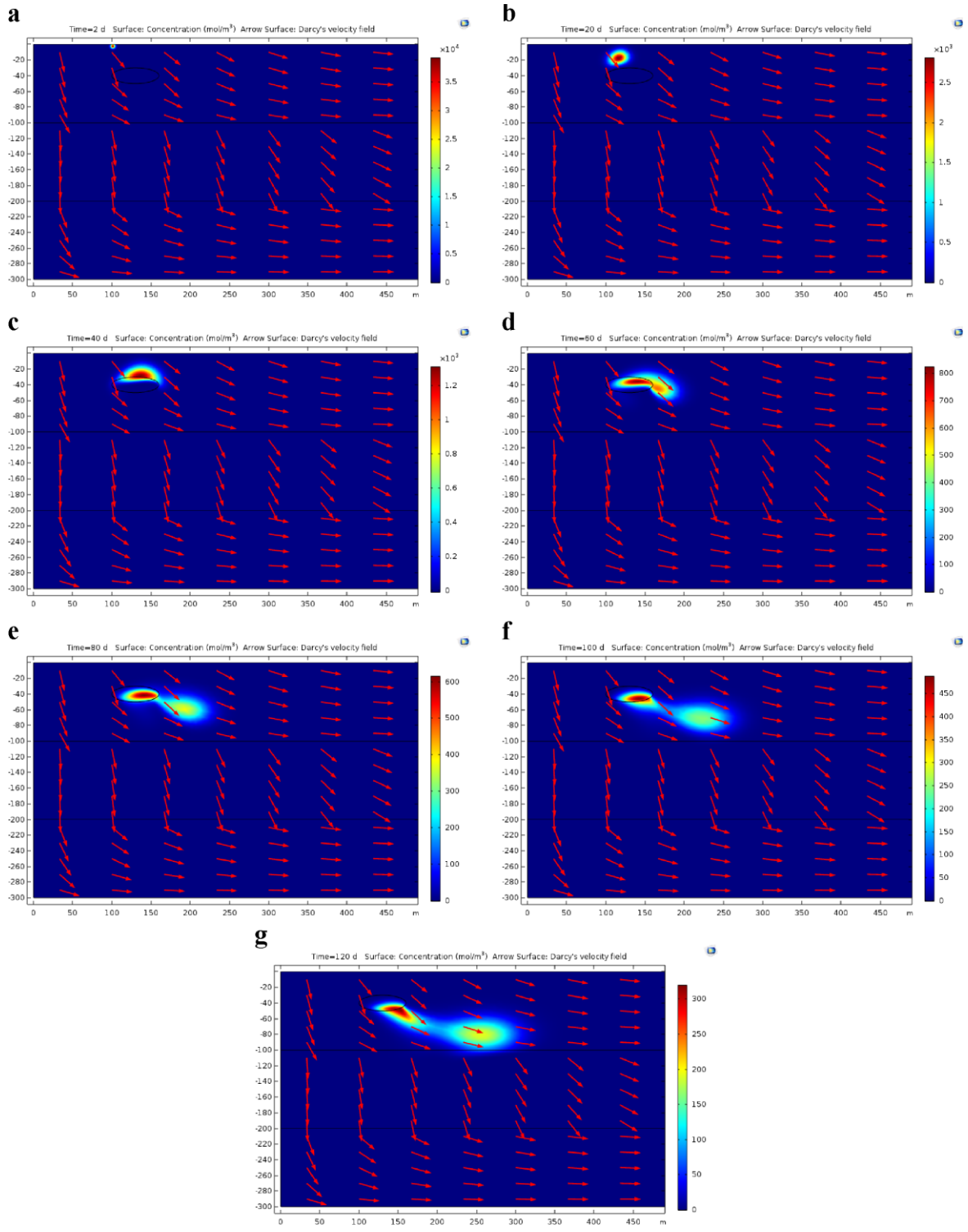

Figure 7.5 Snapshots of pollutant transport in inhomogeneous groundwater flow system. (a) Initial state (*t*=0), (b) after 20 d, (c) after 40 d, (d) after 60 d, (e) after 80 d, (f) after 100 d, and (g) after 120 d. Coloring denotes the concentration of the contamination. Darcy flux direction is shown by red arrows.

7.2.1 Effect of well

The main question is: How can be the polluted water removed from the subsurface? One possible solution is that one or more wells must be pumped around the contamination, so the polluted water can be discharged from the aquifer. As we will see, it is not trivial to plan e.g. the appropriate number, areal distribution, discharge rate of wells. The well in our numerical model will be imitated by a line segment, which is rather a drain when 2D is expanded to 3D. But there is no perfect solution for modeling a well in 2D, **Geometry_R>Line Segment>Start Point>Specify>Coordinates: (400, 0)** m to **Endpoint>Specify>Coordinates: (400, -80)** m, then **BAO**. We will use also a probe to measure the efficiency of the well pumping, **Definitions_R>Probes>Domain Probe>Variable name: c_tot**, **Probe Type>Type: Integral**, **Expression: c**, which calculates how the total/integrated concentration of pollutant water reduces in the model. To set the '2D pumping well' **Darcy's Law_R>Flux Discontinuity>Boundary Selection>Selection: #8** (well), **Inward mass flux: -0.1** kg/(m^{2}s), which would result in about 300 l/min discharge rate for a typical 2D water well. Now, we do not need the pollutant source, **Transport of Diluted Species in Porous Media>Line Mass Source_R>Disable**.

In order to refine the discreatization around the well, **Mesh_R>Size**, move **Size 4** above **Free Triangular**, then **GEL>Boundary>Selection: #8** (well), **Custom>MES: 2** m. Clicking **BA** yields 19814 finite elements. Now, we can continue the calculation by **Study 2>Step 1: Time Dependent>Times: range(120, 1, 240)** d. This setting, however, does not mean that the calculation will be continued from the final result! It configures only the start, output and stop times. To set the initial condition as a final result of the earlier study, **Study 2>Solver configuration>Solution 2>Dependent Variables>General>Defined by study step: User defined**, **Initial Values of Variables Solved For>Method: Solution**, **Solution: Solution 2**, **Time (d): 120**. Now, it is suggested to decrease the maximum time step, **Study 2>Solver configuration>Solution 2>Time-Dependent Solver>Time Stepping> Maximum step: 0.5** d, which is half of the output time step. We might need to reset time settings here, **General>Defined by study steps: Step 1: Time Dependent**. So, we can start the 'environmental precalculation', **Study 2>Compute**.

The solution visualized in **Graphics** window says that the arrows showing the flow direction change, the local flow generated by the pumping well overwrites the topography-driven regional groundwater flow near the well (*Figure 7.6*). The pollution moves toward the well, but cannot inhibit the penetration into the clayey layer. **Probe Plot** illustrates that the total contamination decreases in the model, at the beginning of the calculation *c* decreases quickly, but when the pollution enters the low-permeability clayey layer (at approx. 140 d), the rate of reduction moderates. In the meantime, the size of the anomaly increases, and the magnitude of the anomaly decreases due to diffusion and dispersion processes. In general, the pumping well facilitated the reduction of pollutant concentration; however the tested solution was not perfect. E.g. the well was too far from the actual position of the contamination, so partly aided the pollution to penetrate deeper. That is why the role of numerical modeling is very important in the subsurface contamination transport, too. We have to keep the model, **Save As>Solute transport & well**.

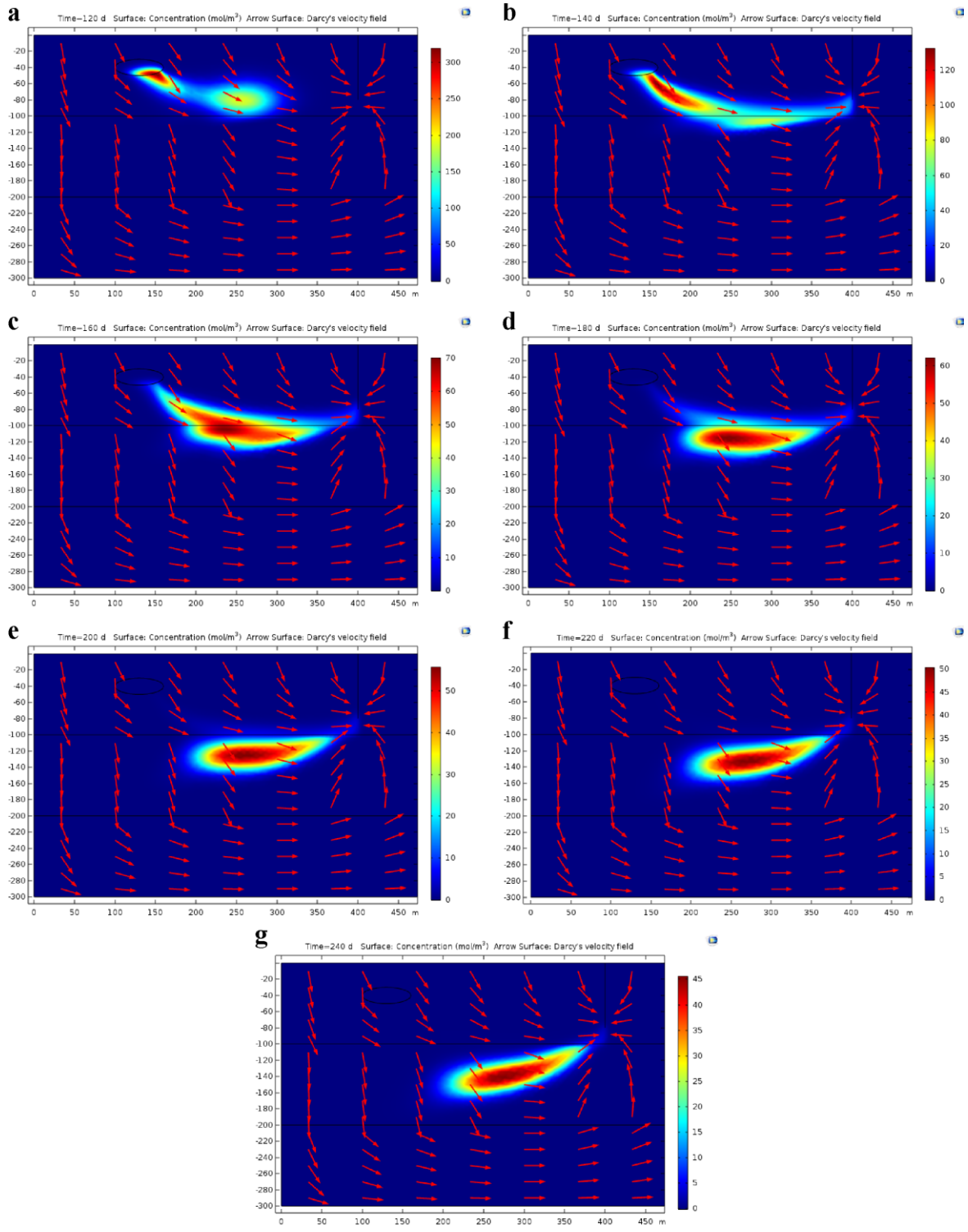

Figure 7.6 Snapshots of pollutant transport in inhomogeneous groundwater flow system including a pumping well at x=400 m. (a) t=120 d (start of pumping), (b) t=140 d, (c) t=160 d, (d) t=180 d, (e) t=200 d, (f) t=220 d and (g) t=240 d. Coloring denotes the concentration of the contamination. Darcy flux direction is shown by red arrows.

8 MANTLE CONVECTION

Numerical modeling of mantle convection is a typical 'multiphysical' problem, since the unknowns of the thermal convection occurring in the mantle are the pressure, the flow velocity and the temperature. The pressure and the velocity is solved by the conservation of mass and Navier–Stokes equation, while the temperature is computed from heat transport equation. In this final part the PDE system is fully coupled, because the temperature depends on the flow field, and the velocity depends on the temperature due to thermal buoyancy. The second part deals with the problem of thermochemical mantle convection, in which also the mass transport equation is coupled to the former PDEs, to build up an imposing multiphysical numerical model.

8.1 Thermal mantle convection

In this model the higher temperature at the base of mantle ensures the driving force that is the thermal buoyancy for the mantle convection. Higher temperature decreases the density of the mantle material due to heat expansion, and induces thermal buoyancy force and ascending of the fluid. When the fluid reaches the cold surface, it starts cooling, its density is increasing, then it descends to the bottom. Moving along the hot core mantle boundary (CMB) the mantle is warming up, its density is decreasing, and the circulation begins from the start. To model thermal mantle convection as simple as possible, **Model Wizard>2D>Fluid Flow>Nonisothermal Flow>Laminar Flow>Add**, which is one of the predefined modules including coupled PDEs in COMSOL. The unknowns are the pressure *p*, the three components of the velocity (*u*, *v* and *w* at least in 3D) and the temperature *T*. Then click **Study>Time Dependent>Done**.

First, the model parameters needs defining in **Global Definitions>Parameters** after *Table 8.1*. In addition, we will use model variables as well, *r* denotes the radius and *rho* defines the linear relation between the density and the temperature (*Table 8.2*).

Name	Expression	Value	Description
R0	6370 [km]	6.37E6 m	Earth radius
R1	3480 [km]	3.48E6 m	Core radius
T0	300 [K]	300 K	Surface temperature
T1	3200 [K]	3200K	CMB temperature
rho0	3300 [kg/m^3]	3300 kg/m^3	Surface density
g	10 [m/s^2]	10 m/s^2	Gravitational acceleration
alpha	2E-5 [1/K]	2E-5 1/K	Heat expansion coefficient

Table 8.1 Model constants

Name	Expression	Unit	Description
r	sqrt(x^2+y^2)	m	Radius
rho	rho0*(1-alpha*(comp1.T-T0))	kg/m^3	Mantle density

Table 8.2 Model variables

Next step is the geometry building, **Geometry_R>Circle>Radius: R0**, and **Geometry>Circle_R>Duplicate>Radius R1**, then **BAO**. To cut the 'core' from the 'Earth', **Geometry_R>Booleans and Partitions>Difference>Objects to add: c1** ('Earth'), and **Objects to subtract: c2** ('core'), then **BAO** again to get the 'mantle'. In order to minimize the time and memory requirement, we will solve the problem only on the one fourth of the model domain, **Geometry_R>Square>Size>Side length: 2*R0** at **Position: (-2*R0, -R0)**

then **Geometry>Square_R>Duplicate**, **Geometry>Square 2>Position: (0, -2*R0)**, then **BAO**. To make a difference, **Geometry_R> Booleans and Partitions>Difference>Objects to add: diff1** (‘mantle’), and **Objects to subtract: sq1, sq2** (two squares), then **BAO** to get quadrant of the ‘mantle’ as the final model geometry. Click **Zoom Extents**.

Now, we specify the model for the flow. To see the equations, **Laminar Flow (spf)>Equation**, you can identify the Navier–Stokes equation (NS) ensuring the momentum conservation and the continuity equation governing the mass conservation in the system. In NS the inertia term (left) is balanced by the right terms: pressure gradient, viscous force and possible external force, for example Lorentz force. Continuity equation is valid also for compressible fluid, so we can simplify the problem to **Physical Model>Compressibility: Incompressible flow**, but the gravitational force is essential, click **Include gravity** to modify NS. Of course, you must designate the downward direction, which varies in the model, **Laminar Flow>Gravity>Acceleration of gravity>g: (-x/r*g, -y/r*g)**. We can add the physical parameters, **Laminar Flow>Fluid Properties>Dynamic viscosity: 1e22** Pas. If the dynamic viscosity depends on the temperature, pressure or/and the stress, it can be defined as a variable. We allow to be moving along the boundaries (free slip), **Laminar Flow>Wall>Wall condition>Slip**. Finally, we need to use a pressure constraint, because only the gradient of the pressure acts in NS, for this we have to switch on **Advanced Physics Option** at the top of **Model Builder** window. So, **Laminar Flow_R>Points>Pressure Point Constraint>Point Selection: #2** (surface), where the pressure is fixed to zero, **Pressure>p_0: 0**.

Now, we can skip to the thermal parameters, **Heat Transfer in Fluids (ht)>Equation** shows that the heat of the fluid parcel depends on the heat advection, heat conduction, heat production, external heat flux, pressure work and the viscous dissipation as it was studied during the course of Earth’s Flow Systems II. To define the necessary parameters, **Heat Transfer in Fluids>Fluid>Thermal conductivity>User defined>k: 5.4** W/(m K), **Density>rho: rho** (as a temperature-dependent fluid density), **Heat capacity at constant pressure>C_p: 1200** J/(kgK), **Ratio of specific heats>γ: 1**, which affirms that there is no difference between specific heat at given pressure and at given volume. In **Heat Transfer in Fluids>Initial Values** we will define a perturbed conductive temperature state to facilitate the start of convective motion, e.g.

$$T = T_1 - \frac{T_1 - T_0}{R_0 - R_1}(r - R_1) + 0.1(T_1 - T_0)\sin\left(\pi \frac{r - R_1}{R_0 - R_1}\right)\sin\left(2\,\mathrm{atan}\,\frac{y}{x}\right), \qquad (8.1)$$

which results in a positive temperature anomaly at an angle of 45º. Thermal insulation, as boundary condition is appropriate for the side walls, but the surface, **Heat Transfer in Fluids_R>Temperature>Boundary Selection: #4** (surface), **T0: T0**, and the CMB, **Heat Transfer in Fluids_R>Temperature>Boundary Selection: #3** (CMB), **T0: T1** is isothermal.

It is suggested switching of the automatic coupling between modules, **Multiphysics>Nonisothermal Flow_R>Disable**, to set it manually. In this case you can define the temperature-dependent density in NS, **Laminar Flow>Fluid Properties>Density>rho: rho**. And, you need to define the velocity in **Heat Transfer in Fluids>Fluid>Velocity field>u: Velocity field (spf)**. So, you can see how the PDEs are coupled.

We decrease the mesh size for the whole model domain, **Mesh_R>Size**, **Size>Custom>MES: 100000** m, and for the boundaries, where thermal boundary layers could evolve in supercritical Rayleigh number convection, **Mesh>Size 1>GEL: Boundary**,

Selection: All, and **Custom>MES: 30000** m. We use triangles for discretization, **Mesh_R>Free Triangular**, then **BA** to get 12719 finite elements.

Before starting the computation we can check the initial settings and tune the visualization properties, **Study_R>Get Initial Value**. In **Results>Temperature>Surface** you can see the perturbed conductive temperature defined above. Please, change the color scale to **Coring and Style>Color table: Rainbow**. It is useful to display also the flow directions, **Temperature_R>Arrow Surface>Arrow Positioning>x grid points>Points: 30** and **y grid points>Points: 30**, **Coloring and Style>Arrow length: Normalized**, **Color: Black**.

Turning back to the solver, **Study 1>Step 1: Time Dependent>Time unit: a**, **Times: range(0, 1e6, 1e8)** a. To see the temperature field and flow direction during the solution, **Results While Solving>Plot>Plot Group: Temperature** at each time steps, **Update at: Time steps taken by solver**. We refine the time stepping, **Study 1>Solver Configurations>Solution 1>Time-Dependent Solver>Time Stepping>Steps taken by solver: Strict** and **Maximum step: 3e5** a. Let us start the simulation, **Study 1>Compute**.

Figure 8.1a shows that the temperature anomaly at 45º evolves to a large thermal instability and reaches the surface after 7–9 Myr. After approx. 20 Myr the warm fluid is located in the upper part of the mantle, and cold fluid are spread above the CMB (*Figure 8.1b*). Temporarily, it seems a stable situation, cold, dense mantle is below the hot, light one. However, the cold upper boundary cools the warm fluid, and vice versa, hot lower boundary warms up the cold fluid. Since this process occurs by heat conduction, it is very slow and endures over 100 Myr. It is suggested saving the model before continuation, **Save>Thermal mantle convection**.

Actually, the phenomenon modeled above is only a transient state, so, if we want to see the flow similarly to the real mantle convection, we need to continue the calculation. But first, we define some probe plots to quantify the flow,

- **Definitions_R>Probes>Boundary Probe>Variable name: q_surf**, as the surface heat flux, **Source Selection>Selection: #4** (surface), **Expression: ht.ntflux** (normal total heat flux) in **Table and plot unit: mW/m^2**, then **Table and Window Setting>Plot window>+ (Add Plot Window): Probe Plot 1**.
- You can duplicate this probe plot to calculate surface velocity, **Definitions>Boundary Pobe 1_R>Duplicate>Variable name: v_surf**, **Expression: spf.U** (velocity magnitude) in **Table and plot unit: cm/yr**, then **Table and Window Setting>Plot window>+ (Add Plot Window): Probe Plot 1**.
- To calculate the average mantle temperature, **Definitions_R>Probes>Domain Probe>Variable name: T_av**, **Expression: T**, then **Table and Window Setting>Plot window>+ (Add Plot Window): Probe Plot 3**.

For the continuation of the calculation, **Study 1>Step 1: Time Dependent>Times: range(1e8, 2e6, 1e9)** a, and **Study 1>Solver Configurations>Solution 1>Time-Dependent Solver 1>Time Stepping>Maximum step: 1e6** a. It is very important to set the initial condition, **Study 1>Solver Configurations>Solution 1>Dependent Variables 1>General> Defined by study step: User defined**, **Initial values of Variables Solved For>Method: Solution**, **Solution: Solution 1** and **Time (a): 1E8**. Now, we can continue the simulation from the end of the former solution, **Study 1>Compute**.

During the solution you can see, how cold instabilities forms from the upper cold surface and try to penetrate the upper hot zone. As their negative thermal buoyancy reduces, they become trapped in the hot zone. However, cold instabilities are able to cool down the upper hot mantle domain (*Figure 8.1c*). The process occurring above the CMB is very similar. By the time the cold/hot thermal instabilities cool down/heat up the upper/lower part of the mantle, thermal mantle convection will have been evolved (*Figure 8.1d*). Since neither the

surface heat flux/velocity nor the average temperature did not reach the quasi-stationary state, we should continue the simulation after **Save As>Thermal mantle convection_t1e9yr**. For the continuation of the simulation, **Study 1>Step 1: Time Dependent>Times: range(1e9, 2e6, 2e9)** a, and **Study 1>Solver Configurations>Solution 1>Dependent Variables 1>Initial Values of Variables Solved For>Time (a): 1E9**, then **Study 1>Compute**.

During this third run a typical convective system is forming, hot plumes are emerging from the hot CMB, while cold downwellings are descending down into the warm mantle.

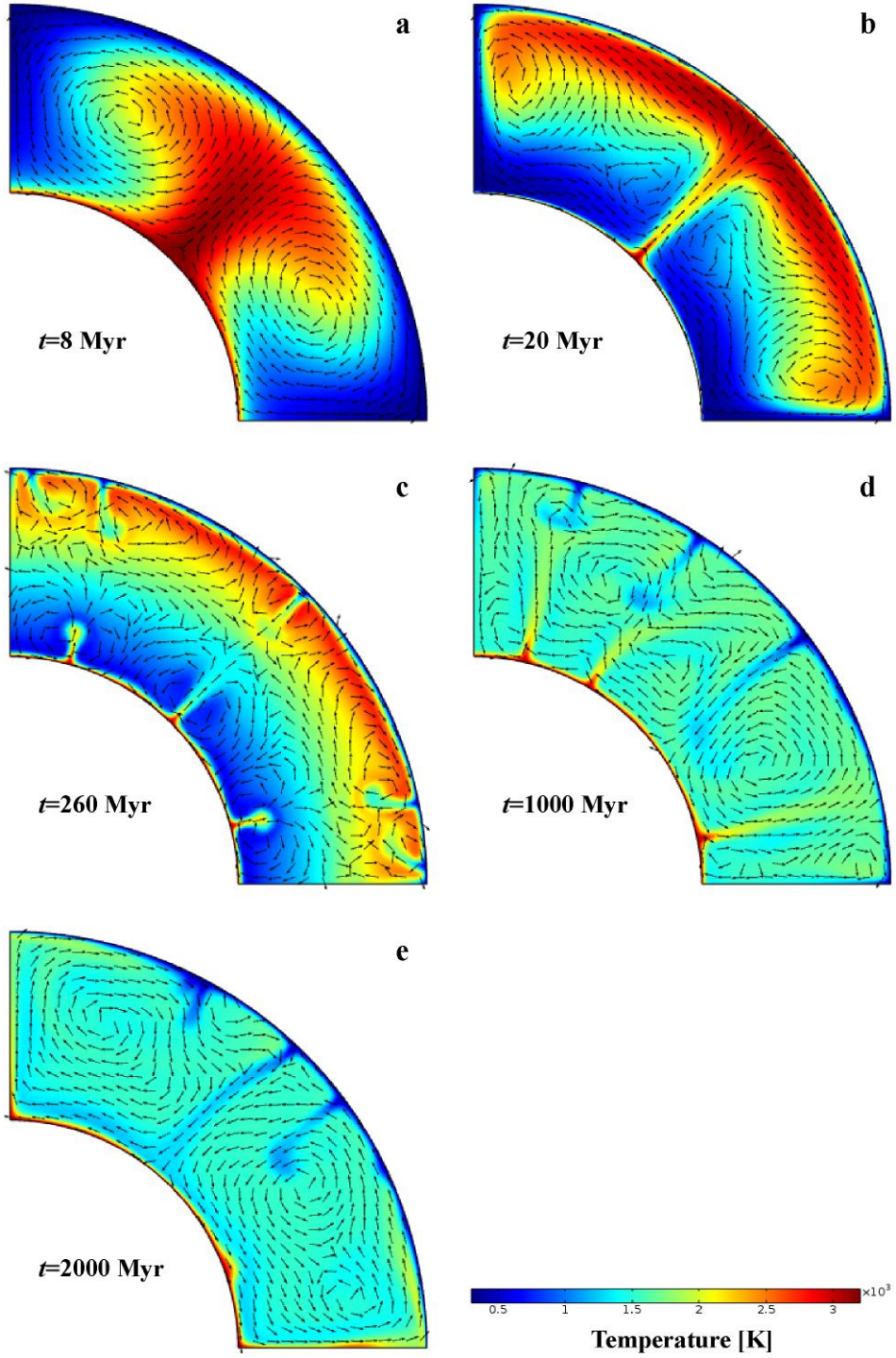

Figure 8.1 Snapshots of the temperature field and the flow velocity direction (black arrow) of thermal mantle convection at (a) *t*=8 Myr, (b) *t*=20 Myr, (c) *t*=260 Myr, (d) *t*=1000 Myr and (e) *t*=2000 Myr.

Plumes are drifted toward a side walls (slip flow condition), while a cold downwelling is stabilized at approx. 45º. The solution is time-dependent, hot and cold instabilities are forming form the thermal boundary layers. Meanwhile, the surface heat flux and the velocity begins to reach the quasi-stationary state tending to about 100–110 mW/m^2 and 2 cm/yr, respectively, which are in accordance with the observation in spite of the simplicity of the numerical model. The average temperature is still decreasing, because this monitoring parameter is stabilizing the most slowly. *Figure 8.1e* illustrates the final result, which will be the initial state of the following thermochemical mantle convection model. But previously, we need to save the solution, **Save As>Thermal mantle convection_t2e9yr**.

8.2 Thermochemical mantle convection

Based on the newest seismological findings it is obvious that the mantle is not homogeneous compositionally. Two large low shear velocity provinces (LLSVP) were detected beneath Africa and Pacific by seismic tomography. In LLSVPs the reduction of S wave velocity is significant (2–4%), on the other hand the, P wave velocity decrease is not relevant (0–1%). This fact and other observations suggest that the lowest part of the mantle is compositionally/chemically distinct from the overlying mantle. In this final part, we will compile a simple thermochemical mantle convection model in which the thermal buoyancy facilitates the convection in the mantle (hot material below), while the 'chemical buoyancy' hinders it (compositionally dense material below). The competition of these two contrary effects forms the thermochemical convection in the mantle (for details see the notes of Earth's Flow Systems II).

To handle the effect of chemical buoyancy, we need to add another module to the PDE system governing the non-isothermal flow problem, **Component 1_R>Add Physics>Chemical Species Transport>Transport of Diluted Species**, **Settings >Equation** shows that the time-dependence of concentration of the dense material is influenced by the diffusion, the advection and other reaction/source terms on the right side. We must define that the density of the chemically dense mantle material is higher by 1%, add another parameter to **Global Definitions>Parameters**, **Name: beta**, **Expression: 0.01** and **Description: Initial relative density contrast**. Back to the **Transport of Diluted Species>Transport properties>Convection>Velocity field: Velocity field (spf)**, which establishes that the velocity in the advection term in the mass transport equation is derived from the velocity computed from NS. Since the mantle is solid, the molecular diffusion of the dense material is negligible, so **Diffusion>Diffusion coefficient>D_c: 0**. We might set that the temperature can be obtained from the heat transport equation, **Model input>Temperature>T: Temperature (ht)**, although the concentration is independent of the temperature, therefore it does not have influence on the solution. It is very important to define the initial condition for the dense material concentration. The primordial location, arrangement and type of the dense zone is very questionable and not solved problem. One of the most frequently used initial condition is a dense layer blanketing the Earth's core. Thus, we suppose a layer with a thickness of 300 km directly above the CMB, which has a continuous transition from the light upper part to the dense lowest part of the mantle. This transition is described by the Heaviside function, **Transport of Diluted Species>Initial Values>Concentration>c: flc1hs((R1+300[km]-r)[1/m], 25000)**, which says that the dense (c=1) layer is 300 km thick, it is located above the CMB (R1), and the thickness of the transition from light to dense mantle material is 50 km (25000 m is the half-width of the transition).

Perhaps, the most difficult part of the model is the appropriate setting of the initial conditions. The initial temperature and the velocity field is the final result of the former solution of thermal mantle convection at a time of $2 \cdot 10^9$ yr. On the other hand, the

concentration should be started from the initial value. To do this, **Study 1>Solver Configurations>Solution 1>Dependent Variables>General>Defined by study step: Step 1: Time Dependent**, and you should click off **Study 1>Step 1: Time-Dependent: Transport of Diluted Species**, not to solve this module. In order to get the temperature and the velocity field from the end of the former simulation, **Values of dependent variables>Initial values of variables solved for>Settings: User controlled**, **Method: Solution**, **Study: Study 1** and **Time (a): Last**. In order to get the concentration from the initial value defined above, **Values of variables not solved for>Settings: User controlled**, **Method: Initial expression**, **Study: Study 1** and **Time (a): Last**. Now, we can check the initial conditions, **Study 1_R>Get Initial Value**.

After this, we can prepare the plot what we want to see during the simulation, **Results_R>2D Plot Group** and **2D Plot Group_R>Surface>Expression: c** within the **Range>Manual color range: -0.1** to **1.1**. It is worth renaming the plot, **2D Plot Group_R>Rename: Concentration**. To illustrate also the temperature contours in this plot, **Results>Concentration_R>Contour>Expression: T**, **Levels>Number of levels>Total levels: 10**, and we will not need the color legends, so click off **Color legend**. *Figure 8.2a* illustrates the initial condition of the concentration and temperature field of the thermochemical mantle convection model.

In the thermochemical model, it is clear, that the mantle density depends both the

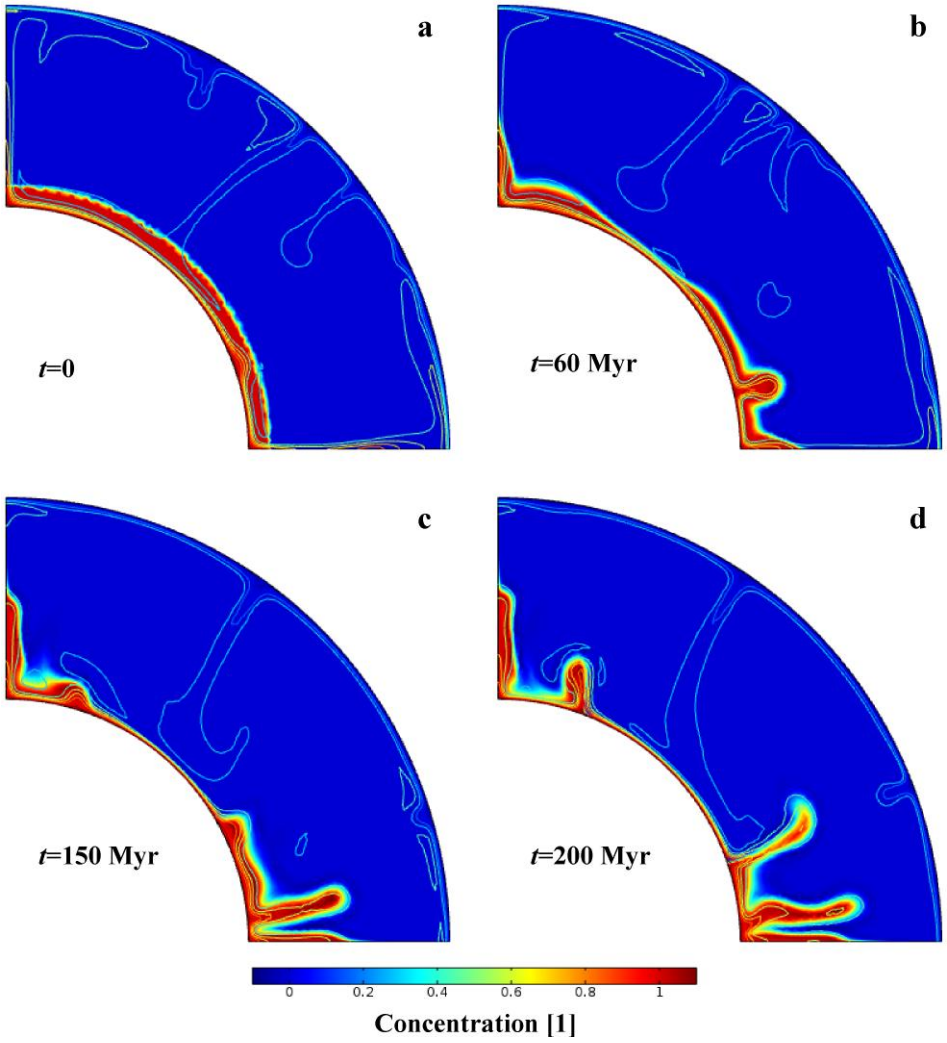

Figure 8.2 Snapshots of the concentration of the dense material and the temperature (contours) in the thermochemical mantle convection model at a time of (a) *t*=0 Myr, (b) *t*=60 Myr, (c) *t*=150 Myr and (d) *t*=200 Myr.

temperature and the concentration of the dense material, **Global Definitions>Variables> rho>Expression: rho0*(1-alpha*(comp1.T-T0)+beta*comp1.c [m^3/mol])**.

Finally, we need to set the parameter of time-dependent solution, **Study 1>Step 1: Time Dependent>Times: range(0, 1e6, 2e8)** a, to see the time-variation of the concentration during the solution, **Results While Solving>Plot Group: Concentration**, and you should not forget to click **Physics and Variables Selection>Transport of Diluted Species** to solve the coupled thermochemical problem. To stabilize the computation, **Study 1>Solver Configurations>Solution 1>Time-Dependent Solver>Time Stepping>Initial step: 1e3** a and **Maximum step: 3e5** a. Now, we can start the solution, **Study 1>Compute**.

After 60 Myr a depression forms beneath the cold and thermally dense downwelling, while the compositionally dense mantle is lifted up along the side walls and within the model by ascending hot plumes (*Figure 8.2b*). *Figure 8.3c* displays that the primordial dense layer disintegrated after 150 Myr. Dense layer around the CMB retains the heat from below and moderates the intensity of convection, as a consequence both the surface heat flux (from 108 to 76 mW/m^2) and surface velocity (from 2.2 to 1.1 cm/yr) decreases (**Probe Plot 1 and 2**). The average temperature shows a long-term decreasing trend.

Buoyancy ratio defines the ratio of the stabilizing chemical buoyancy and the destabilizing thermal buoyancy,

$$B = \frac{\beta \Delta c}{\alpha \Delta T} = \frac{0.01}{2 \cdot 10^{-5} \frac{1}{\mathrm{K}} \cdot 2900\mathrm{K}} \cong 0.17, \tag{8.2}$$

where α and β denotes the heat expansion coefficient and the initial compositional density difference between the dense and light mantle material, as well as Δc and ΔT are the maximum concentration and temperature difference in the model. The value of $B \approx 0.17 < 1$ indicates that the effect of thermal destabilization is stronger, so the disintegration, the breaking-up, then the homogenization of the primordial dense layer is expectable during geological time scale. At higher compositional density difference β, that is larger buoyancy ratio *B*, the evolution of the thermochemical mixing is slowed down. The process of thermochemical convection can be continued in a manner presented in the previous part to accomplish the simulation till the homogenization of the dense layer. This model should be saved, **Save as>Thermochemical mantle convection**.

ACKNOWLEDGEMENTS

The project was supported by the János Bolyai Research Scholarship of the Hungarian Academy of Sciences.